SESSION IV

BASIC PHYSICS, MATERIALS AND FUELS

S. Pilate (BN) – H. Takano (JAERI)

SESSION IV
BASIC PHYSICS, MATERIALS AND FUELS

SUB-SESSION IV-A:
BASIC PHYSICS

NUCLEAR DATA MEASUREMENTS FOR P&T AND FUTURE PLANS IN JNC

H. Harada, S. Nakamura, K. Furutaka, T. Baba
Japan Nuclear Cycle Development Institute
4-33 Muramatsu, Tokai-mura, Naka-gun, Ibaraki 319-1194, Japan

Abstract

Measurements of thermal neutron capture cross-sections (σ_0) and resonance integrals (I_0) of some important fission product (FP) nuclides, performed at JNC for partitioning and transmutation (P&T) studies, are presented. Method of the measurements and the results are reviewed, and possible reasons for discrepancies between the present data and that obtained by other researchers are discussed. Future plans on nuclear data measurements for P&T studies are presented.

1. Introduction

The reduction of the environmental loads is one of the important issues of the countries all over the world. In the field of nuclear energy production, the amount of radioactive nuclear wastes should be reduced. To reduce the amount, some methods have to be designed to transform these radioactive nuclides into stable ones.

One of the ways to transform these radioactive nuclides is the transmutation using the reactor neutrons. In order to study schemes of nuclear transmutation using the reactor neutrons, it is essential to know precise values of neutron cross-sections of these radioactive nuclides. Looking at the nuclear data of neutron reactions for these radioactive FP nuclides, the data are rather scarce, and the existing data are old and sometimes poor in accuracy. In this point of view, we have performed measurements of thermal (2 200 m/s) neutron capture cross-sections (σ_0) and resonance integrals (I_0) of some important radioactive FP nuclides and some the surrounding stable nuclides, using an activation method. These nuclides include ^{133,134,135,137}Cs, ^{90}Sr, ^{99}Tc and ^{127,129}I.

In this paper, our experimental method to determine σ_0 and I_0 of these radioactive FP nuclides, and the obtained results are reviewed. Then, our future plans on nuclear data measurements are presented.

2. Nuclear data measurements for P&T by JNC from 1990 to 1999

JNC has organised some researches on nuclear data measurements by several universities in Japan. These researches include:

- Measurements of fast neutron induced fission cross-section of americium isotopes (Department of Quantum Science and Energy Engineering, Tohoku University).
- Neutron capture cross-section measurement of ^{237}Np with lead slowing-down spectrometer (Research Reactor Institute, Kyoto University).
- Preliminary experiment of neutron capture cross-section of ^{99}Tc with lead slowing-down spectrometer (Research Reactor Institute, Kyoto University).
- Measurement of neutron capture cross-sections of ^{99}Tc (Research Laboratory for Nuclear Reactors, Tokyo Institute of Technology).
- Measurement of fission cross-section and fission neutron spectrum of ^{237}Np by an advanced technique (Department of Quantum Science and Energy Engineering, Tohoku University).

At the same time, JNC has continued their own effort on measurements of neutron capture cross-sections of long-lived FP nuclides (LLFP) using some research reactors in Japan, from 1990 until now [1-9]. This paper concentrates on the latter topic, and describes our experimental methods and results.

The experimental procedure to determine σ_0 and I_0 is based on an activation method, in which samples are irradiated with neutrons and then γ rays are measured which are emitted during de-excitations of the daughter of the capture products, to determine reaction rate R of the capture reaction. For the γ-ray measurements, a high purity Ge detector with a large volume is used. This enables determination of γ-ray yield in an efficient and reliable manner and thus the reaction rate R is determined precisely in case the precise values of emission probabilities of the γ-rays are available. In

order to determine σ_0 and I_0, at the same time, irradiations and measurements are also done for samples with a Cd shield.

The procedure to determine σ_0 and I_0 from the obtained R is based on Westcott's convention [10]. It was already described elsewhere [1], and only a brief summary is given here:

In the Westcott's convention, the reaction rate R in well-moderated neutron fields is expressed as:

$$R = n\,\upsilon_0\,\sigma_{\mathrm{eff}}$$

where in the convention $n\upsilon_0$ is the "neutron flux" with neutron density n including thermal and epithermal neutrons and with velocity υ_0=2 200 m/s, and σ_{eff} an effective cross-section. The σ_{eff} is written as:

$$\sigma_{\mathrm{eff}} = \sigma_0\,[g\,G_{\mathrm{th}} + r(T/T_0)^{1/2}\,s_0\,G_{\mathrm{epi}}]$$

where σ_0 is the reaction cross-section for 2 200 m/s neutrons and g the measure of deviation of the cross-section from the $1/\upsilon$ law in the thermal energy region. In the analysis the g is assumed to be unity. The quantity $r(T/T_0)^{1/2}$ gives the fraction of epithermal neutrons in the neutron spectrum, and s_0 is defined as:

$$s_0 = 2I'_0/((\pi)^{1/2}\sigma_0)),$$

with I'_0 the reduced resonance integral, i.e. the resonance integral after subtracting the $1/\upsilon$ component. The G_{th} and G_{epi} are self-shielding factors for thermal and epithermal neutrons, respectively. The above equations are combined to read:

$$R/\sigma_0 = G_{\mathrm{th}}\,\phi_1 + s_0\,G_{\mathrm{epi}}\,\phi_2,$$

where ϕ_1 and ϕ_2 represent simplified flux factors. The ϕ_1 and ϕ_2 can be determined by using flux monitors whose cross-sections and resonance integrals are already determined precisely. As flux monitors, we use Co and Au, which differ in sensitivities to thermal and epithermal neutrons. By using two flux monitors with different sensitivities to thermal and epithermal neutrons, ϕ_1 and ϕ_2 can be determined unambiguously. The self-shielding factors G_{th} and G_{epi} are usually almost unity and can be calculated by considering geometries of irradiations.

From the obtained reaction rates R and flux factors ϕ_1, ϕ_2 for irradiations with and without Cd shield the cross-sections σ_0 and the reduced integrals I'_0 are deduced. The resonance integral, I_0, is deduced from I'_0 using the following relation:

$$I_0 = I'_0 + 2\,\sigma_0\,(E_0/E_{\mathrm{Cd}})^{1/2}$$

where E_0 and E_{Cd} are neutron energy at 2 200 m/s and Cd cut-off energy.

In Table 1, the results obtained by the present authors are summarized [1-9] along with the data previously published by other research groups [11-18]. The table includes results of the neutron capture cross-sections and resonance integrals for long-lived FP nuclides (LLFP) as well as those for their stable isotopes: the latter are also important because these stable nuclides absorb neutrons and affect transmutation rates of LLFP, and also these stable nuclides can be transformed into radioactive ones by absorbing neutrons.

Some of the data obtained by the present author do not differ significantly from those obtained previously. For example, for ^{134}Cs nuclide, the effective cross-section obtained by Bayly *et al.* [17]

agrees ours within limits of errors. Also, the thermal neutron cross-section and the resonance integral of ^{129}I nuclide obtained by the present authors are close to those published by Eastwood *et al.* [14].

On the other hand, for some nuclides, the results obtained by the present authors differ considerably from others. An example of the discrepancy is the result for ^{99}Tc nuclide. Although the thermal neutron cross-section does not differ much, the result of the reduced resonance integral obtained by the present authors [4] are about twice as large as that obtained by Lucas *et al.* [13], as depicted in Figure 1. The origin of this discrepancy may be ascribed to the characteristics of their irradiation: their analysis was based on the same convention as ours which is valid only for well moderated neutron spectrum, but at one of their irradiation positions, the index for the epithermal neutrons, *r*, is as large as 0.15. Even with our data, the number of existing data of resonance integral for ^{99}Tc nuclide is only two. It should be stressed that, in order to be certain that correct values of σ_0 and I_0 are obtained, at least two different types of measurements have to be done. This is also true for other radioactive FP nuclides such as ^{90}Sr and ^{137}Cs.

It should also be noted that the data presented in [4] do not include the error of γ-ray emission probabilities: because of its short life, γ-ray emission probabilities of ^{100}Tc nuclide are determined with an error of as large as 17% [22]. In order to obtain σ_0 and I_0 of ^{99}Tc nuclide more accurately, accurate values of γ-ray emission probabilities of ^{100}Tc nuclide are needed.

3. Future plans on nuclear data measurements for P&T in JNC

Following the decision of the Atomic Energy Commission in Japan that the basic study on P&T should be continued JNC resumes the nuclear data measurement under a basic study scheme for P&T from 2000. Now we are planning to extend our area of nuclear data measurements over capture cross-sections, fission cross-sections and decay data for important LLFP and MA for the energy region from thermal to a few MeV. The plan includes the following researches and developments:

- More precise determination of the capture cross-sections of nuclides such as ^{99}Tc and ^{129}I.
- Development of prompt γ-ray spectroscopic method for the determination of the neutron capture cross-sections of LLFP.
- Development of a new spectroscopic method to measure neutron cross-sections for energy range from thermal to a few MeV.

3.1 More precise determination of the capture cross-sections

As already mentioned above, γ-ray emission probabilities of ^{100}Tc nuclide are not determined with enough accuracy because of its short life. To obtain more precise values for capture cross-sections of the ^{99}Tc nuclide, the γ-ray emission probabilities of ^{100}Tc should be determined more accurately. In order to achieve this, a β-γ coincidence measurement system has been developed for the determination of γ-ray emission probabilities of short-lived nuclides [23]. An experiment has been already performed using the system to precisely determine γ-ray emission probabilities of ^{100}Tc nuclide.

3.2 Prompt γ-ray spectroscopy

For the determination of capture cross-sections of nuclides whose capture products are stable, a conventional activation method can not be applied in which de-excitation γ-rays are observed of daughter nuclides of the capture products. These include some important long-lived FP nuclides such as ^{93}Zr, ^{79}Se and ^{107}Pd. In order to determine capture cross-sections of such nuclides, a prompt γ-ray spectroscopic method is being developed, in which complete level schemes are constructed by in-beam γ-γ coincidence measurements using thermal neutron beam and then γ-ray emission probabilities are determined. By using the obtained emission probabilities, neutron capture cross-sections are determined.

This method is also applicable to nuclides whose capture products are not stable ones: measurements in this method will confirm the results that are already obtained by using other methods such as an activation technique.

3.3 Development of a new spectroscopic method for neutron cross-sections in a wide energy region

In order to efficiently determine neutron cross-sections of LLFP and minor actinides over a broad energy range from thermal to MeV region, some new experiments will be required. The present authors are planning to start the international collaborations from 2001 Japanese fiscal year.

Table 1. **Neutron capture cross-sections at 2 200 m/s neutron energy and resonance integrals for some important fission product nuclides, obtained by the present authors as well as other researchers**

Nuclide	Half-life (year)	Previous data (barns) (Authors and published year)	Data obtained by JNC (barns)
^{137}Cs	30	$\sigma_{eff} = 0.11 \pm 0.03$ (Stupegia 1960 [11])	$\sigma_0 = 0.25 \pm 0.02$ $I_0 = 0.36 \pm 0.07$ (1990 [1], 1993 [2])
^{90}Sr	29	$\sigma_{eff} = 0.8 \pm 0.5$ (Zeisel 1966 [12])	$\sigma = (15.3 + 1.3 - 4.2) \times 10^{-3}$ $I_0 \leq 0.16$ (1994 [3])
^{99}Tc	2.1×10^5	$\sigma_0 = 20 \pm 2$ $I'_0 = 186 \pm 16$ (Lucas 1977 [13])	$\sigma_0 = 22.9 \pm 1.3$ $I = 398 \pm 38$ ($I' = 388 \pm 38$) (1995 [4])
^{129}I	1.6×10^7	$\sigma_0 = 27 \pm 2$ $I_0 = 36 \pm 4$ (Eastwood 1958 [14])	$\sigma_0 = 30.3 \pm 1.2$ $I_0 = 33.8 \pm 1.4$ (1996 [5])
^{127}I	(stable)	$\sigma_0 = 4.7 \pm 0.2$ $I_0 = 109 \pm 5$ (Friedmann 1983 [15])	$\sigma_0 = 6.40 \pm 0.29$ $I_0 = 162 \pm 8$ (1997 [6])
^{135}Cs	2.3×10^6	$\sigma_0 = 8.7 \pm 0.5$ $I_0 = 61.7 \pm 2.3$ (Baerg 1958 [16])	$\sigma_0 = 8.3 \pm 0.3$ $I_0 = 38.1 \pm 2.6$ (1997 [7])
^{134}Cs	2	$\sigma_{eff} = 134 \pm 12$ (Bayly 1958 [17])	$\sigma_{eff} = 141 \pm 9$ (1999 [8])
^{133}Cs	(stable)	$\sigma_0 = 30.4 \pm 0.8$ $I_0 = 461 \pm 25$ (Baerg 1960 [18])	$\sigma_0 = 29.0 \pm 1.0$ $I_0 = 298 \pm 16$ (1999 [9])

Figure 1. **Thermal neutron capture cross-sections (upper) and resonance integrals (lower) of ^{99}Tc nuclide**

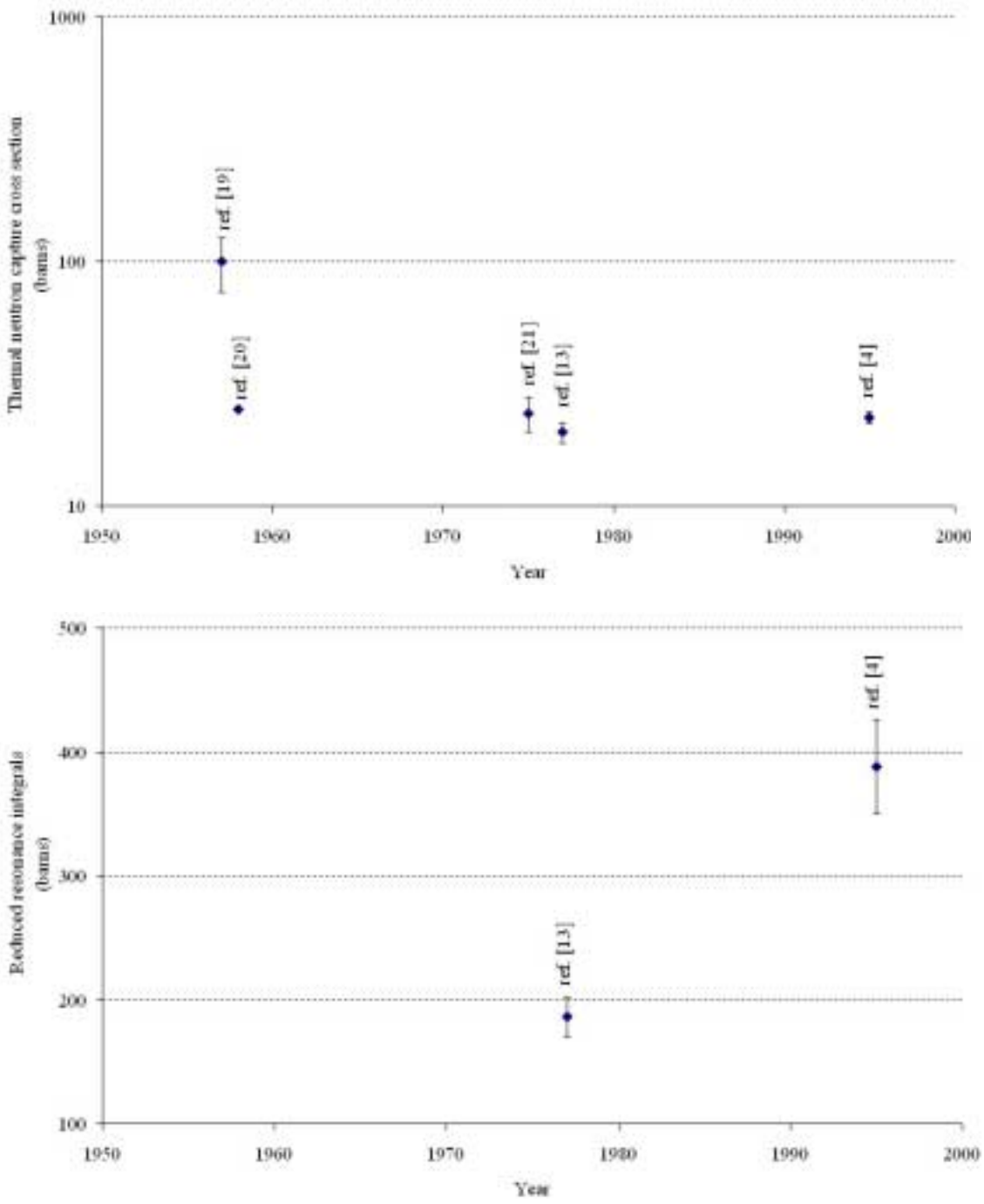

REFERENCES

[1] H. Harada, H. Watanabe, T. Sekine, Y. Hatsukawa, K. Kobatasyi, T. Katoh, J. Nucl. Sci. Tech., 27 (1990), pp. 577-580.

[2] T. Sekine, Y. Hatsukawa, K. Kobayashi, H. Harada, H. Watanabe, T. Katoh, J. Nucl. Sci. Tech., 30 (1993), pp. 1099-1106.

[3] H. Harada, T. Sekine, Y. Hatsukawa, N. Shigeta, K. Kobayashi, T. Ohtsuki, T. Katoh, J. Nucl. Sci. Tech., 31 (1994), pp. 173-179.

[4] H. Harada, S. Nakamura, T. Katoh, Y. Ogata, J. Nucl. Sci. Tech., 32 (1995), pp. 395-403.

[5] S. Nakamura, H. Harada, T. Katoh, Y. Ogata, J. Nucl. Sci. Tech., 33 (1996), pp. 283-289.

[6] T. Katoh, S. Nakamura, H. Harada, Y. Ogata, J. Nucl. Sci. Tech., 36 (1999), pp. 223-231.

[7] T. Katoh, S. Nakamura, H. Harada, Y. Hatsukawa, N. Shinohara, K. Hata, K. Kobayashi, S. Motoishi, M. Tanase, J. Nucl. Sci. Tech., 34 (1997), pp. 431-438.

[8] T. Katoh, S. Nakamura, H. Harada, Y. Hatsukawa, N. Shinohara, K. Hata, K. Kobayashi, S. Motoishi, J. Nucl. Sci. Tech., 36 (1999), pp. 635-640.

[9] S. Nakamura, H. Harada, T. Katoh, J. Nucl. Sci. Tech., 36 (1999), pp. 847-854.

[10] C.H. Westcott, W.H. Walker, T.K. Alexander, in Proceedings of 2nd International Conference on Peaceful Uses of Atomic Energy, Geneva, Vol. 16, p. 70 (1958).

[11] D.C. Stupegia, J. Nucl. Energy, Part A: Reactor Science, 1960, pp. 16-20.

[12] G. Zeisel, Acta Physica Austriaca, 23, (1966), pp. 66.

[13] M. Lucas, R. Hagemann, R. Naudet, C. Renson, C. Chevalier, IAEA-TC-199/14 (1977), pp. 407-432.

[14] T.A. Eastwood, A.P. Baerg, C. B. Bigham, F. Brown, M.J. Cabell, W.E. Grummitt, J.C. Roy, L.P. Roy, R.P. Schuman, in Proceedings of the International Conference on the Peaceful Uses of Atomic Energy, (United Nations: Geneva, 1958), 54-63.

[15] L. Friedmann, D.C. Aumann, Radiochimica Acta, 33 (1983), pp. 183-187.

[16] A.P. Baerg, F. Brown, M. Lounsbury, Can. J. Phys., 36 (1958), pp. 863-870.

[17] J.G. Bayly, F. Brown, G.R. Hall, A.J. Walter, J. Inorg. Nucl. Chem., 5 (1958), pp. 259-263.

[18] A.P. Baerg, R.M. Bartholomew, R.H. Betts, Can. J. Chem., 38 (1960), pp. 2147-2531.

[19] *Neutron Cross-section*, BNL-325 and Suppl. 1, (1955 and 1957).

[20] N.J. Pattenden, in Proceedings of 2nd International Conference on Peaceful Uses of Atomic Energy, Geneva, Vol. 16, p. 44 (1958).

[21] V.V. Ovechkin *et al.*, in Proceedings of Conference on Neutron Physics, Kiev (1973), Vol. 2, p. 131.

[22] R.B. Firestone, V.S. Shirley (Eds.), *Table of Isotopes*, (8th ed.), John Wiley & Sons, New York (1996).

[23] K. Furutaka, S. Nakamura, H. Harada, T. Katoh, J. Nucl. Sci. Tech., 37 (2000), pp. 832-839.

NEW DATA AND MONTE CARLO SIMULATIONS ON SPALLATION REACTIONS RELEVANT FOR THE DESIGN OF ADS

J. Benlliure
Universidad de Santiago de Compostela
15706 Santiago de Compostela, Spain

Abstract

The main European experimental programs to characterise spallation reactions used as neutron sources are reviewed. The neutron production is described in terms of the multiplicities, spatial and energy distributions. Experiments to determine the residual nuclei production in the spallation target are also discussed. These data are used to benchmark existing nuclear model calculations.

1. Introduction

Nowadays it is well established that spallation reactions constitute an optimum neutron source to feed a sub-critical reactor in an accelerator driven system (ADS). However, the present knowledge about this reaction mechanism is not accurate enough for any technical application. Two main aspects will play a major role in the design and construction of the target assembly of the spallation neutron source used in an ADS: the neutron yields and the residual nuclei produced in the reaction.

The neutron production should be characterised in terms of the neutron multiplicity and their spatial and energy distributions. The neutron multiplicity will determine the intensity of the proton-driver accelerator while their energy and spatial distribution should be considered to design the geometry of the spallation target and the shielding to high-energy neutrons.

Spallation reactions do not only produce neutrons but also residual nuclei. Most of these nuclei are radioactive, therefore, activation problems should be considered in the design of the target. In Figure 1 we report an example of the simulated activity induced in a cylindrical lead target by a 1 mA proton beam. As it is showed in the figure, both the cooling time and the total activity induced in the target are not negligible. In addition the residual nuclei will contribute to the corrosion of the target and to the radiation damages in the target, accelerator window and structural materials.

Figure 1. **Calculated radioactivity induced in a cylindrical lead target (120 cm long and 46 cm diameter), by a 1 GeV proton beam of 1 mA after one year of irradiation. Calculations done with the Lahet Code system by D. Ridikas [1].**

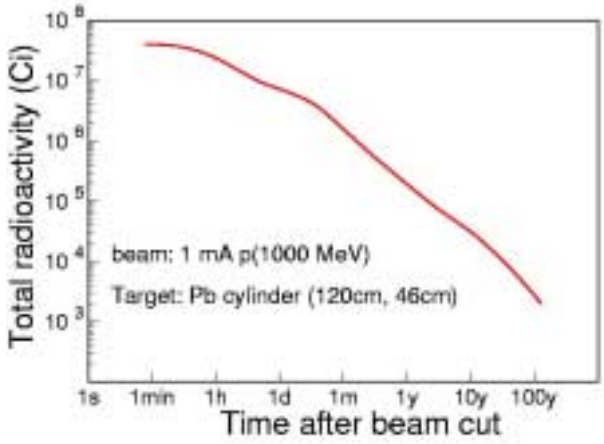

Although spallation reactions are understood qualitatively, they are not known with the degree of accuracy needed for any technical application. In this sense, most of the existing codes used to describe these reactions have a limited predictive power. Therefore a large experimental program has been initiated in Europe few years ago in order to improve our knowledge on these reactions. These experiments will provide accurate data to benchmark more reliable model calculations. In the following sections we will describe some of these experiments.

2. General considerations on spallation reactions

Spallation reactions are collisions induced by light-energetic projectile on a heavy-ion target. These reactions can be described as a two-stage process. First the incoming projectile induces quasi-free nucleon-nucleon collisions with the nucleons of the target nucleus. These collisions lead to the prompt emission of few neutrons and protons. A fraction of the kinetic energy of the incoming projectile will be transferred to the target nucleus as excitation energy, e.g. a 1 GeV proton deposits on average 200 MeV in the target nucleus. The rest of the energy will be shared between the prompt emitted nucleons. This emission of fast nucleons will play an important role in the development of an inter-nuclear cascade process inside the target.

In a second step the residual nuclei produced in the collisions will de-excite by evaporation of low energy protons and neutrons or fissioning. In principle, neutron evaporation is favoured since to evaporate protons or to fission the system needs extra energy to overcome the Coulomb barrier. The energy of the evaporated nucleons is determined mainly by the temperature reached by the residual nucleus in the collisions and will be in the range of a few MeV.

To describe the full interaction of a relativistic projectile with a target material we should consider that the most probable interaction of this projectile with the target material will be governed by electromagnetic processes. The main consequence of the electromagnetic interaction of the projectile with the electrons of the target material will be the slow down of the projectile and heat load of the target.

Figure 2. **Range of protons in lead as a function of their energy**

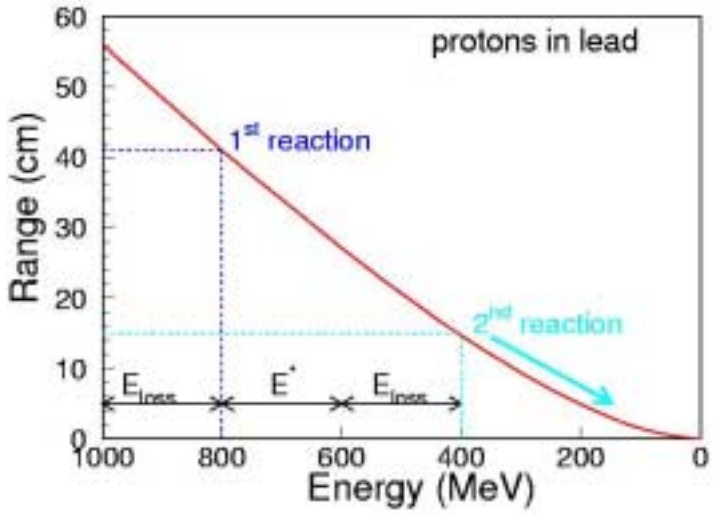

The nuclear interaction between the projectile and the target is determined by the total reaction cross-section. In the case of the reaction proton on lead at 1 GeV the reaction cross-section corresponds to a mean free path of protons on lead around 15 cm. In contrast, the mean free path for electromagnetic interaction is much shorter, consequently the incoming projectile will be slowed down before any nuclear interaction. The electromagnetic interaction can be characterised in terms of the range of the incoming particle in the traversed medium. In Figure 2 we represent the range of protons in lead as a function of their energy. As can be seen the range of a proton with 1 GeV in lead is around 55 cm.

In order to describe the inter-nuclear cascade inside the target we should estimate the energy balance in the interaction of the projectile with the target. If we consider that on average the nuclear interactions take place at 15 cm, the mean energy loss of the incoming projectile before the reaction will be 200 MeV. In addition the energy dissipated in the first spallation reaction is around 200 MeV. This excitation energy leads to a large population of different residual nuclei. The remaining kinetic energy ≈ 600 MeV will be shared between the four or five prompt nucleons emitted during the first stage of the reaction. These nucleons will lead to secondary reactions in the target (inter-nuclear cascade).

The maximum energy of the prompt emitted nucleons is expected to be lower than 300 MeV. According to Figure 2, at this energy the range of protons in lead is few centimetres, therefore most of the secondary protons will be stopped before they induced any secondary reactions. The inter-nuclear cascade will be then induced mainly by neutrons with energies lower than 300 MeV. At this energy the spallation reaction is less violent and only few nucleons will be produced with an energy range lower than 100 MeV. Consequently the final reaction residues will be very close in mass and atomic number to the target nucleus.

In summary we can conclude that an incoming proton at 1 GeV on a lead target will induce on average two spallation reactions. The first one at high energy will determine mostly the residual nuclei produced in the target. The second reaction at lower energy will contribute to the multiplication and moderation of the neutrons.

3. Neutron production in spallation reactions

The neutron yield produced in spallation reactions will depend strongly on the projectile-target combination. In principle the heavier the target nucleus the larger the neutron excess leading to a larger neutron yield. Nevertheless the gain factor between heavy and light targets is not larger than a factor of five. In contrast, the radiotoxicity induced in the spallation target can be drastically reduced when using lighter targets as discussed in [2].

In addition to the neutron yields, reliable information on the energy and spatial distributions of the neutrons is required. This information can be used in the design of the spallation-target assembly geometry or the shielding to high-energy neutrons.

Neutron detection is not an easy task since neutrons only feel the strong interaction. This is the reason why different experimental devices are needed to characterise the neutron production in spallation reactions. In the following we will consider two examples.

3.1. Measurement of neutron yields

Neutron multiplicities can be investigated using liquid-scintillator based detectors with a large angular acceptance. A clear example is the detectors BNB (Berlin Neutron Ball) [3] and ORION [4] used by the NESSI collaboration (Berlin-Ganil-Jülich). This collaboration has performed a large experimental program to determine the neutron yields produced in thin and thick targets for a large range of primary projectiles and energies. To fulfil this programme experiments were done at GANIL (France) [4], Jülich (Germany) [3] and CERN (Switzerland) [5].

Figure 3. **Average neutron multiplicity per incident proton as a function of target thickness and beam energy for Pb, Hg and W materials obtained by the NESSI collaboration [3]**

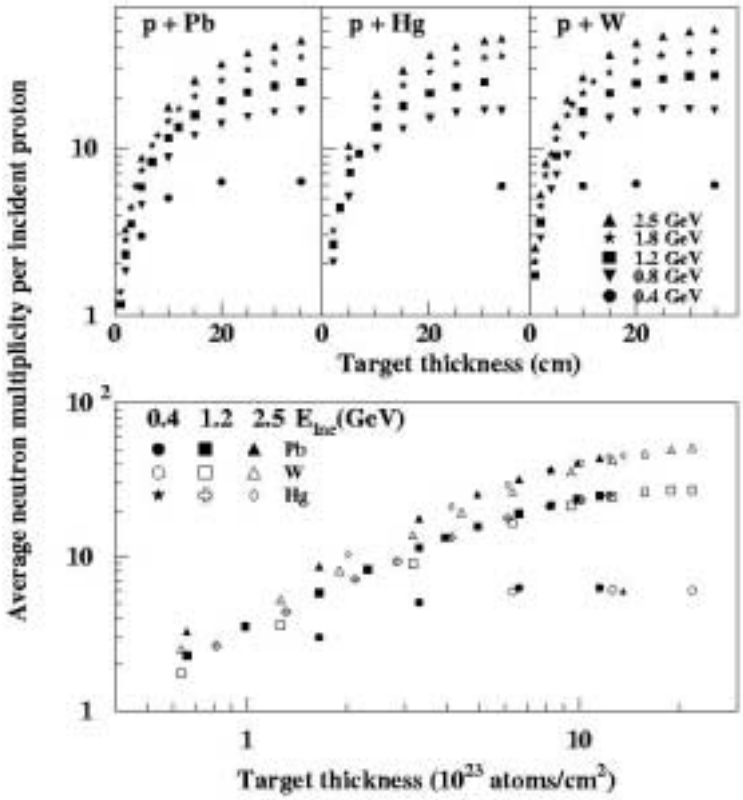

Figure 3 shows some representative results obtained by this collaboration at Jülich with the BNB detector. This figure represents the measured average neutron multiplicity per incident proton as a function of target thickness and beam energy for Pb, Hg and W materials. As can be seen, for the different target materials, the neutron multiplicity saturates at a given target thickness which increase with the proton energy. This saturation corresponds to the previous picture where every incident proton originates on average two collisions with a mean free path of 15 cm.

3.2. Energy and spatial distribution of neutrons

Specific experimental set-ups are needed to measure the spatial and energy distribution of the neutrons produced in spallation reactions. A clear example is the experiments performed by the "transmutation" collaboration at Saturne (France). These measurements use two different experimental techniques to cover the full energy range of the neutrons produced in the reaction. The detection of neutrons with energies lower than 400 MeV was based in a measurement of their time of flight between the incident proton beam, tagged by a plastic scintillator, and a neutron-sensitive liquid scintillator [6]. Neutrons with higher energies were measured using (n,p) scattering on a liquid hydrogen converter and reconstruction of the proton trajectory in a magnetic spectrometer [7]. An additional collimation system allowed determining the angular distribution of the neutrons.

This experimental technique was used to investigate the neutron production in reactions induced by protons with energies between 0.8 and 1.6 GeV on thin and thick lead targets. In Figure 4 we report some of the results obtained with a 1.2 GeV proton beam on a two centimetres thick lead target. This

kind of measurements allow to characterise the spallation process. High energy neutrons emitted at low angles are representative of the first stage of the collision while low energy neutrons emitted isotropically correspond to the evaporation phase. Measurements done with thicker targets are representative of the inter-nuclear cascade leading to the multiplication and moderation of neutrons.

Figure 4. **Neutron production double-differential cross-sections measured in 1.2 GeV induced reactions on a 2-cm thick Pb target [8]. The histograms represent calculations using the Bertini INC Code [9] while the dotted lines corresponds to calculation done with the Cugnon INC Code [10].**

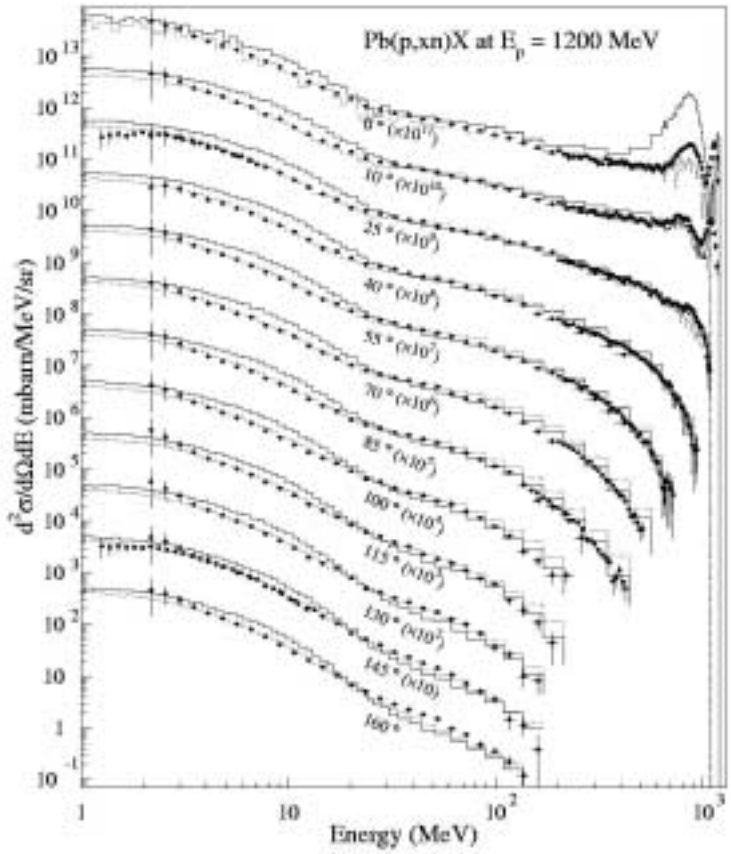

4. Residue production in spallation reactions

Residue production in spallation reactions can be investigated using two different experimental approaches. In the standard one, the reaction is induced in direct kinematics, the light-energetic projectile hits a heavy target. In this case the recoil velocity of the residues produced in the reaction is not sufficient to leave the target and γ-spectroscopy or mass spectrometry techniques are used to identify those residues. The main limitation of this technique is that for most of the residues the measurement is done after β decay and consequently only isobaric identification is possible.

Better suited seems to be the measurement of the spallation residues in inverse kinematics. In this case the heavy nucleus is accelerated at relativistic energies and impinges a light target. Due to the kinematical conditions, the reaction residues leave easily the target and can be identified in a short time using the appropriate technique.

4.1 Measurement of residue production in inverse kinematics

One of the most outstanding experiments are the ones performed by a German-Spanish-French collaboration at GSI. The technique used in these experiments takes advantage of the inverse kinematics and the full identification in mass and atomic number of the reaction residues by using a magnetic spectrometer.

The experiments have been performed at the SIS synchrotron at GSI. Primary beams of ^{197}Au, ^{208}Pb and ^{238}U accelerated up to an energy of 1 A GeV impinged on a liquid hydrogen or deuteron target. The achromatic spectrometer FRS [11] equipped with an energy degrader, two position sensitive scintillators and a multisample ionisation chamber allowed to identify in atomic and mass number all the reactions products with half lives longer than 200 ns and with a resolving power of $A/\Delta A \approx 400$. Figure 5 represents an example of the resolution achieved with this experimental technique. The final production cross-sections are evaluated with an accuracy around 10%. In addition, the magnetic spectrometer allows determining the recoil velocity of the reaction residues. This information is relevant for the characterisation of the damages induced by the radiation in the accelerator window or the structural materials. More details about these experiments can be found in [12-15].

Figure 5. **Example of identification matrix obtained with the Fragment Separator at GSI [13]**

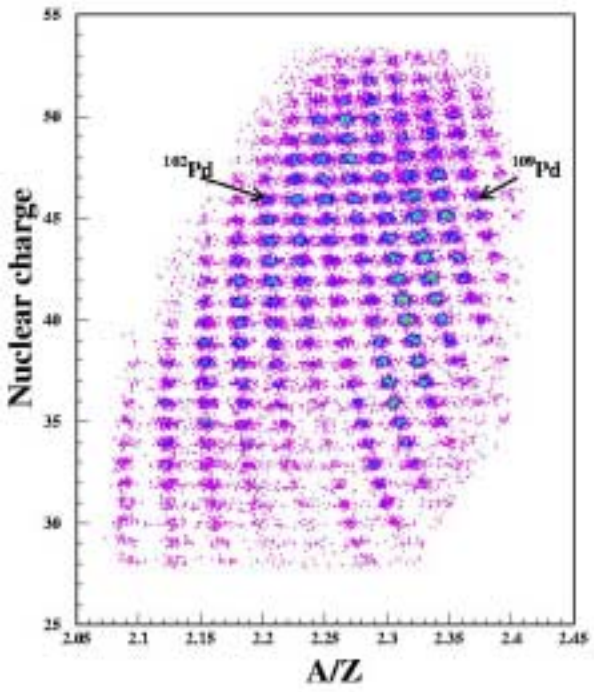

Figure 6. **Two-dimensional cluster plot of the isotopic production cross-sections of all the spallation residues measured at GSI in the reaction ^{208}Pb(1 A GeV) + p shown as chart of nuclides [15]**

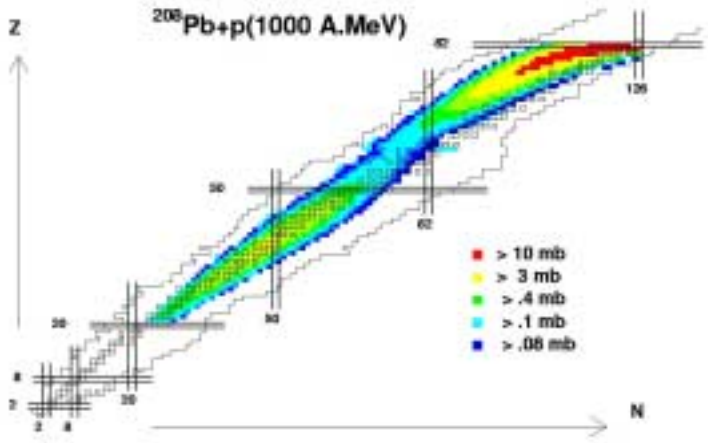

In Figure 6 we present in a chart of the nuclides all the residues measured in the reaction ^{208}Pb(1 A GeV) + p. More than 1 000 different spallation residues were identified in this reaction. As can be seen in this figure, the spallation residues populate two different regions of the chart of the nuclide. The upper region corresponds to the spallation-evaporation residues which populate the so-called evaporation-residue corridor. The second region populates medium-mass residues produced in spallation-fission reactions. Both reactions mechanism, fission and evaporation, should be considered to describe the production of spallation residues in these reactions.

The measured isotopic production cross-sections for some selected elements are presented in Figure 7. This figure shows clearly the quality of the measured data that can be used to benchmark any model calculation.

Figure 7. **Isotopic production cross-sections for some of the elements produced in the reactions ^{208}Pb + p at 1 A GeV [15]. The data are compared with two model calculations, the dark line correspond to the results obtained with the Lahet Code [16] while the hell line was obtained with the intra-nuclear cascade model of Cugnon [10] coupled to the evaporation-fission Code ABLA from GSI [17,18].**

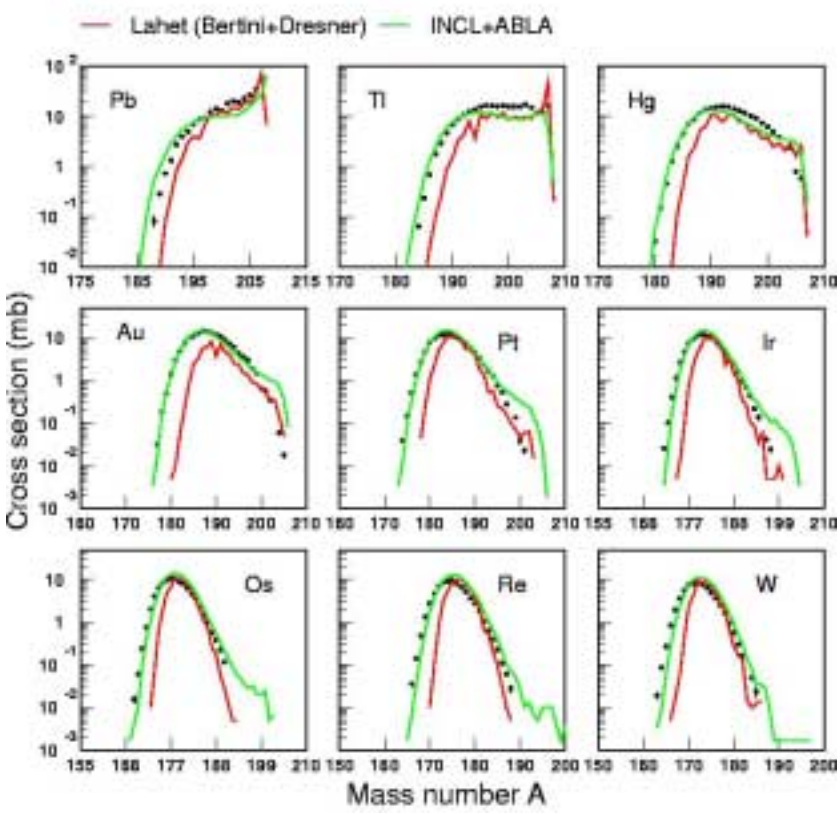

4.2 Measurement of residue production in direct kinematics

Although this method only allows isobaric identification after β-decay, for some shielded isotopes it is possible to determine their primary production cross-sections. In principle this experimental technique is less beam time consuming than the inverse kinematics. Therefore full excitation functions can be established for selected isotopes as shown in Figure 8. In addition this method can be applied to thin and thick targets.

From the results shown in Figure 8 we can conclude that the low energy reactions produced mainly residues close to the target nucleus, while most of the reaction residues populating a large part of the nuclear chart are produced by energetic particles. The two most important experimental programs in Europe using this technique are the ones performed by the group of R. Michel at the University of Hanover [19] and Y.E. Tiratenko at the ITEP in Moscow [20].

Figure 8. **Excitation functions for some selected isotopes produced in the interaction of protons with lead measured with γ-spectroscopy techniques [21]**

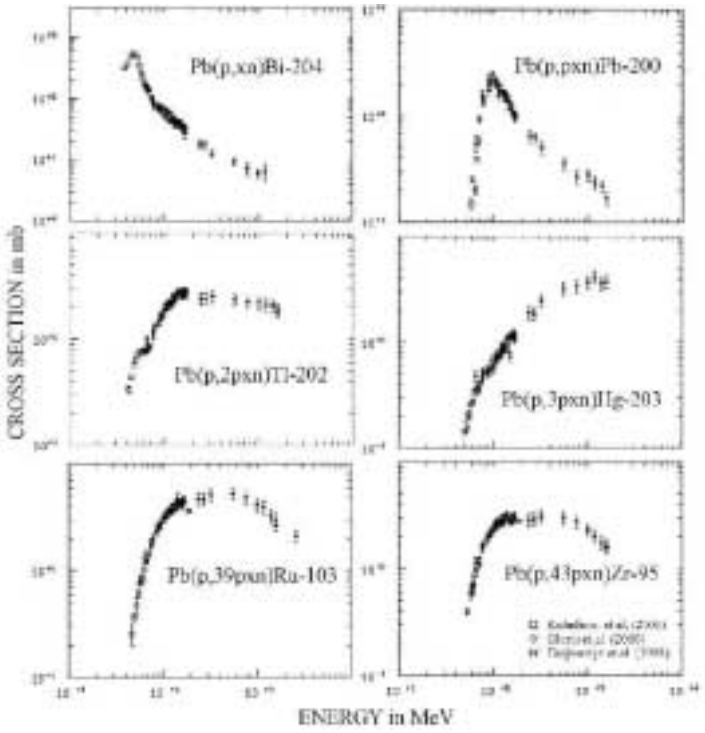

5 Reactions in the 20-200 MeV energy range

Reactions induced by neutrons and light-charged particles in the energy range between 20 and 200 MeV are representative of the inter-nuclear cascade in the spallation target. This reactions will play a major role in the multiplication and moderation of the neutrons. The energy dissipated in these reactions leads to the emission of few particles and consequently only residual nuclei close in mass and atomic number to lead will be produced.

These experiments intend to measure the double-differential production cross-sections of neutrons and light-charged particles. It is out to the scope of this work to review on all the experimental programs investigating these reactions. Most of them contribute to the Hindas project of the Fifth Framework Programme of the European Commission. The experiments take advantage of a large network of European facilities delivering protons and neutrons in the investigated energy range: KVI (Netherlands), Louvain-la-Neuve (Belgium) and Uppsala (Sweden). More detailed information about this program can be found in the contributions of N. Marie, F.R. Lecolley and J.P. Meulders to this conference.

6. Model simulations

Most of the existing models to simulate spallation reactions describe the first stage of the collision in terms of semi-classical nucleon-nucleon collisions (intra-nuclear cascade) and a statistical de-excitation of the hot residue. The main inputs of the intra-nuclear cascade are the elastic and inelastic nucleon-nucleon cross-sections and the distribution of the nucleons in the target nucleus in position and momentum space. The statistical evaporation of particles is generally based in the Weisskopf

formalism while fission can be describe according to the prescription of Bohr. In this case the main parameters are the description of the level density and the Coulomb barriers for charged-particles emission or fission. Another critical parameter is the coupling time between the intra-nuclear cascade and the evaporation.

The last model intercomparison done by NEA [22] revealed important deficiencies in most of the existing codes to describe spallation reactions. In fact these deficiencies can be understood due to the lack of experimental information. The new data provided by the present experimental programs will help to improve this situation. In Figure 7 we compare the measured isotopic production cross-sections for some of the elements produced in the reactions ^{208}Pb + p at 1 A GeV at GSI [15] with two model calculations. In this figure, the dark line correspond to the results obtained with the Lahet Code (Bertini + Dresner) [16] while the hell line was obtained with the intra-nuclear cascade model of Cugnon [10] coupled to a new the evaporation-fission Code ABLA from GSI [17,18]. As can be seen, the new models provide a much better description of the experimental data.

7. Conclusions

Spallation reactions are considered as an optimum neutron source to feed an ADS. However this reactions are not known with the degree of accuracy needed for the design of such devices. This is the main justification for a large experimental program initiated in Europe few years ago to collect high quality data about neutron and residual nuclei production in these reactions. This experimental program takes advantage of most of the existing heavy-ion facilities in Europe in order to cover the full energy range involved in the interaction of light-energetic projectiles with heavy-ion targets. Most of these programs are supported by different programs of the European Commission like Hindas or the European Spallation Source (ESS).

REFERENCES

[1] D. Ridikas, thesis, University of Caen, 1999.

[2] D. Ridikas and W. Mittig, Nucl. Instr. and Methods A 414 (1998) 449.

[3] A. Letourneau *et al.*, Nucl. Instr. and Methods B 170 (2000) 299.

[4] B. Lott *et al.*, Nucl. Instr. and Methods A 414 (1998) 117.

[5] D. Hilscher *et al.*, Nucl. Instr. and Methods A 414 (1998) 100.

[6] F. Borne *et al.*, Nucl. Instr. and Methods A 385 (1997) 339.

[7] E. Martinez *et al.*, Nucl. Instr. and Methods A 385 (1997) 345.

[8] X. Ledoux *et al.*, Phys. Rev. Lett. 82 (1999) 4412.

[9] H.W. Bertini *et al.*, Phys. Rev. 131 (1963) 1801.

[10] J. Cugnon *et al.*, Nucl. Phys. A 620 (1997) 475.

[11] H. Geissel *et al.*, Nucl. Instr. Methods B 70 (1992) 286.

[12] W. Wlazlo *et al.*, Phys. Rev. Lett. 84 (2000) 5736.

[13] J. Benlliure *et al.*, Nucl. Phys. A, in print.

[14] F. Farget *et al.*, Nucl. Phys. A, in print.

[15] T. Enqvist *et al.*, Nucl. Phys. A, in print.

[16] R.E. Prael *et al.*, Los Alamos National Laboratory, Report LA-UR-89-3014.

[17] A.R. Junghans *et al.*, Nucl. Phys. A 629 (1998) 635.

[18] J. Benlliure *et al.*, Nucl. Phys. A 628 (1998) 458.

[19] R. Michel *et al.*, Nucl. Instr. and Methods B 129 (1997) 153.

[20] Y.E. Titarenko *et al.*, Nucl. Instr. and Methods A 414 (1998) 73.

[21] M. Gloris *et al.*, Nucl. Instr. and Methods B (2000), in print.

[22] R. Michel, P. Nagel, *International Codes and Model Intercomparison for Intermediate Energy Activation Yields*, NSC/DOC(97)-1, NEA/P&T No. 14.

THE MUSE EXPERIMENTS FOR SUB-CRITICAL NEUTRONICS VALIDATION AND PROPOSAL FOR A COMPUTER BENCHMARK ON SIMULATION OF MASURCA CRITICAL AND SUB-CRITICAL EXPERIMENTS

R. Soule
CEA-Cadarache, DRN/DER/SPEx
Building 238, 13108 Saint-Paul-Lez-Durance, France

E. Gonzalez-Romero
CIEMAT, FACET Project
Av. Complutense 22, 28040 Madrid, Spain

On behalf of the MUSE collaboration

Abstract

Accelerator driven systems (ADS) are being explored in France in the frame of the research programme on radioactive waste management options. Besides studies aimed to clarify the motivations for ADS, a significant programme has been started to validate experimentally the main physics principles of these systems. This experimental programme was initiated at CEA-Cadarache in 1995, with the sponsorship of EdF and Framatome. Since 1997, the CNRS has joined the programme, which is now a common CEA-CNRS-EdF-Framatome programme, open to external partners, in particular since October 2000 the European Community in the frame of the 5th FW Programme.

1. Introduction

Since 1991, the Commissariat à l'Énergie Atomique (CEA) MASURCA (MAquette SURgénératrice de CAdarache) has studied the physics of hybrid systems, involving a sub-critical reactor coupled with an accelerator.

These studies are being explored in France in the frame of the research programme on radioactive waste management options.

The potential of this kind of systems is to be found in:

- The concentration of waste in a limited number of dedicated facilities.
- The sub-criticality of such a system, which is a particularly attractive argument in favour of the safety of such concepts and which, more particularly, allows for the introduction of new fuels.

Besides studies aimed to clarify the motivations for ADS, a significant programme has been started to validate experimentally the main principles of these systems, in terms of the physical understanding of the different phenomena involved and their modelling, as well as in terms of experimental validation of coupled systems, sub-critical environment/accelerator.

This validation must be achieved through mock-up studies of the sub-critical environments coupled to a well-known source of external neutrons which represents the spallation source. The experimental investigations on the physics of sub-critical external source-driven systems are performed at the CEA Cadarache MASURCA facility, in the frame of the MUSE (MUltiplication of an external Source Experiments) programme.

2. Neutronic validation of source-driven sub-critical systems

2.1 Principles

Neutronic studies of fast critical systems have been largely performed in the past and the associated calculations tools (including both recommended nuclear data and calculation tools) and bias factors developed for the predictions of such systems have been mainly based on integral experiments in critical facilities. Validated experimental techniques have also been developed, directly applied to power critical operating systems.

In order to validate the physics characteristics of a source-driven sub-critical multiplying system, the main original idea has been to separate the experimental validation of the sub-critical multiplication phenomena of the external neutron source, from the validation of the external source characteristics. This can be done using a well-known (in energy spectrum and geometrical position) external source to drive the multiplying sub-critical core.

The neutron source (e.g. a spontaneous fission source or a fixed energy neutron generator), can be surrounded by a "buffer" medium, simulating the diffusing properties of a spallation source. The leakage neutrons through the "buffer" zone are then used as an external source but with a modified energy spectrum. The source neutrons, after having travelled approximately one mean-free path in the multiplying medium, become distributed, in energy and space, as the neutrons generated by fission in the multiplying medium.

The experimental programmes allow to validate both nuclear data and calculation methods used to describe the sub-critical core, in terms of sub-critical reactivity level, spatial flux distributions, neutron spectra, spectrum indexes and source neutron worth (the φ* parameter) [1]. If the source can be used in continuous and pulsed modes, static and dynamic reactivity measurements are possible. This point is of relevance, since the experimental investigation of the different techniques to monitor the sub-criticality level during operation of an ADS is still an open question.

2.2 The MUSE experiments

This validation experimental programme was started at CEA (with the sponsorship of EdF and Framatome) in 1995 with the short exploratory MUSE-1 experiment [1], providing some insight into the physical behaviour of the neutron population in the sub-critical system. The MUSE-2 experiment [2], (2 months in 1996) was devoted to the experimental study of diffusing materials (sodium and stainless steel) placed around the external source to modify the neutron importance of the external source.

Since 1997, the French Scientific Research Committee (the CNRS) has joined this programme, which is now a common CEA-CNRS-EdF-Framatome programme in the frame of the joint research programme GEDEON (Waste management with innovative options programme).

In 1998, during three months the MUSE-3 experiments have been performed [3]. The external neutron source of about 1.0 E+08 n/s was produced by a commercial neutron generator based on the (d,t) reaction. This neutron generator operating in both continuous and pulsed modes allowed to complete the study of diffusing materials (sodium and pure lead) and to explore the dynamic behaviour of the multiplying medium for different sub-criticality levels (≈-0.16, -1.6, -3.2, -4.7 $ respectively). The expected dependence of monitors responses in function of the sub-criticality has been observed.

The MUSE programme is entered a new phase starting in 2000.

First of all, the installation at MASURCA of a ad-hoc deuton accelerator (the GENEPI), especially developed and built at the CNRS/IN2P3/ISN Grenoble, with improved performances (in terms of the quality of the neutron pulse and source intensity), and the use of both (d,d) and (d,t) reactions, will enable to explore different neutron spectra, different source worths and their ratios to the fission neutron worth (the φ* parameter). Accurate dynamic measurements based on the pulsed mode operation of the GENEPI will allow new experimental reactivity determination of the sub-critical multiplying media.

Secondly, the MUSE experiments have been opened to the international collaborations via the 5th Framework Programme of the European Community and also via bilateral collaborations between CEA and Argonne National Laboratory (USA) and JAERI (Japan) respectively.

The future MUSE experiments will investigate several sub-critical configurations loaded in the MASURCA facility driven by the GENEPI external neutron sources. The foreseen configurations will have MOX fuel (with ≈25% enrichment in Pu) with sodium, gas or lead coolant. Physical presence of a spallation source will be simulated by surrounding the GENEPI neutron source with a pure lead zone (see Figure 3). Several levels of sub-criticality will be investigated (from -0.2 to -16 $). Foreseen measurements concern the sub-criticality levels by classical Source Multiplication Method but also via dynamic and noise methods, the neutron spatial distributions, the neutron spectra, the effective delayed neutron fraction and the neutron source importance parameter. Extensive cross-comparisons of codes and nuclear data are foreseen.

Experimental reactivity control techniques, related to sub-critical operation, will be developed and inter-compared. *In particular, in the field of reactivity control related to sub-critical operation, development, inter-comparison and improvement of experimental techniques will be performed.* Description of experimental conditions, techniques and associated results with uncertainties will be set up.

Complementary experiments (the SAD experiments) will be performed at Dubna (Russian Federation) in the frame of a sub-contract of the 5th FWP of the European Community, studying different spallation neutron sources (Pb, Pb-Bi, W targets) produced by the 660 MeV protons of the Dubna synchrotron. These experiments will allow the experimental characterisation of the spallation neutrons propagation into materials (target, fuel and structural materials) encountered in ADS.

The analysis of the whole experiments allows to develop a reference calculation route (including both recommended nuclear data, validated calculation tools and associated residual uncertainties) for the design of ADS and for the deep spallation neutrons transport penetration to optimise the neutron shielding, with a special attention to a "forward" direction (behind the target area).

3. The MASURCA facility

The MASURCA facility is dedicated to the neutronic studies of fast reactor lattices. The materials of the core are contained in cylinder rodlets, along with in square platelets. These rodlets or platelets are put into wrapper tubes having a square section (4 inches) and about 3 meters in height. These tubes are hanged vertically from a horizontal plate supported by a structure of concrete. The core itself can reach 6 000 litres. To build such cores the tubes are introduced from the bottom in order to avoid that the fall of a tube corresponds to a positive step in reactivity.

The reactivity control is fulfilled by absorber rods in varying number depending of core types and sizes. The control rods are composed of fuel material in their lower part, so that the homogeneity of the core is kept when the rods are withdrawn. The core is cooled by air and is surrounded by a biological shielding in heavy concrete allowing operation up to a flux level of 10^9 n/cm^2/sec. Core and biological shielding are inside a reduced pressure vessel, relative to the outside environment. The limited maximum operating power of the facility is limited to 5 kW_{th}.

4. The GENEPI accelerator

The GENEPI (GÉnérateur de NEutrons Pulsé Intense) accelerator has been especially formed for the MUSE experiments in the MASURCA facility for brief neutron injections with a very fast intensity decrease.

It will produce a pulsed neutron beam of about 1 μs during a maximum relative time of $5 . 10^{-3}$ s, that is a maximum frequency of about 5 000 Hz.

In this way, deuton impulses are created, then focalised, accelerated and guided to a deuterium or tritium target. The (D,D) or (D,T) nuclear reactions produce neutrons of about 2.67 MeV or 14.1 MeV respectively. For incident deutons of about 250 keV, the neutron yield is greater for the (D,T) reaction than for the (D,D) reaction.

This accelerator is a classical electrostatic one with a lower mean neutrons production than the same type of accelerators. The main originality of GENEPI concerns its operating mode based on high ions peak current (50 mA) and a decreasing time of the neutron impulse of some 100 μs.

The GENEPI accelerator is mainly composed of:

- A deuton source.
- The extraction and focusing electrodes.
- The 250 keV electrostatic accelerator.
- The mass separator.
- The deuterium or tritium target , as indicated in the Figure 1.

The main characteristics of the ion beam are indicated in the Table 1.

Table 1. **Deuton beam characteristics**

Beam energy	140 to 240 keV
Peak current	50 mA
Repetition rate	10 to 5000 Hz
Minimum pulse duration	700 nanoseconds
Mean beam current	(200 μA (for a duty cycle of 5 000 Hz)
Spot size	Diameter ≈20 mm
Pulses reproducibility	Fluctuations at the 1% level

The characterisation of the neutron production by both deuterium and tritium targets has been performed by the ISN Grenoble team. The characterisation of the neutron source intensity is based on the activation of a Si detector by:

- The recoiled protons produced by the (d,d) reaction on the deuterium target and in the magnet chamber due to deuterium implantation.
- The recoiled protons and alpha particles produced by the (d,t) reaction on the tritium target.

This alpha monitoring gives a neutron pulse shape very similar to this obtained by ionic current as indicated in Figure 2.

The characterisation of the neutron production spectrum is based on the activation analysis of ^{58}Ni foils. For the 2.67 MeV neutrons produced by the D(d,n)^{3}He reaction, the ^{58}Ni(n,p)^{58}Co is used. The 14 MeV neutrons spectrum produced by the T(d,n)^{4}He reaction is determined by both the ^{58}Ni(n,2n)^{57}Ni and ^{58}Ni(n,np)^{57}Co reactions representative of the neutrons with an energy higher than 13 MeV. For a natural Ni target of 20 mm diameter (corresponding to a mass of about 580 mg) irradiated during 14 hours at 2 000 Hz with a pulse width of 700 nanoseconds FWHM, the neutrons/pulse intensities, indicated in the Table 2 have been measured.

Table 2. **Neutron intensities**

Target characteristics*	Nuclear reaction	Neutrons/pulse
D in 1mg/cm^2 Ti deposit (Φ 30mm)	D(d,n)^{3}He	4.0 E+04
T (1Ci) in 0.25 mg/cm^2 Ti deposit (Φ 25mm)	D(t,n)^{4}He	1.7 E+06**
T (10 Ci) target	idem	Expected: 3.0 to 9.0 E+06

*D/Ti or T/Ti atomic ratio is close to 1.5.
**Measurement done after a 50% decrease of the tritium content of the target.

An accurate monitoring of the external neutron source in term of intensity and pulse form is of prime importance for a good and accurate understanding of the dynamic measurements. The target beam current, the proton and alpha + proton spectroscopy signals and the alpha + protons time distribution referenced to the neutron source pulse will be available for the physicists during the future MUSE experimental campaigns.

5. The MUSE-4 experiments

As the MUSE experiments are based on a parametric approach, the MUSE-4 configurations are based on the ZONA2 fuel cell (see Figure 2), representative of a Pu fast burner core (Pu enrichment of ≈25% with ≈18% content of ^{240}Pu) with sodium coolant. The fuel zone is radially and axially reflected by a stainless steel/sodium (75/25) shielding. The GENEPI deuteron guide is horizontally introduced at the core mid-plane and the deuterium or tritium target is located at the core centre (see Figure 3). To compensate the spatial effect due to the presence of the GENEPI beam guide in the north part of the loading, the south symmetric part will be loaded with pure lead. To simulate the physical presence of a spallation source, a pure square (20 cm thick) lead zone will be introduced around the GENEPI target (see Figure 3).

Six different experimental configurations will be studied:

- A critical one, the GENEPI being shut off, in which all the safety and neutron flux level and spectrum measurements will be performed. In this configuration the reactivity scale will be experimentally determined by classical pilot rod shutdown measurement.
- Three sub-critical configurations (k_{eff} being successively of about 0.994: the SC1 configuration, 0.97: the SC2 configuration and 0.95: the SC3 configuration). These three configurations will be obtained by replacing radially some peripheral fuel cells by stainless steel/sodium cells. The west/east symmetry along the beam guide axis will be preserved.
- Two complementary asymmetrical sub-critical configurations, with k_{eff} of about 0.95 and 0.93, obtained from the reference critical one and from the above SC1 sub-critical respectively, by complete insertion of the same safety rod. These two last configurations will be of interest in the frame of studying the decoupling effects and the excitation of high order flux harmonics by the external source.

A very extensive experimental programme has been planned for one year, including the active participation of the different partners as indicated in the Table 3. In support to the transmutation studies of minor actinides, fission rates of ^{232}Th, ^{233}U, ^{237}Np, ^{240}Pu, ^{241}Pu, ^{242}Pu, ^{241}Am, ^{243}Am and ^{244}Cm will be measured using fission chambers. Transmutation of some long-lived fission products will be

also experimentally determined using activation foils such as ^{197}Au, ^{115}In, ^{160}Dy, natural Mn, representative of the LLFP's of interest in term of capture cross-sections.

6. Benchmark on computer simulation of MASURCA critical and sub-critical experiments

The study of the neutronic of accelerator driven systems, in which an intense external neutron source maintains a stationary power level, requires the extension and validation of appropriated computational tools to solve steady-state and time–dependent problems, from the standard codes and nuclear data libraries developed for critical reactors. The MASURCA nuclear assembly used in the MUSE experiment, that has been and will be configured as a critical and sub-critical reactor, offers a unique opportunity for test and validation of the available and new computational tools. For these purposes we propose to organise in collaboration with the OCDE Nuclear Energy Agency a benchmark on computer simulation of MASURCA critical and sub-critical experiments particularly concentrated on the MUSE-4 experiments. The fact that the results can be compared with already available experimental data and data to be obtained in very short time will allow to go beyond the simple observation of the coincidence and discrepancy between codes or nuclear data libraries.

The benchmark model would be oriented to compare simulation predictions based on available codes and nuclear data libraries between themselves and with experimental data related to: TRU transmutation, criticality constants and space and time evolution of the neutronic flux following source variation, in the framework of liquid metal fast sub-critical systems.

The benchmark could be divided in three steps:

- First step will allow understanding the simulation methods of the different groups and tuning of the simulations programmes with the experimental data of one already measured critical configuration (COSMO).
- In the second step, the MUSE-4 reference configuration is proposed for simulation of the different reactor parameters (criticality constant, flux distribution...) in a nearly critical configuration, critical-2$.
- The third step is oriented to the simulation of reactor time response to the external source in the sub-critical reference configuration.

To allow the use of the widest range of simulation codes to participate in the benchmark the geometry and material compositions will be described in detail but homogenised at the tube level. The errors introduced by the homogenisation approximation have been checked by the MUSE collaboration, and they are very small, typically from less than 0.1% in k_{eff} to a maximum of 8% in the absolute flux at the worst tube (k_{eff} = 0.995). Detailed figures and tables will clarify this geometrical description of the MASURCA configurations and of the reference points for requested calculations. Special attention will be paid to insure that most of the requested calculations can be compared with directly measurable parameters.

In the case of the COSMO critical MASURCA configuration the requested calculations will include: the criticality constant, k_{eff}, ^{235}U fission rate as a function of the position at the available experimental channels (horizontal and vertical); spectral index from the reaction rates in the available detectors and activation foils and the energy dependence of the neutron spectrum in a few characteristic positions (to clarify discrepancies between codes).

For the critical-2$ MUSE-4 reference configuration calculations the requested parameters should include: the criticality constant, k_{eff}, ^{235}U fission rate as a function of the position at the available

experimental channels (horizontal and vertical); spectral index from the reaction rates in the available detectors and activation foils and the energy dependence of the neutron spectrum in a few characteristic positions; the ^{235}U fission rate in the available experimental positions as a function of the time after the deuteron-tritium source pulse and the neutron mean lifetime.

Finally for the sub-critical MUSE-4 reference configuration calculations the requested parameters should include: the ^{235}U fission rate as a function of the position at the available experimental channels (horizontal and vertical); spectral index from the reaction rates in the available detectors and activation foils and the energy dependence of the neutron spectrum in a few characteristic positions; the ^{235}U fission rate in the available experimental positions as a function of the time after the deuteron-tritium source pulse; the neutron mean lifetime; the change in neutron multiplication from the critical-2$ to the sub-critical configuration and the difference between k_{eff} and k_{source} for the sub-critical configuration.

The probable situation that some of the calculations will be made before the experiments are performed is the best warranty for making blind simulations and to understand the potentialities and accuracy of the different computational tools.

7. Conclusions

From the year 2000, the MUSE experiments begin an international test stand for the inter-comparison and development of specific experimental techniques and for the validation of a reference calculation route, including recommended nuclear data, validated calculation tools and associated residual uncertainties related to the neutronics specificities of the accelerator driven systems. During the MUSE-4 experiments in year 2001, the coupling between the GENEPI accelerator and a MOX fuel with sodium coolant will be studied. During the two following years, the GENEPI accelerator will be coupled with a MOX fuel with gas coolant representative of Fast Gas Cooled sub-critical system. A small MOX fuel zone with lead coolant will be also investigated.

A first important conclusion of the European collaboration during the definition of the MUSE-4 critical and sub-critical configurations concerns the important discrepancy observed between deterministic code and stochastic codes using *a priori* the same nuclear libraries. The understanding of this discrepancy should be obtained via an international calculation benchmark based, in a first step on very simplified experimental configurations, in terms of geometrical description and material compositions. In a second step, real critical and sub-critical configurations studied during the MUSE-4 experiments will be proposed.

Acknowledgements

The authors wish to thank all the partners of the MUSE collaboration with a special mention for their fruitful participation to Mrs. C.A. Bompas (CEA-Cadarache), Mrs. Billebaud, Messrs Giorni, Loiseaux, Brissot and Wachtarczyk (ISN-Grenoble), Mr. Plaschy (PSI, Villingen), Mr. Villamarin (CIEMAT, Madrid) and Mr. Seltborg (5KTH Stockholm).

REFERENCES

[1] M. Salvatores, M. Martini, I. Slessarev, R. Soule, J.C. Cabrillat, J.P. Chauvin, P. Finck, R. Jacqmin, A. Tchistiakov in *Proceedings of the Second International Conference on Accelerator Driven Transmutation Technologies and Applications*, (ADTTA'96), Kalmar, Sweden, June 3-7, 1996.

[2] R . Soule, M. Salvatores, R. Jacqmin, M. Martini, J.F. Lebrat, P. Bertrand, U. Broccoli, V. Peluso in *Proceedings of the International Conference on Future Nuclear Systems*, (Global'97), Yokohama, Japan, October 5-10, 1997, Vol. 1, pp. 639-645.

[3] J.F. Lebrat, R. Soule, M. Martini, J.P. Chauvin, C.A. Bompas, P. Bertrand, P. Chaussonnet, M. Salvatores, G. Rimpault, A. Giorni, A. Billebaud, R. Brissot, S. David, D. Heuer, J.M. Loiseaux, O. Meplan, H. Nifenecker, J.B. Viano, J.F. Cavaignac, J.P. Longequeue, J. Vergnes, D. Verrier in *Proceedings of the Third International Conference on Accelerator Driven Transmutation Technologies and Applications*, (ADTTA'99), Prague, Czech Republic, June 1999.

Figure 1: Schematic view of the GENEPI-MASURCA coupling

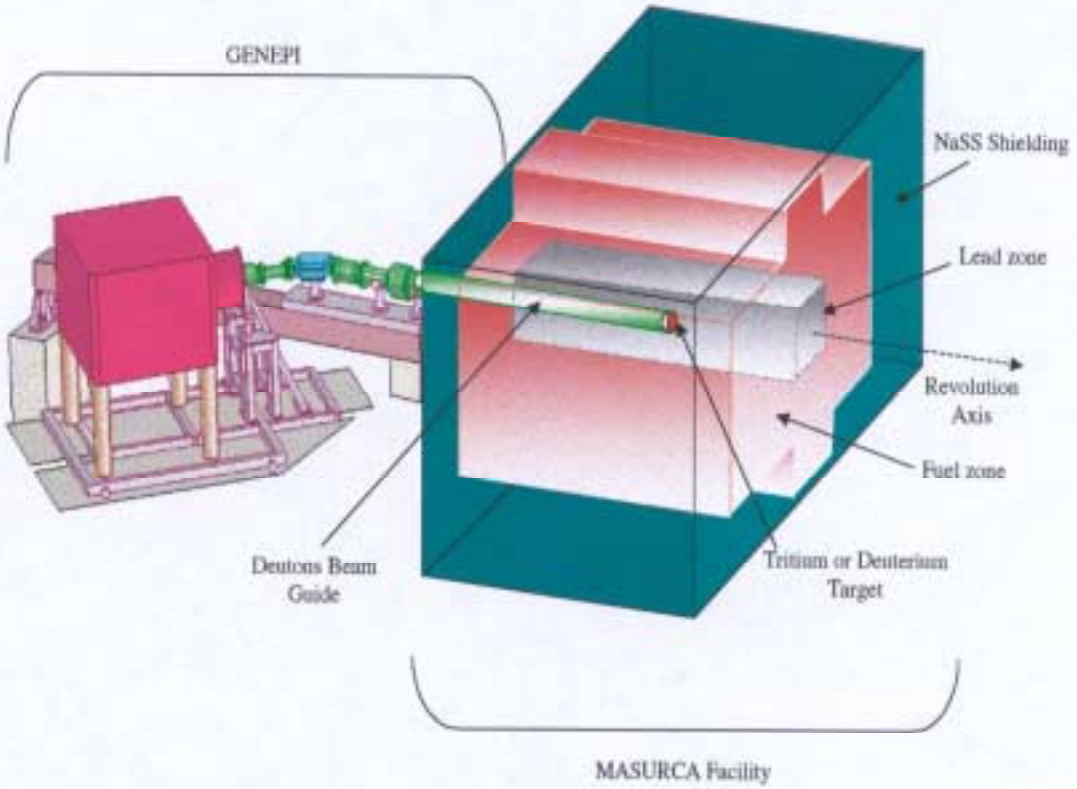

Figure 2: Fuel basic cell for the MUSE-4 experiments

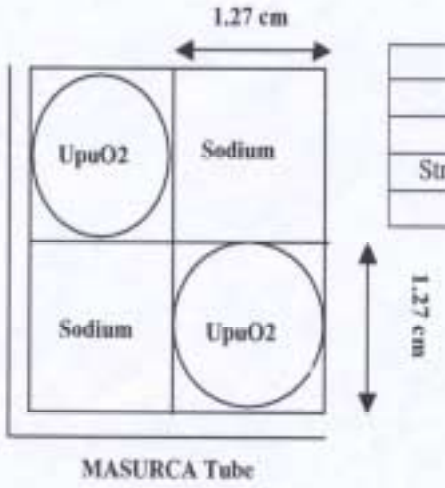

	Volumetric composition %
UpuO2 fuel	≈ 34
Sodium coolant	≈ 43
Structural materials (SS)	≈ 12
Void	≈ 11

Figure 3. **XY loading (at the core mid-plane) of the MUSE-4 reference critical configuration (provisional)**

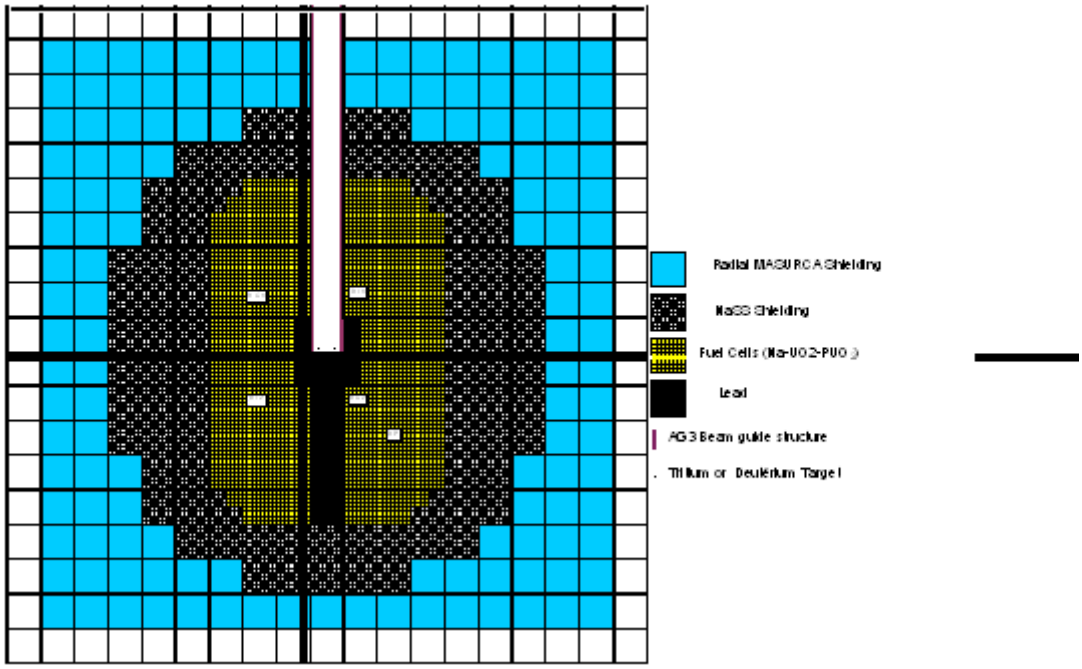

Figure 4. **Neutron pulse time spectrum**

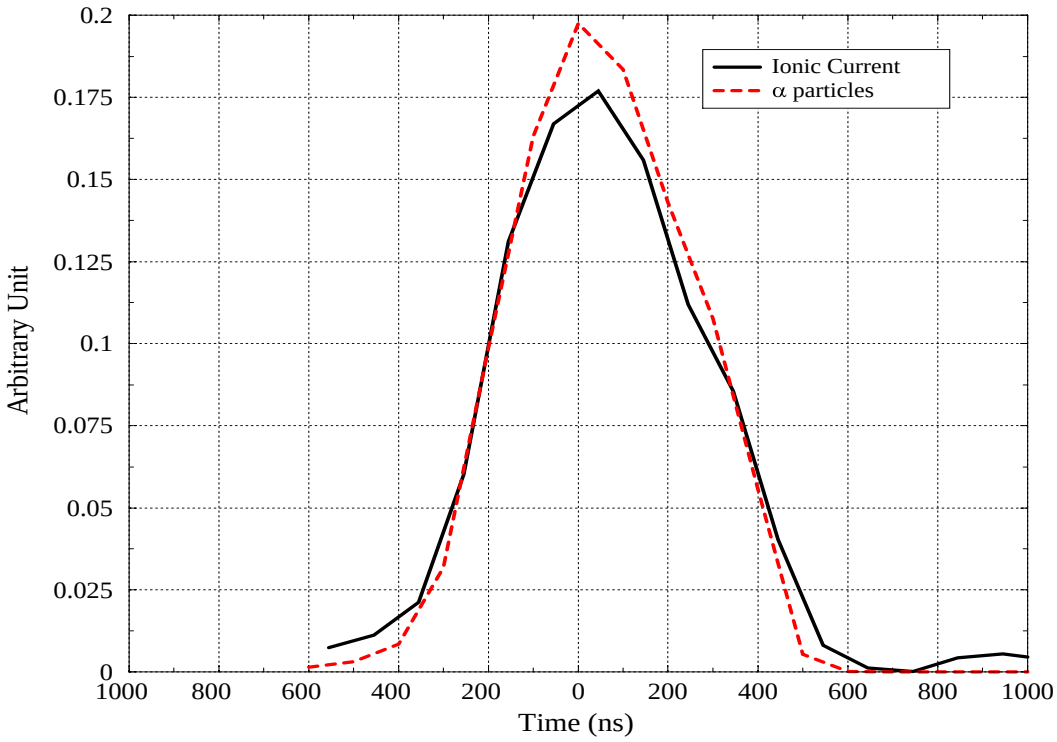

Table 3. **Planned experimental programme during the MUSE-4 experiments**

	REF	SC1					SC2				SC3		SC3	SC2
		OFF		(d,d)	(d,t)		OFF		(d,t)		OFF	(d,t)	(d,d)	(d,d)
		SYM	ASY		SYM	ASY	SYM	ASY	SYM	ASY				
Operating														
Rod worth	**X**	**X**					**X**				**X**			**X**
Monitor calibration	**X**	**X**					**X**				**X**			**X**
Reactor calibration	**X**	**X**					**X**				**X**			**X**
Chamber inter-calibration	**X**													
GENEPI monitoring				**X**	**X**									
Target control study				**X**	**X**				**X**			**X**	**X**	**X**
Statics														
Source multiplication	**X**	**X**					**X**				**X**			
Radial traverses	**X**			**X**	**X**	**X**			**X**	**X**		**X**	**X**	**X**
Axial traverses	**X**			**X**	**X**	**X**			**X**	**X**		**X**	**X**	**X**
Spectrum indices	**X**								**X**					**X**
Foil activation	**X**			**X**	**X**				**X**			**X**	**X**	
^{3}He spectrum				**X**	**X**				**X**			**X**	**X**	**X**
^{252}Cf source importance		**X**	**X**					**X**			**X**			
GENEPI source importance				**X**	**X**	**X**			**X**	**X**		**X**	**X**	**X**
Dynamics														
Reactor noise	**X**	**X**												
Transfer function				**X**	**X**				**X**			**X**	**X**	**X**
Frequency modulation				**X**	**X**				**X**			**X**	**X**	**X**
Pulsed source methods				**X**	**X**	**X**			**X**	**X**		**X**	**X**	**X**
Rossi- & Feyman-α methods	**X**	**X**		**X**	**X**		**X**		**X**		**X**	**X**	**X**	**X**

- For each sub-critical configuration (SC1, SC2 and SC3) the GENEPI will be shut OFF/ON with deuterium target and ON with tritium target.
- SYM configurations correspond to “clean” configurations.
- ASYM configurations correspond to the above “clean” configurations, but with BC2 safety rod completely inserted.

OECD/NEA BENCHMARK CALCULATIONS FOR ACCELERATOR DRIVEN SYSTEMS

M. Cometto
CEA/PSI
5232 Villigen, Switzerland

B.C. Na
OECD/NEA
Le Seine Saint-Germain, 12, blvd des Iles, 92130 Issy-les-Moulineaux, France

P. Wydler
5452 Oberrohrdorf, Switzerland

Abstract

In order to evaluate the performances of the codes and the nuclear data, the Nuclear Science Committee of the OECD/NEA organised in July 1999 a benchmark exercise on a lead-bismuth cooled sub-critical system driven by a beam of 1 GeV protons. The benchmark model is based on the ALMR reference design and is optimised to burn minor actinides using a "double strata" fuel cycle strategy. Seven organisations (ANL, CIEMAT, KAERI, JAERI, PSI/CEA, RIT and SCK•CEN) have contributed to this exercise using different basic data libraries (ENDF/B-VI, JEF-2.2 and JENDL-3.2) and various reactor calculation methods. Significant discrepancies are observed in important neutronic parameters, such as k_{eff}, reactivity swing with burn-up and neutron flux distributions.

1. Introduction and benchmark specification

Recognising a need for code and data validation in the area of accelerator driven systems (ADS), the OECD/NEA Nuclear Science Committee organised in 1994 a benchmark on a sodium cooled sub-critical system with a tungsten target and minor actinide (MA) and plutonium nitride fuel [1]. In that benchmark, considerable differences in calculated initial k_{eff} and burn-up reactivity swing indicated a need for refining the benchmark specification and continuing the exercise with a wider participation [2,3]. The present benchmark was therefore launched in July 1999 to resolve the discrepancies observed in the previous exercise and to check the performances of reactor codes and nuclear data for ADS with unconventional fuel and coolant. The choice of lead-bismuth as a coolant and target material reflects the increased interest in this technology.

The ADS is designed to operate as a MA burner in a "double strata" strategy, featuring a fully closed fuel cycle with a top-up of pure MA. Two fuel compositions are prescribed in accordance with this strategy. In the start-up core, MAs are mixed with plutonium from UOX-fuelled LWRs. In the equilibrium core, the fuel represents an asymptotic composition reached after an indefinite number of cycles. Both fuel compositions differ strongly from the usual U-Pu mixed oxide (MOX) composition. The fuel is diluted with zirconium as an inert matrix for the core to give a k_{eff} of about 0.95 at BOL. Since the emphasis is on code and data validation in the energy region below 20 MeV, a predefined spallation neutron source, produced with HETC assuming a proton energy of 1 GeV and a beam radius of 10 cm, was provided to the participants.

The R-Z benchmark model, shown in Figure 1, comprises four regions: a central lead-bismuth target zone, a void zone in the beam duct region, a multiplying region which consists of homogenised fuel, cladding and lead-bismuth coolant and, finally, an outer reflector zone. The reactor operates at a nominal power of 377 MW_{th} and the core has a residence time of 5 years. To simulate a load factor of 0.85, the power is reduced to 320 MW_{th} in the burn-up calculations. At EOL the fuel reaches an average burn-up of approximately 200 GWd/t_{HM}.

Figure 1. **R-Z model of ADS**

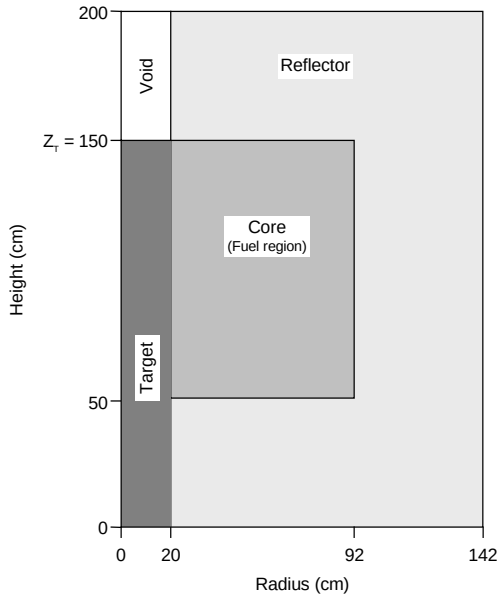

The choice of adopting the ALMR reference system as a basis for the benchmark model has the advantage that a detailed plant concept is available and the characteristics of the plant with normal cores has already been analysed in great detail, including transient and beyond design basis behaviour. The present benchmark model is therefore also suited for transient benchmarks.

As a follow-up to the present benchmark, a transient benchmark dealing with the beam trip problem of the ADS is currently being defined. Preliminary results of the current benchmark exercise were presented in November 1999 at the OECD/NEA Workshop on Utilisation and Reliability of High Power Accelerators in Aix-en-Provence [4].

2. Results and discussion

Seven institutions participated in the benchmark, using nuclear data mainly from ENDF/B-VI, JEF-2.2 and JENDL-3.2. For the core analysis, both deterministic and Monte Carlo methods were applied. The list of participants, basic libraries and codes used are summarised in Table 1.

Table 1. **List of participants, basic data libraries and codes**

Organisation	Basic library	Codes used	Method
ANL (USA)	ENDF/B-VI ENDF/B-V for lumped FP	MC^2-2, TWODANT, REBUS-3	Deterministic
CIEMAT (Spain)	JENDL-3.2 ENDF/B-VI for fission yields	EVOLCODE system (NJOY, MCNP-4B, ORIGEN-2.1)	Monte Carlo
KAERI (Korea)	JEF-2.2 JENDL-3.2 for Pb and ^{242m}Am	TRANSX-2.15, TWODANT, DIF3D-7.0, REBUS-3	Deterministic
JAERI (Japan)	JENDL-3.2	ATRAS (SCALE, TWODANT, BURNER, ORIGEN-2)	Deterministic
PSI/CEA (CH/France)	ERALIB I (JEF-2.2 based)	ERANOS, ORIHET	Deterministic
RIT (Sweden)	JEF-2.2	NJOY, MCNP-4B, MCB, ORIGEN-2	Monte Carlo
SCK•CEN (Belgium)	JEF-2.2 ENDF/B-VI for Pb and ^{233}U	NJOY97.95, MCNP-4B, ORIGEN-2	Monte Carlo

In addition to their reference solution, some participants provided additional results obtained with different methods or basic libraries. In particular, RIT provided neutron flux distributions for the equilibrium core obtained with ENDF data and k_{eff} results for the start-up core based on the JENDL library.

In the following, we summarise the most important results of the benchmark exercise. In particular, we focus on the one-group microscopic cross-sections, the neutron spectrum, the neutron flux distributions, the integral parameters k_{inf} and k_{eff} as well as the k_{eff} variation with the burn-up. Other important parameters such as the external neutron source strength and safety parameters are also discussed.

In the analysis of the results, it is necessary to consider how the participants accounted for the nuclear power in the system. Whereas ANL, CIEMAT, KAERI and PSI/CEA took into account the energy coming from both fissions and captures, JAERI and SCK•CEN considered only the energy coming from fissions and RIT neglected both the energy coming from captures and from delayed

neutrons. Since the neutron flux is normalised to the given reactor power of 377 MW, neglecting the contribution of some reactions to the power leads to an overestimation of the flux. The effect can be estimated to be about 4% for JAERI and SCK•CEN and about 9% for RIT; it therefore has an important influence, especially on the fuel burn-up and on the neutron flux distributions.

The main neutronic characteristics reported by the participants are summarised in Tables 2 and 3. Table 2 refers to the start-up core and Table 3 refers to the equilibrium core.

Table 2. **Main neutronic characteristics of the start-up core**

	Organisation						
Parameters	***ANL***	***CIEMAT***	***JAERI***	***KAERI***	***PSI/CEA***	***RIT***	***SCK•CEN***
Library	ENDF	JENDL	JENDL	JEFF	JEFF	JEFF	JEFF
k_{inf}	1.15894	1.13732	1.15920	1.13256	1.13141	1.149	1.14729
k_{eff} at BOL	0.98554	0.9570	0.9650	0.94546	0.94795	0.9590	0.9590
P/A ratio *	1.307	1.245	1.253	1.226	1.228	1.220	1.241
Source (n/s)-BOL	6.1E17	1.65E18	1.25E18	4.11E18	2.26E18	2.54E18	2.29E18
Source (n/s)-EOL	4.12E18	3.51E18	2.88E18	7.33E18	3.96E18	4.83E18	4.54E18
Neutron's median energy (keV)	210	212	162	222	214	220	220
Coolant void reactivity (pcm) **	3 161 2 433	3 905 3 214	3 813 3 048	3 686 2 596	2 870 1 655	2 904 1 863	2 896 1 681
Fuel Doppler effect (pcm) ***	0 13	38.2 323.7	20.2 31.9	16.5 27.2	6.2 12.4	48 53	11 48.7
β_{eff} at BOL (pcm)	156	246	173.5	–	184.0	195	–

Table 3. **Main neutronic characteristics of the equilibrium core**

	Organisation						
Parameters	***ANL***	***CIEMAT***	***JAERI***	***KAERI***	***PSI/CEA***	***RIT***	***SCK•CEN***
Library	ENDF	JENDL	JENDL	JEFF	JEFF	JEFF	JEFF
k_{inf}	1.14420	1.11629	1.14192	1.13366	1.13165	1.150	1.14884
k_{eff} at BOL	0.96895	0.9370	0.9494	0.94174	0.94374	0.9570	0.95509
P/A ratio *	1.308	1.241	1.258	1.258	1.260	1.245	1.274
Source (n/s)-BOL	1.39E18	2.54E18	1.94E18	4.49E18	2.55E18	2.70E18	2.47E18
Source (n/s)-EOL	3.18E18	2.38E18	2.00e18	5.80E18	2.86E18	3.39E18	2.64E18
Neutron's median energy (keV)	185	188	152	181	179	188	183
Coolant void reactivity (pcm) **	3 318 2 154	4 511 2 582	4 138 2 821	3 902 2 034	2 732 1 925	3 045 1 605	3 144 1 681
Fuel Doppler effect (pcm) ***	20 12	17.1 277.6	30.4 45.8	23.0 43.7	4.2 5.8	45 49	98 103
β_{eff} at BOL (pcm)	116	221	145.2	–	155.9	188	–

* Ratio between production and absorption reaction rates in the heavy metals.

** Calculated as $k_{eff}^{voided} - k_{eff}^{ref}$ for the BOL (first row) and EOL (second row).

*** Calculated as $\left(k_{eff}^{980K} - k_{eff}^{1580K}\right)/\left(k_{eff}^{980K} \cdot k_{eff}^{1580K}\right)$ for the BOL (first row) and EOL (second row).

2.1 One-group microscopic cross-sections and k_{inf}

The one-group microscopic cross-sections provided by ANL, KAERI, PSI/CEA and SCK•CEN are obtained by means of a cell calculation; i.e. the fundamental mode neutron spectrum of the fuel cell is used for averaging the cross-sections. CIEMAT, JAERI and RIT derived one-group microscopic cross-sections from a reactor calculation; the latter cross-sections represent averages over the core fuel zone and, therefore, differ from those obtained from cell calculations. As shown by additional calculations made by PSI/CEA and SCK•CEN, the differences due to the averaging method are between 4.5% and 13% for the one-group capture cross-sections and less than 6% for the one-group fission cross-sections.

The figures at the end of this section show microscopic one-group capture cross-sections of the most relevant isotopes in the equilibrium core. Figure 2 compares cell averaged and Figure 3 compares core averaged one-group cross-sections.

The cross-sections show some correlation with the basic data used: the JENDL-based cross-sections are in good agreement for all the isotopes. Some discrepancies appear between the JEFF-based cross-sections: when comparing the core averaged data, RIT and SCK•CEN give very close results which, however, differ from the PSI/CEA results for the majority of isotopes. When comparing the cell averaged data, the results provided by KAERI, PSI/CEA and SCK•CEN generally differ from one another.

A direct comparison of both cell- and core-averaged cross-sections requires caution. Nevertheless, the following general conclusions can be made: when comparing one-group cross-sections, based on different basic libraries, good agreement can be observed only for uranium isotopes (not presented in the figures). Large discrepancies are observed for plutonium isotopes, particularly for the capture cross-sections. Compared to other libraries, ENDF gives a higher value for ^{238}Pu and lower values for the other isotopes. The values obtained with JEFF and JENDL are closer, except for the isotopes 238 and 241.

Considerable discrepancies between cross-sections based on different libraries are observed also for neptunium, americium and curium. For example, JENDL gives by far the highest capture cross-sections for ^{243}Cm, ^{246}Cm and ^{247}Cm, and ENDF gives significantly lower fission cross-sections for ^{242}Cm, ^{243}Cm and ^{245}Cm (not presented in this paper).

The k_{inf} results (presented in Tables 2 and 3) show quite a spread. The maximum differences are 2.5% for the start-up core and 3.0% for the equilibrium core. Interestingly, no clear correlation with the nuclear data used can be observed. Significant discrepancies are observed between the two JENDL-based results (about 2.0%). The four JEFF-based results can be grouped into two classes, characterised by high (RIT and SCK•CEN) and low (KAERI and PSI/CEA) values. Another interesting effect is that JEFF predicts similar k_{inf} values for both cores, whereas ENDF and JENDL predict a k_{inf} difference of about 1.5% between the start-up and the equilibrium cores.

Figure 2. **Microscopic capture cross-sections for the equilibrium core (cell averaged)**

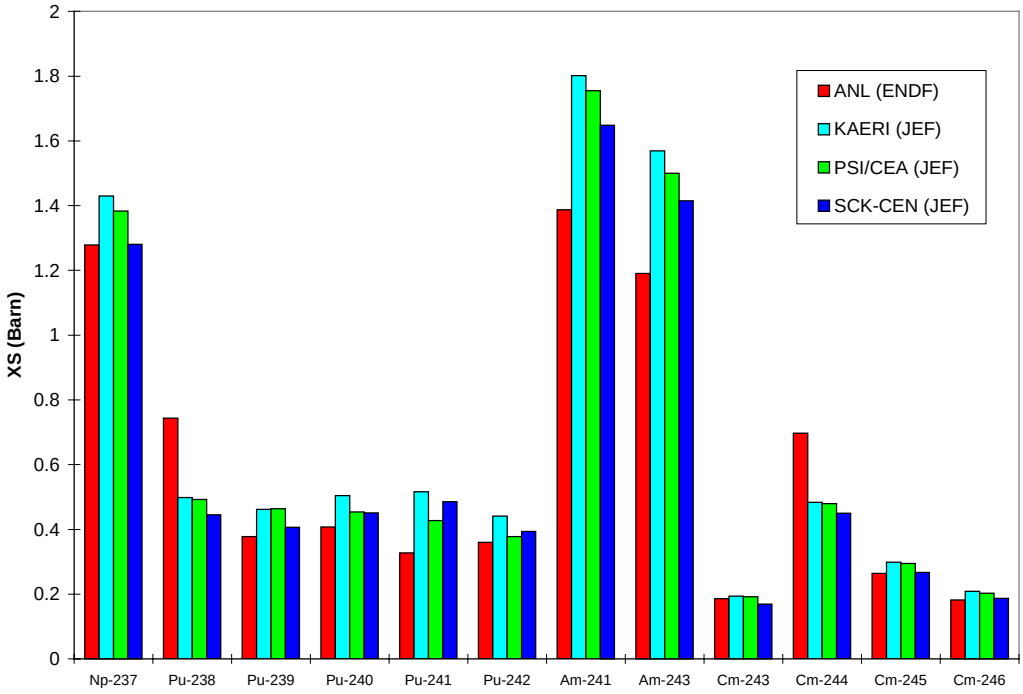

Figure 3. **Microscopic capture cross-sections for the equilibrium core (core averaged)**

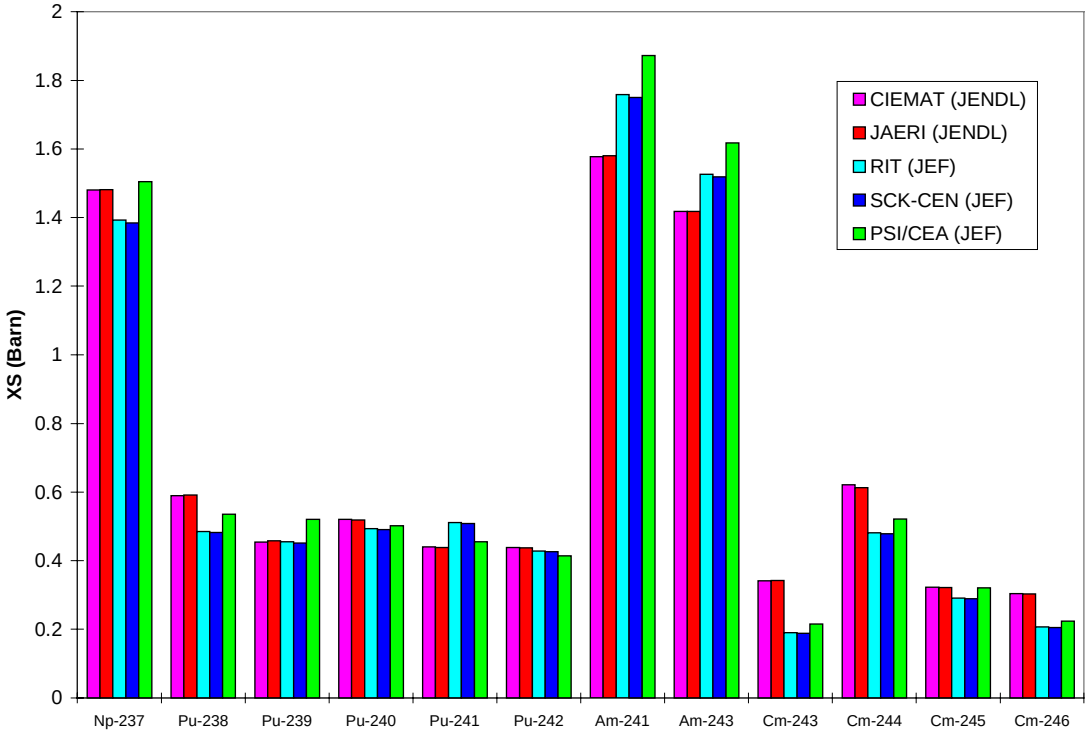

2.2 k_{eff} at beginning of life and k_{eff} variation

The k_{eff} values at beginning of life (see Tables 2 and 3) show a maximum discrepancy of 4% for the start-up core; the spread in the k_{eff} values is slightly reduced for the equilibrium core. The k_{eff} values do not show a clear correlation with the library used, indicating that the sensitivity of the results to the data processing route and/or the neutron transport approximation also has to be investigated. 1% of the discrepancies arise from the two ENDF-based calculations and 0.8% from the three JENDL-based results. The four JEFF-based results can be grouped into two classes characterised by high (RIT and SCK•CEN) and low (KAERI and PSI/CEA) k_{eff} values. However, comparing these results is difficult because only RIT used the complete JEF-2.2 library. PSI/CEA used the library ERALIB1 (adjusted from JEF-2.2) and KAERI and SCK•CEN used data for Pb from JENDL and ENDF respectively.

A systematic sensitivity analysis performed by KAERI using a simplified 1-D model of the start-up core enables us to estimate the impact of the nuclear data on k_{eff} [5]. The results show that the k_{eff} values are lower by 2 250 pcm for JEF and by 1 160 pcm for JENDL, when all the important actinides are substituted from the reference ENDF-based calculation. Overall, the k_{eff} obtained using JEFF is 2 070 pcm lower than the reference ENDF-based result; the differences arise mainly from heavy metals (-2 250 pcm), lead (+680 pcm) and ^{15}N (-420 pcm) while the contribution of bismuth is small (-73 pcm). JENDL also gives a lower k_{eff} value (-2800 pcm) mainly due to the contribution of lead (-1 100 pcm) and heavy metals (-1 160 pcm). The contribution of ^{15}N and bismuth (-450 and -77 pcm) is similar to that for JEFF.

From the reaction rates provided by the participants, the production over absorption (P/A) ratio is calculated for all the heavy nuclides and it is presented in Tables 2 and 3. ANL (ENDF) predicts by far the highest values for both core configurations, whereas the other results are closely grouped. The two JENDL-based results are similar and, for the four JEFF-based results, SCK•CEN gives the highest value and RIT the lowest value for both core compositions. The ratios of production to absorption are similar for the start-up and the equilibrium cores when using ENDF and JENDL data. However, all four JEFF-based results give larger values (+2.5%) for the equilibrium core than for the start-up core. Interestingly, the k_{eff} values are not correlated in a systematic way with P/A ratios as one would expect. In particular, all four JEFF-based solutions give a lower P/A ratio but a higher k_{eff} in the start-up core. ANL, CIEMAT and JAERI calculated similar P/A values but different multiplication factors for both cores.

The multiplication factors for the two cores do not exhibit consistent biases. This may be due to the fact that the two cores are not dominated by the same producers and absorbers. From the submitted reaction rate balance components, it can be deduced that the production rate is dominated by ^{239}Pu, ^{241}Am and ^{241}Pu in the start-up core and by ^{238}Pu and ^{245}Cm in the equilibrium core. The absorption rate is dominated by ^{241}Am, ^{239}Pu and ^{243}Am in the start-up core and by ^{243}Am and ^{238}Pu in the equilibrium core.

The k_{eff} variations with burn-up are shown in Figures 4 and 5 and the respective burn-up reactivity drops, k_{BOC}-k_{EOC}, including decomposition of the global reactivity drop into actinide and fission product components, are given in Tables 4 and 5. In addition to the solution obtained with the JEFF library, RIT presented, for the start-up core, an additional solution obtained with JENDL data.

Figure 4. **k_{eff} variation in the start-up core**

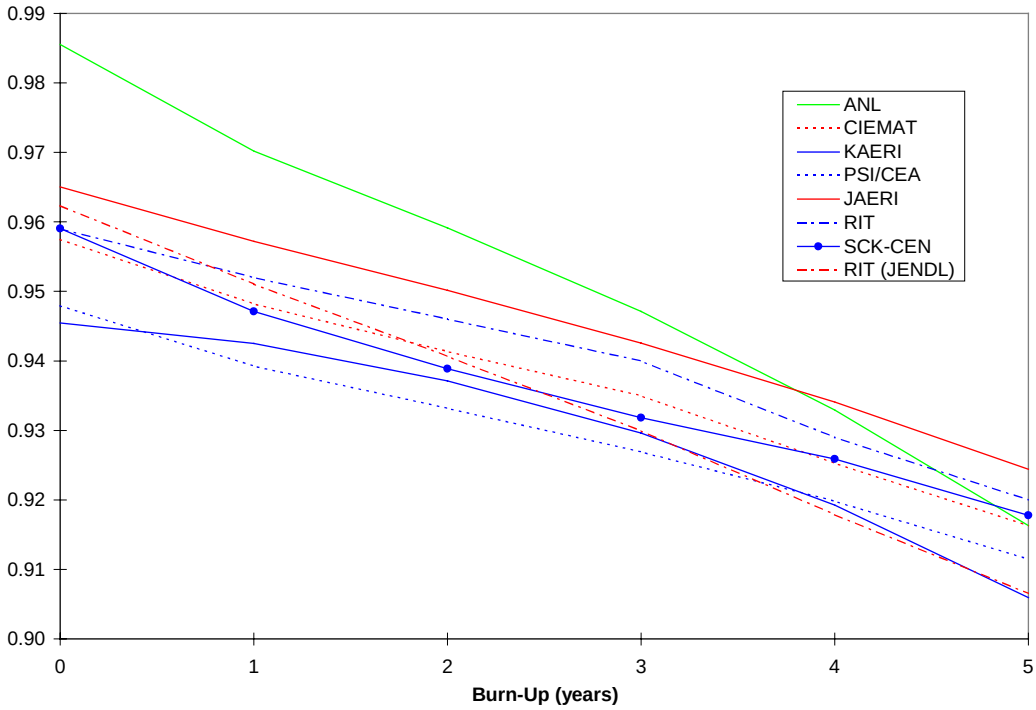

Figure 5. **k_{eff} variation in the equilibrium core**

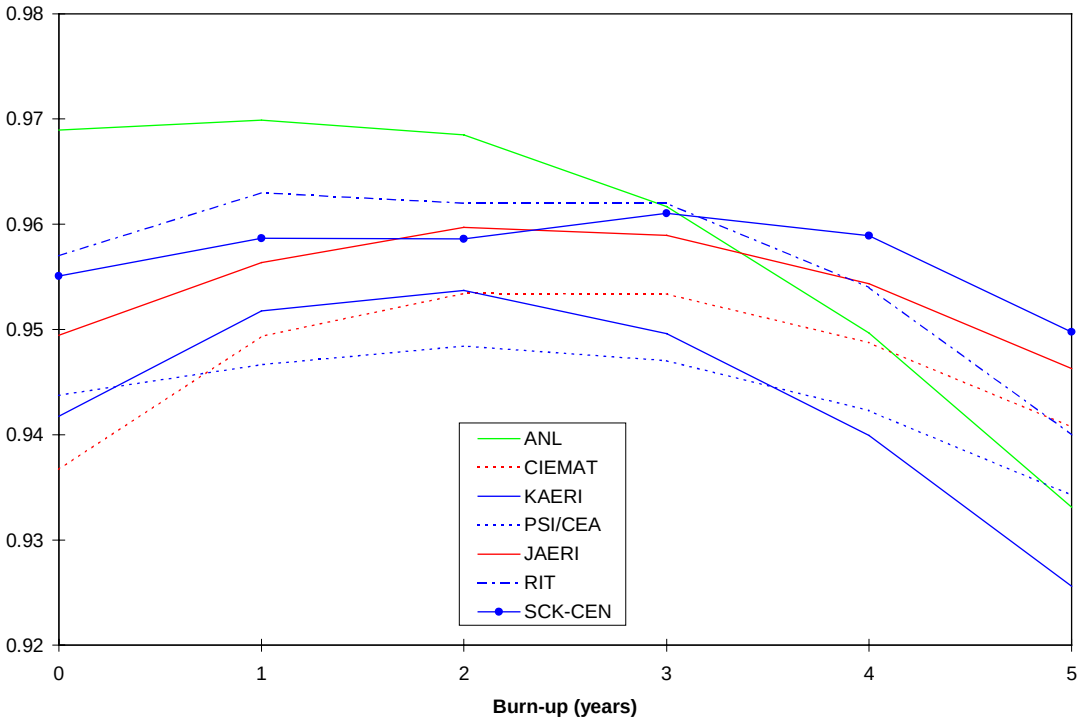

The burn-up reactivity drop values, k_{BOC}-k_{EOC}, range from 0.036 to 0.069 in the start-up core and from -0.004 to 0.036 in the equilibrium core. ANL (ENDF) predicts, in both cases, by far the highest reactivity drop. The total reactivity drop values in the start-up core are close for five participants (CIEMAT, KAERI, JAERI, JEFF-based RIT and SCK•CEN) with values between 3 900 and 4 100 pcm but this result hides compensating effects between fission products and heavy metals contributions and is fortuitous. The results are more spread for the equilibrium core.

Neither the actinide nor the fission product components are well correlated with the nuclear data library used. Only the contribution of the actinides gives similar results for three of the four JEFF-based results. Other possible causes of discrepancies can be related to the treatment of fission products. In particular, it is questionable whether lumped fission products generated for U and Pu can be representative for a system where a significant fraction of the fissions arise from minor actinides with a higher mass number, such as Am and Cm. However no obvious correlation can be observed related to the use of individual or lumped fission products.

Table 4. **Start-up core: end of cycle reactivity drop components (in units of 10^3 Δk)**

Δk from	**ENDF**	**JENDL**			**JEFF**			
	ANL	***CIEMAT***	***JAERI***	***RIT***	***KAERI***	***PSI/CEA***	***RIT***	***SCK•CEN***
Actinides	28	28	14	22	3	8	4	16
FP's	41	13	27	34	37	28	35	25
Total	69	41	41	56	40	36	39	41

Table 5. **Equilibrium core: end of cycle reactivity drop components (in units of 10^3 •k)**

Δk from	**ENDF**	**JENDL**		**JEFF**			
	ANL	***CIEMAT***	***JAERI***	***KAERI***	***PSI/CEA***	***RIT***	***SCK•CEN***
Actinides	-11	-18	-27	-27	-26	-27	-17
FP's	45	14	30	43	35	44	22
Total	36	-4	3	16	9	17	5

2.3 Neutron spectrum

Neutron spectra are calculated for both cores at R = 56 cm and Z = 100 cm; this point corresponds to the centre of the fuel region where the neutron spectrum is dominated by the fission neutrons. From the submitted neutron spectra, median energies were calculated (see Tables 1 and 2).

Good agreement is observed for most of the participants except for JAERI, which predicts a clearly softer spectrum (its median energy is about 20% lower than the others). The spectra provided by the other six participants show a good agreement especially for the energy range above 5-10 keV that covers approximately 95% of the neutrons. It is only in the lower resonance region (between 100 eV and 1 keV) that the differences between the results become pronounced. Finally, it is interesting to notice that the spectrum in the equilibrium core is softer than that in the start-up core.

2.4 Neutron flux distribution

One radial flux distribution corresponding to the mid-plane and two axial flux distributions corresponding, respectively, to the centre of the target and the fuel zone were requested. Considerable differences between the participants are observed, especially for the radial neutron flux distribution and for the axial flux distribution in the target zone. In particular, ENDF-based results (ANL and RIT) estimate by far the lowest neutron flux through the target. The discrepancies are also significant in the fuel region, where differences in flux level and in peak flux position appear. These discrepancies can be partially explained by the different level of sub-criticality: a system with a lower k_{eff} needs more external neutrons in order to maintain the chain reaction. This results in a more peaked axial flux in the target, at the interface with the duct, and a displacement of the axial flux peak in the fuel towards the upper part of the core.

An additional study was performed with ERANOS in order to assess the impact of the k_{eff} value on the neutron flux distribution. By modifying appropriately the ν values for reproducing the k_{eff} values submitted by the participants, neutron flux distributions were recalculated for each participant. From these distributions, spatial dependent correction factors were obtained. Finally, the neutron flux distributions supplied by the participants were rescaled for the reference k_{eff} value of 0.95 using these spatial dependent correction factors. The rescaled neutron flux distributions are presented in Figures 6, 7 and 8 and refer to the equilibrium core.

Figure 6. **Axial flux distribution in the target region; results scaled to a k_{eff} value of 0.95**

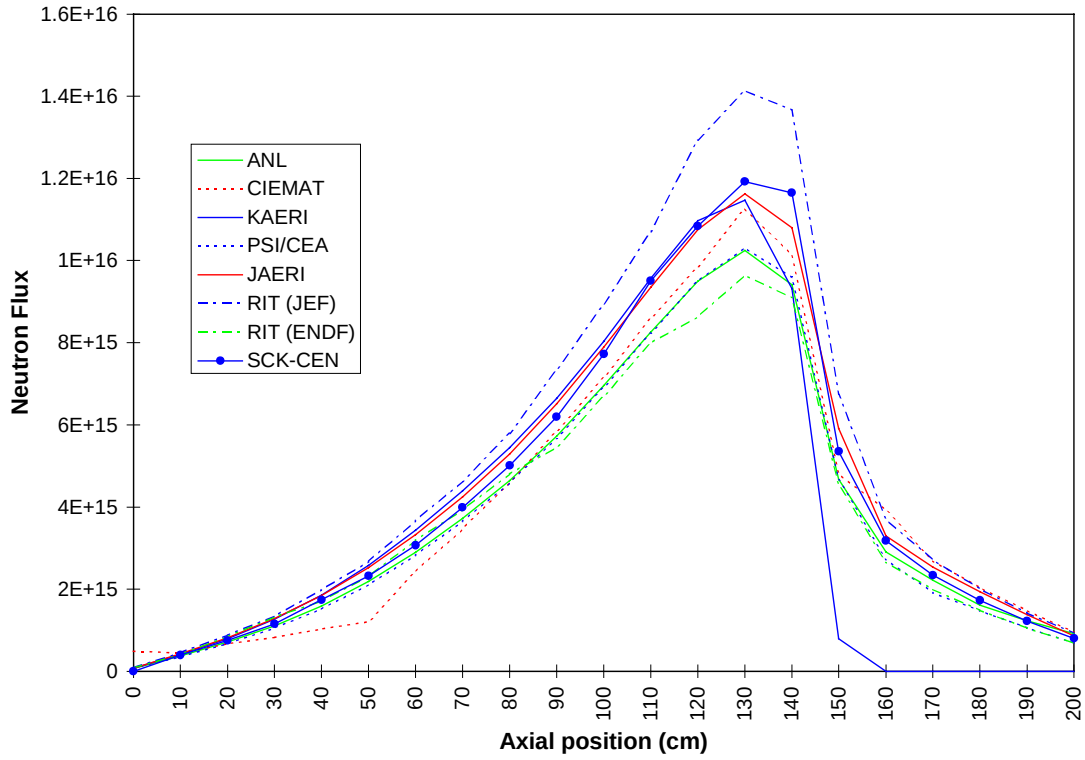

Figure 7. **Axial flux distribution in the fuel region; results scaled to a k_{eff} value of 0.95**

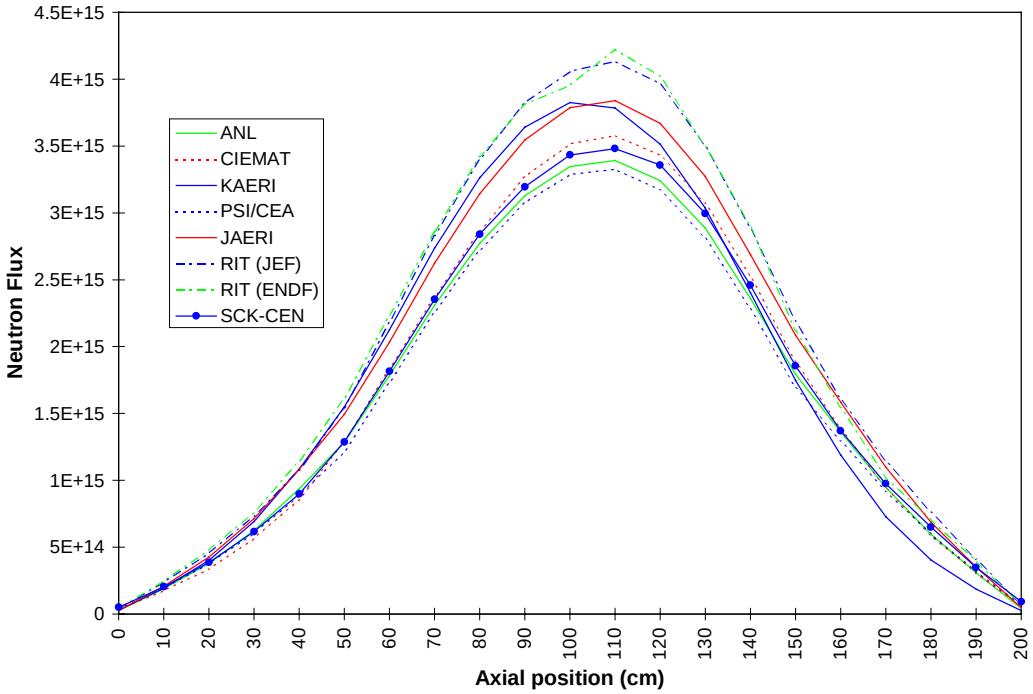

Figure 8. **Radial flux distribution in the mid-plane; results scaled to a k_{eff} value of 0.95**

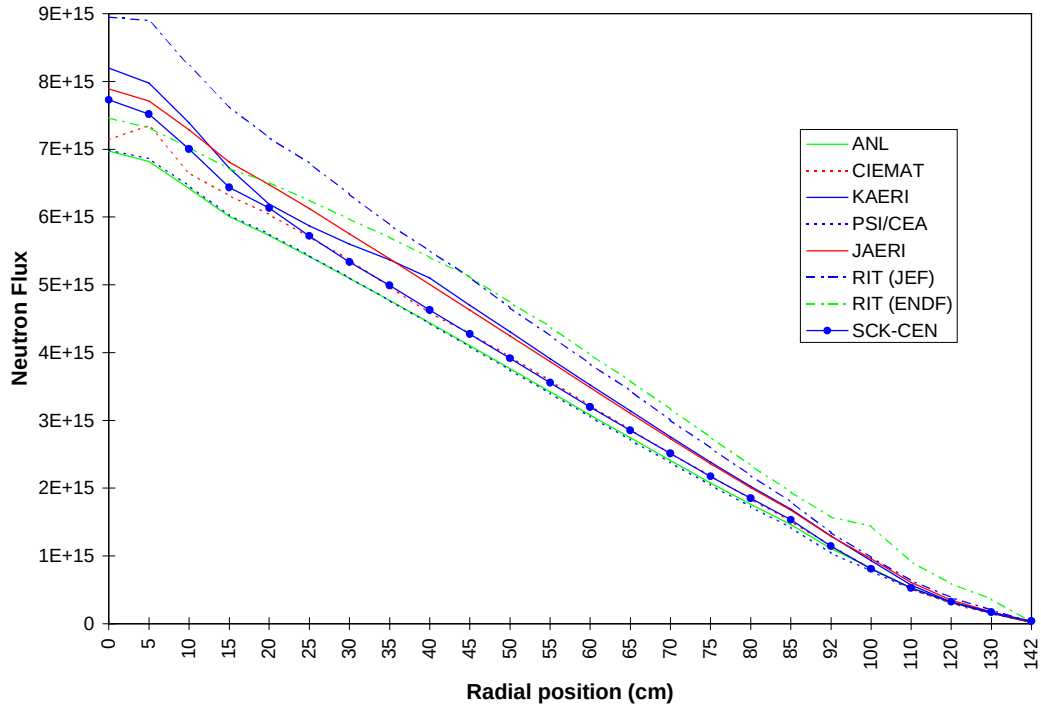

In the fuel region, the shape of the axial neutron flux distributions is in good agreement for most participants. However, the peak position reported by KAERI is shifted to the core centre (Z = 100 cm). The spread in the absolute value of the flux is still significant and the difference

between the highest and the lowest value (obtained by RIT and PSI/CEA respectively) is about 20%. As expected, the discrepancies in the axial neutron distributions in the target region become considerably smaller after the adjustment. The shapes of the flux distributions have a similar trend and the values are less spread. Similar considerations apply to the radial neutron flux distributions corresponding to the mid-plane. Referring to the normalisation of flux to power mentioned earlier, the neutron flux values provided by RIT, SCK•CEN and JAERI are overestimated with respect to the other participants and should be reduced correspondingly (9% for RIT, 4% for JAERI and SCK•CEN).

Even with the adjustment taking into account the k_{eff} effect, there still remain differences in the flux distributions, especially in the absolute value of the flux and its shape. Large discrepancies are observed in the shape of the axial flux in the target calculated by CIEMAT and KAERI. The CIEMAT result shows a distinct feature in the lowest part of the target region, due to the geometry model used: the lowest part of the target (the first 50 cm) was replaced by a void region. The KAERI result has a vanishing flux in the void zone; that is probably due to the diffusion approximation.

2.5 Source strength

The source strength, i.e. the number of neutrons per second that the ADS needs in order to maintain the chain reaction, is an important parameter because it is directly proportional to the required accelerator power. Its value is given by the following equation [6]:

$$N = \frac{P_{th} \cdot \nu_k}{E_f} \cdot \left(\frac{1}{k} - 1 \right) \cdot \frac{1}{\varphi^*}$$

where N is the number of neutrons/s, P_{th} the thermal power, ν_k and E_f, respectively, the average number of neutrons and the average energy released per fission in the fuel, k the multiplication factor of the system without source and φ^* the importance of spallation neutrons relative to fission neutrons.

The results, presented in Tables 2 and 3, for the beginning and for the end of irradiation, show quite a spread: at BOL, the ratio between the highest (KAERI) and the lowest (ANL) values is about 7 for the start-up core and 3 for the equilibrium core. The other three JEFF-based results lie in a similar range (maximum difference of about 10%) and the two JENDL-based results show a difference of about 30% for both core configurations.

As the above equation indicates, the required number of external neutrons is strongly dependent on the multiplication factor. It may be interesting to isolate that effect by dividing the source strength value by (1/k-1) in order to remove the differences due to the multiplication factor (at least partially, knowing that φ^* is also dependent on k). The numerical value obtained in that way is dependent on P_{th}, ν_k, E_f and φ^* and therefore should be close for all the participants. The values obtained are quite discrepant, KAERI presenting by far the highest value. Interestingly, the correlation between the three other JEFF-based results turns out to be fortuitous; RIT and SCK•CEN results are closer and the PSI/CEA value is similar to that obtained by ANL. The two JENDL-based results lie in a similar range.

2.6 Isotopic composition at end of irradiation

From the submitted results (not shown in this paper), significant discrepancies in the isotopic

composition at the end of irradiation are observed. The results seem only partially correlated with the nuclear data libraries used.

Before analysing the isotopic composition of the irradiated fuel, it is interesting to calculate the fraction of heavy metals that fissioned after five years of irradiation. Surprisingly, the values are strongly different and can be grouped into two classes characterised by a high "burn-up" (KAERI, RIT and SCK•CEN, all using the JEFF library) and a low "burn-up". The former values are between 21.3% and 22% and the latter between 18.5% and 18.8%. The discrepancy in the total number of heavy metals at EOL is therefore considerable (more than 15%) and is not fully understood.

As for the isotopic compositions at the end of irradiation, a clear dependence on the "burn-up" is observed. In comparison with the other participants, RIT, JAERI and SCK•CEN (high burn-up) report lower values for burned-up isotopes during the irradiation, such as ^{237}Np, ^{241}Am and ^{243}Am and higher values for build-up isotopes (in the start-up core only), such as ^{238}Pu, ^{242}Cm and ^{244}Cm.

The discrepancies are important not only for the minor actinides such as ^{237}Np, ^{241}Am and ^{243}Am (up to 10% relative to the average) but also for the Pu isotopes. Large differences are observed especially for ^{238}Pu, ^{240}Pu and ^{241}Pu where the results of SCK•CEN strongly deviate from the others.

Some discrepancies in the results are also related to differences in the branching ratios or to different treatment of some reactions. For example, the differences observed in the ^{242}Cm and ^{242m}Am concentrations are due to discrepancies in the branching ratios used for the (n,γ) reaction of ^{241}Am. Most participants used the 0.2/0.8 values, whereas RIT used 0.225/0.775, PSI/CEA 0.15/0.85 and SCK•CEN 0.09/0.91. Consequently RIT gives the highest and PSI/CEA and SCK•CEN the lowest concentration of ^{242m}Am. As expected, an opposite effect is observed on the ^{242}Cm. Discrepancies are observed in the concentrations of ^{236}U and ^{235}U in the KAERI and SCK•CEN results. In the start-up core, very low concentrations of these isotopes are reported, whereas in the equilibrium core their results are in acceptable agreement with the other participants. This probably indicates a different treatment of the (n, 2n) reaction for ^{237}Np, which should be thoroughly investigated.

2.7 Safety parameters

Coolant void reactivity calculations are traditionally difficult. Only integral values for the coolant void reactivity from k_{eff} difference calculations are available. The JENDL-based calculations by CIEMAT and JAERI give similar results (agreement within about 10%). Assuming that the Monte Carlo calculations by CIEMAT and RIT can be considered as reference calculations which are only sensitive to differences in nuclear data, the decrease in the BOL coolant void reactivity arising from the substitution of JENDL by JEFF is about 30% (26% for the start-up core and 32% for the equilibrium core). For the other JEFF-based coolant void reactivity predictions, one observes a maximum deviation of 30% with respect to the RIT prediction. It is interesting to notice that, in the ANL and JAERI case, the voided core becomes supercritical.

A general observation on the calculated Doppler reactivity is that it represents an almost "zero effect" on the system. Knowing that the magnitude of the Doppler reactivity in fast spectrum systems was demonstrated with an uncertainty of ±15%, it is difficult to make a comparison of these small values dispersed around zero. Nevertheless, since the Doppler reactivity comes essentially from capture reactions in the thermal energy region, a more thorough insight into the calculation procedures used by the participants, especially energy self-shielding treatment in their calculations, would be necessary to understand the origin of discrepancies among them.

The isotope specific β_{eff} values calculated from the two libraries (ENDF/B-VI and JEF-2.2) are in good agreement. However, ANL (ENDF/B-VI) gives a total β_{eff} value smaller than that of JAERI because the contributions of ^{242m}Am, ^{243}Am and Cm isotopes were not taken into account (the delayed neutron data for these isotopes are not available in ENDF/B-VI used by ANL). JAERI used the delayed neutron data of ^{242m}Am, ^{243}Am and ^{245}Cm isotopes from JENDL-3.2. PSI/CEA took into account the contribution of all the isotopes; its results therefore give the largest value among the results from ANL, JAERI and PSI/CEA. The Monte Carlo calculations give larger β_{eff} values. RIT used the delayed neutron data based on ENDF/B-VI, but did not consider ^{242m}Am, ^{243}Am and Cm isotopes, whereas CIEMAT used the delayed neutron data based on JENDL-3.2 in its calculations. In general, it is seen that the results of the β_{eff} calculations depend on the accuracy of the delayed neutron data used.

3. Conclusions

Seven organisations contributed to this benchmark exercise using different basic data libraries and reactor analysis codes and applying both deterministic and Monte Carlo methods. The analysis of the results shows significant discrepancies in important neutronic parameters, such as k_{inf}, k_{eff} and burn-up reactivity swing. Strong discrepancies appear also in the estimation of the external neutron source, i.e. a parameter which determines the requested accelerator power.

As demonstrated by a separate parametric study, the impact of the different basic nuclear data on these integral parameters is important but it is not sufficient to fully explain the discrepancies observed in the results. In future benchmark exercises which may be based on an experimental result, attention should therefore be given to both the data processing route and the neutron transport approximations. Concerning the burn-up calculations, attention should be given to the treatment of the fission products and to the actinide decay chains noting that in minor actinide burner cores different isotopes are involved compared to MOX-fuelled cores.

Acknowledgements

The authors express their gratitude to all the participants who devoted their time and effort to this benchmark exercise.

REFERENCES

[1] OECD/NEA NSC Task Force on Physics Aspects of Different Transmutation Concepts, *JAERI Proposal of Benchmark Problem on Method and Data to Calculate the Nuclear Characteristics in Accelerator-based Transmutation System with Fast Neutron Flux*, NEA/NSC/DOC(1996), 10 April 1996.

[2] H. Takano *et al.*, *Benchmark Problems on Transmutation Calculation by the OECD/NEA Task Force on Physics Aspects of Different Transmutation Concepts*, Proc. Int. Conf. on the Physics of Nuclear Science and Technology, 5-8 October 1998, Long Island, USA, 1462.

[3] *Calculations of Different Transmutation Concepts: An International Benchmark Exercise*, OECD/NEA report, NEA/NSC/DOC(2000)6, February 2000.

[4] B.C. Na, P. Wydler and H. Takano, *OECD/NEA Comparison Calculations for an Accelerator-driven Minor Actinide Burner: Analysis of Preliminary Results*, NEA-NSC Workshop on Utilisation and Reliability of High Power Accelerators, 22-24 November 1999, Aix-en-Provence, France, (To be published).

[5] J.D. Kim and C.S. Gil, KAERI, Private Communication.

[6] H. Takahashi and H. Rief, *Concepts of Accelerator Based Transmutation Systems*, Proc. of the Specialists' Meeting on Accelerator-based Transmutation, 24-26 March 1992, PSI Villigen, Switzerland, 2-26.

SESSION IV
BASIC PHYSICS, MATERIALS AND FUELS

SUB-SESSION IV-B:
MATERIALS

STAINLESS STEEL CORROSION IN LEAD-BISMUTH UNDER TEMPERATURE GRADIENT

Dolores Gómez Briceño, Fco. Javier Martín Muñoz, Laura Soler Crespo, Federico Esteban Ochoa de Retana, Celia Torres Gurdiel
Nuclear Fission Department, CIEMAT
Av. Complutense 22, Madrid 28040, Spain

Abstract

Austenitic steels can be used in ADS in contact with liquid lead-bismuth at temperatures below 400ºC. At higher temperatures, martensitic steels are recommended. However, at long times, the interaction between structural material and eutectic leads to the dissolution of some elements of the steel in the liquid metal. In a non-isothermal loop, the material dissolution takes place at the hot leg and, due to mass transfer, deposition occurs at the cold leg. Formation of oxide layers on structural materials improves its performance. F82Hmod. and 2¼ Cr-Mo steels have been tested in a small natural convection loop built of austenitic steel (316L), which has been operating for 3 000 hours. During all the operation, a gas with 10 ppm oxygen content has been bubbling in the hot area. The obtained results show that an oxide layer is formed on the samples introduced in the loop at the beginning of the operation and this layer increases with time. However, the samples introduced at intermediate times are not protected by oxide layers and present different levels of attack.

1. Introduction

Due to its excellent physic-chemical and nuclear characteristics, lead-bismuth has been proposed both as a coolant and a spallation target for hybrid systems, so called accelerator driven systems (ADS) [1]. However, heavy liquid metals, and particularly lead-bismuth, present a high corrosivity to most of structural materials.

Austenitic steels may be used in a hybrid system in contact with liquid lead-bismuth if the operating temperature is not beyond 400ºC. For higher temperatures, martensitic steels are recommended [2]. However, with long operation times, the interaction between the structural material and the eutectic leads to the solution of some elements of the steel (Ni, Cr and Fe, mainly) in the liquid metal. In a non-isothermal lead bismuth loop, the material dissolution takes place at the hot leg of the loop and, due to mass transfer, deposition occurs at the cold leg. The available experience, proceeding from the Former Soviet Union, shows that one of the possible ways to improve the performance of structural materials in lead-bismuth is the formation and maintenance of a protective oxide layer, which would constitute a barrier between the liquid metal and the steel.

2. Experimental

Tests have been performed in a small thermal convection loop built of austenitic stainless steel type 316, containing a lead-bismuth volume of 1.2L. A scheme of the loop is shown in Figure 1. The maximum temperature is of 550ºC with a temperature gradient between 50 and 100ºC. Thermocouples placed in several points of the loop, embedded in the lead-bismuth, were used to control the loop temperatures. The eutectic and the gas for controlling the atmosphere were introduced into the loop from an expansion tank placed on top of it.

Figure 1. **Thermal convection loop**

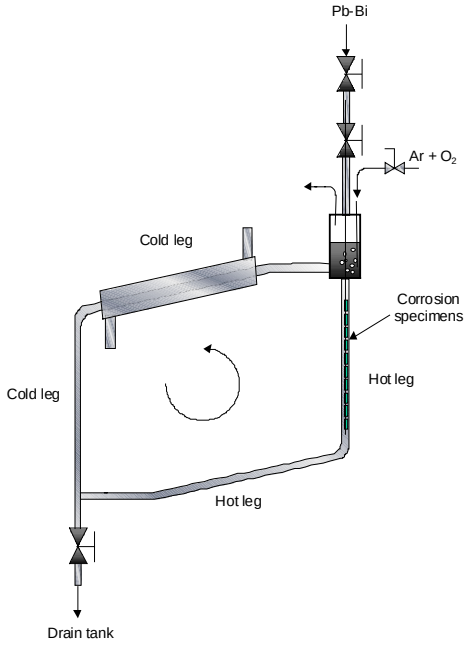

Cylindrical specimens (10 mm length and 7 mm of diameter) of martensitic steel F82Hmod. and low alloy steel 2¼ Cr-Mo, named P22, have been tested. The materials composition is shown in

Table 1. Specimens were inserted and removed at several times from the test zone placed at the hot leg (500ºC) during loop operation, without stopping the flowing of lead-bismuth, according with the scheme shown in Figure 2. In this scheme, samples A, B, C and D correspond to F82H steel and P, Q, R and S correspond to P22 steel. Some samples have been in the loop during all the operation (A_3 and P_3) and others have lived different times and periods of loop life. During the tests, a flow of 40 cc/min of argon with 10 ppm of oxygen was bubbling in the hot area of the loop.

Table 1. **Materials composition**

% weight	**F82Hmod**	**2¼ Cr-1Mo**
Fe	Bal.	Bal.
Cr	7.750	2.250
Ni	0.015	
Al	0.004	
Mo	0.010	1.000
C	0.100	0.090
Si	0.230	0.200
Ta	0.005	
Ti	0.004	
Mn	0.160	0.450
Nb	<0.01	
S	0.003	<0.015
B	40×10^{-3}	
Co	30×10^{-4}	
Cu	0.030	
V	0.140	<0.030
P	–	<0.015

After the tests, specimens were examined by optical and scanning electron microscopy (SEM). Auger spectroscopy was used to obtain the depth profile compositions of the oxide layers formed on the specimens during the tests. The loop structural material (austenitic steel) was also examined. At the end of the operation, the lead-bismuth was frozen inside the loop and several cuts were made at different points of the loop. Cross-sections of these areas were prepared and examined by optical microscopy and SEM.

Figure 2. **Tests scheme**

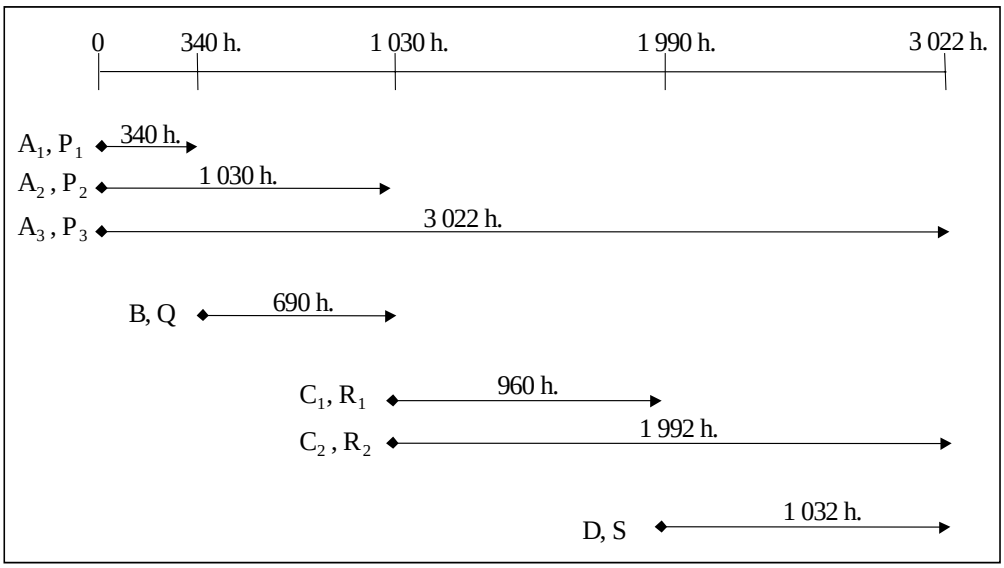

Figure 3. **Temperature evolution during loop life**

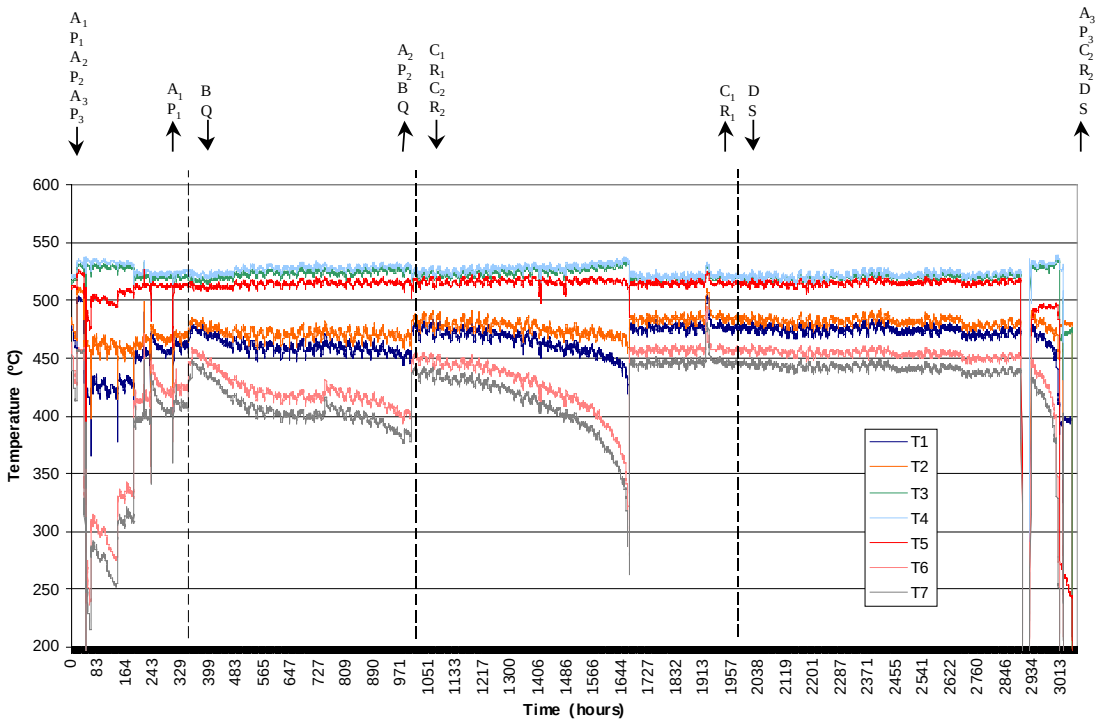

3. Results

The temperature evolution in different points of the thermal convection loop is represented in Figure 3. Specimens insertion and removing times are also indicated in this figure. According with the temperature registration, loop operation can be divided in four steps. During all the steps, the

thermocouples placed in the hot zone of the loop present uniform values with a light decrease over time. However, the cool zone temperature oscillates during the first step and stabilises at the beginning of the second step. From this level, it decreases 50ºC, and it soars to a higher level than the existent at the beginning of the second step. All this process occurs in a time bracket of 1 000 hours of operation. During the third step, the temperature decreases again, reaching lower minimum values than in the previous case, after 1 700 hours of operation. During the last step, the temperatures stabilise again until the end of the loop operation, keeping a temperature gradient between the hot and the cool zones of 80ºC aprox. Temperature decreases may be due to slags formation hindering lead-bismuth flowing. Sudden minimum temperature increases in the cool zones may be due to slag dissolution. A constant flow of gas was kept during all the operation.

As mentioned above, three different steels were examined, the steel samples (F82H and P22) and the structural material (316L austenitic steel). All the samples were examined by optical and scanning electron microscopy and, in some cases, Auger spectroscopy was carried out to obtain the depth profile composition of the oxide layers formed on the sample surfaces.

In general, the specimens of martensitic steel F82H mod. have shown a slightly better behaviour than the 2¼ Cr-Mo specimens although the evolution is the same for both steels. This means that both types of steel formed an oxide layer when the samples were tested from the beginning of the operation and both presented attack at intermediate states.

The six specimens (type A and P) incorporated into the loop at the beginning of the operation show a good corrosion resistance. For F82Hmod., all the specimens are covered by an homogenous oxide layer, with minor spalling areas in samples A_2 and A_3. Type A_1 specimens, tested for 340 hours, present a thin oxide layer of 2.5-3.5 μm, formed by two sub-layers. The outer layer, of 1-1.5 μm thickness, is iron oxide and the inner layer is formed by iron, chromium and oxygen with a chromium concentration higher than its value in the alloy, as can be seen in the Auger depth profiles, Figure 4. A slight depletion of chromium in the underlying alloy was detected. For 2¼ Cr-Mo, P_1 specimens present thicker oxide layers with a wrinkled aspect that let the lead-bismuth penetrate and be placed between the oxide layer and the steel (Figure 5). Due to the thickness of oxide layers formed on 2¼ Cr-Mo specimens, it was not possible to carry out Auger analysis in most of the samples.

Figure 4. **Auger depth profile concentrations. A_1 specimens, 340 hours**

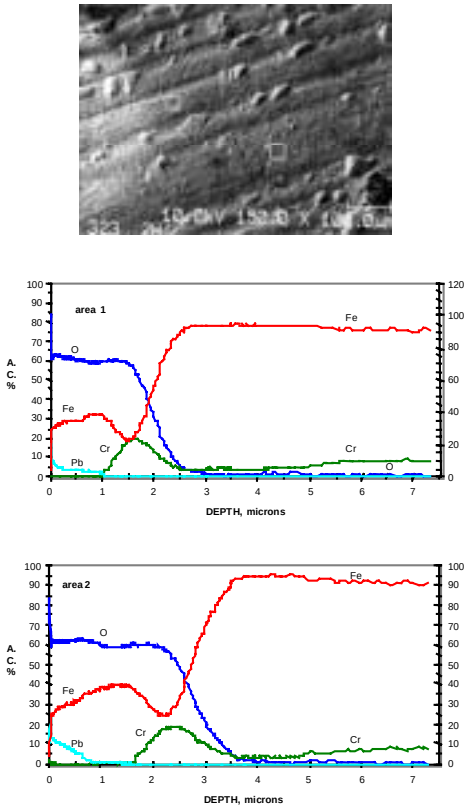

Figure 5. **Oxide layers on P_1 specimens, 340 hours**

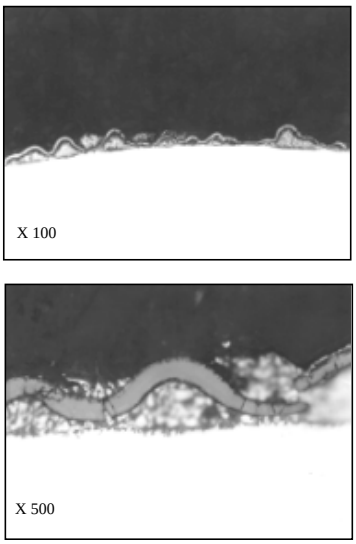

Type A_2 specimens (F82Hmod.), tested for 1 030 hours, show an oxide layer very similar in composition and thickness to the ones detected in A_1 specimens. However, A_3 specimens (F82Hmod.), tested for 3 022 hours, from the beginning to the end of the loop operation, present an oxide layer with a thickness of 20 µm but with similar composition to A_1 and A_2 specimens. Figure 6 shows that in A_3 specimens the outer layer is formed by iron and oxygen (magnetite), whereas the inner layer has iron, chromium and oxygen, with the higher concentration of chromium placed in the interface between the inner layer and the alloy. In all A specimens, the outer layer composition corresponds to magnetite whereas inner layer is an $Fe(Fe_{2-x})Cr_xO_4$. Lead-bismuth eutectic (named lead in all the figures) is incorporated to the outer layer in all A specimens. All type P specimens (2¼ Cr-Mo) present an oxide layer with the same characteristics as P_1 sample. Figure 7 shows the comparison between A_3 and P_3 specimens.

Figure 6. **Auger depth profile concentrations. A_3 specimens, 3 022 hours**

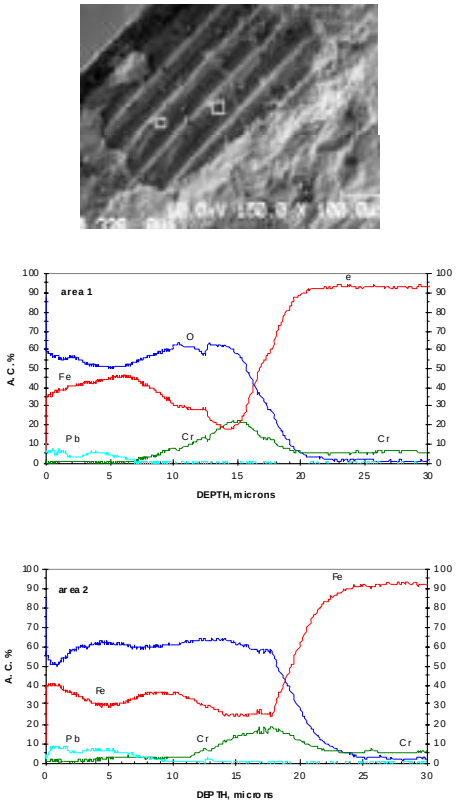

Figure 7. **Appearance of A_3 and P_3 specimens, 3 022 hours**

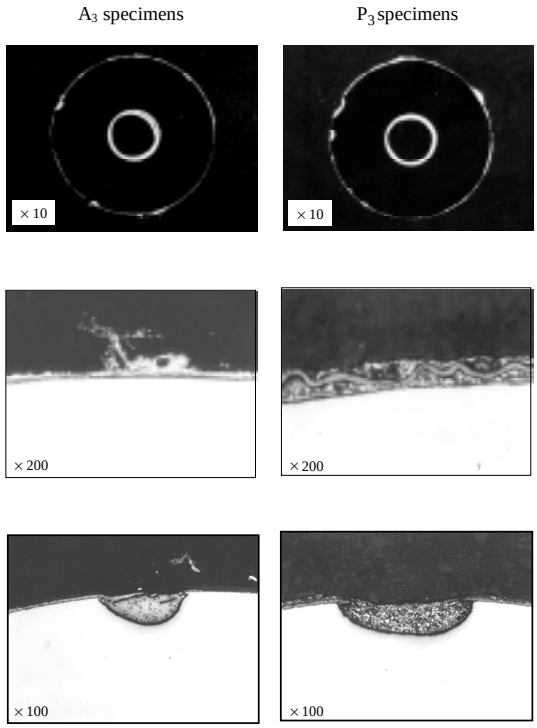

Both present a quite high corrosion resistance, but P_3 present a thicker and slightly less protective oxide layer.

Type B (F82Hmod.) and Q (2¼ Cr-Mo) specimens were introduced into the loop after 340 hours from the operation beginning, and removed 690 hours later. These specimens present a general solution in most of the surface with a depth attack up to 50 µm for F82H sample and 60 µm for 2¼ Cr-Mo. Small areas covered by a very thin oxide layer have been detected. Auger analysis shows a single oxide layer formed by chromium and oxygen. Type C (F82Hmod.) and R (2¼ Cr-Mo) specimens inserted into the loop after 1 030 hours from the operation beginning were removed 960 hours (C_1 and R_1 specimens) and 1992 hours afterwards (C_2 and R_2 specimens). C_1 samples present a deeper attack than R_1, which present only a slight attack. C_2 samples also present a worse behaviour than R_2, but both show general corrosion with a depth attack up to 140 µm. Small surface areas covered by a thin oxide layer are still visible. The thickness and the composition of this oxide layer are similar to the observed in type B specimens, Figure 8.

Type D (F82Hmod.) and S (2¼ Cr-Mo) specimens were introduced into the loop 2 000 hours after the beginning of the operation and removed at the end of the tests together with A_3 and P_3 specimen. No dissolution was observed in these samples. Auger analysis shows a single thin layer of less than 1 µm covering the entire specimen, with a high chromium concentration and without iron, Figure 9. In this sample, lead is incorporated to the oxide layer rich in chromium. In this case, S specimen behaves slightly better than D.

Figure 8. **Auger depth profile concentrations. C_2 specimens, 1 992 hours**

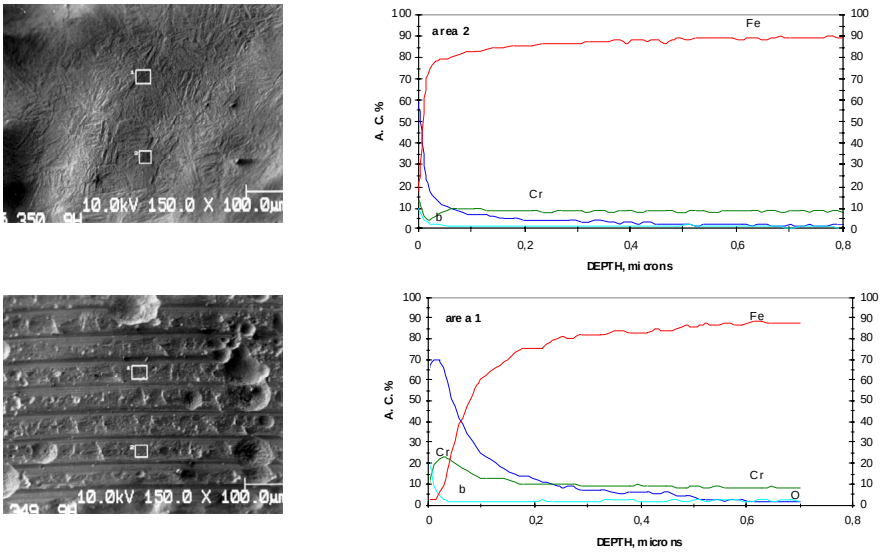

Figure 9. **Auger depth profile concentrations. D specimens, 1 032 hours**

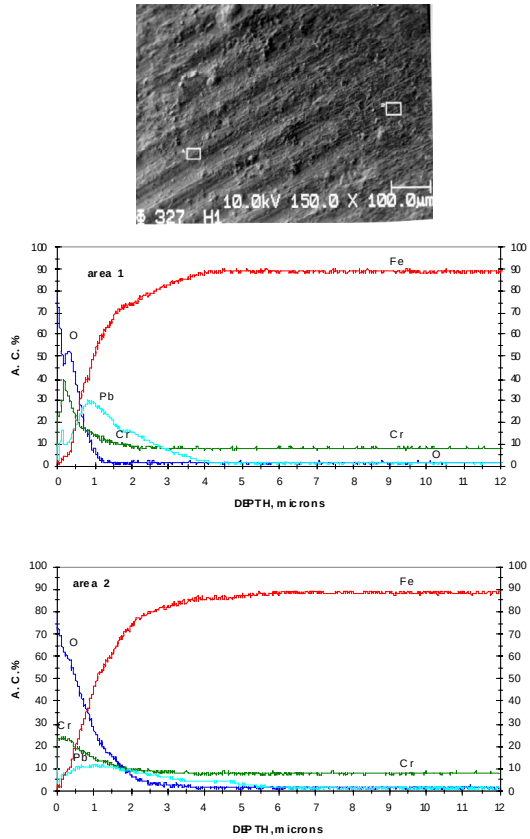

After 2 000 hours from the beginning of the operation a lead-bismuth sample was taken out from the loop in order to measure impurities. This sample had 265 ppm nickel, 5.4 ppm chromium and 17 ppm iron. Iron concentration is higher than iron solubility in eutectic (3.6 ppm), while nickel and

chromium concentration values are lower than their solubility values at 530ºC (30 212 and 13.8 ppm respectively).

After the end of the tests, the loop was cut to be destructively examined. The structural austenitic steel presented material solution, especially at the hottest areas. Figure 10 shows a cut of the coldest area of the loop in which particle deposition was observed. This deposition was also detected at the upper corner of the cold leg. Two different kinds of particles were identified. The round particles closer to the steel wall are formed by chromium, iron and oxygen and the particles with geometrical shape are an intermetallic compound of nickel and bismuth.

Figure 10. **Slags deposition detected in the cold leg loop**

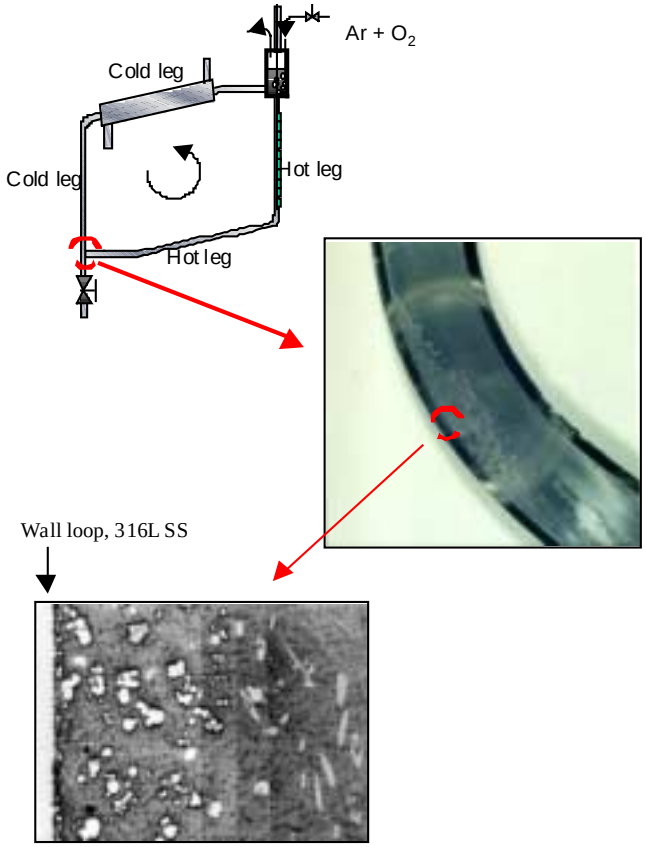

Samples of solidified lead–bismuth from the hot and cold zones were taken to measure oxygen by LECO. A heterogeneous oxygen distribution was observed in the samples. At the core, 2 ppm oxygen were observed in the hot zone, and 1 ppm oxygen in the cold zone. Near the walls, 9 ppm oxygen were measured in the hot zone and 6 ppm oxygen in the cold zone.

4. Discussion

Liquid metal corrosion depends on the solution rate and the solubility value of the solid metal in the liquid metal. Lead alloys, and in particular lead-bismuth eutectic, show a higher agressivity to the structural materials than the alkali liquid metals. In a static system, solution of the solid metal occurs until the solubility value of the main elements of the alloy is reached. In a dynamic system with temperature gradient, a mass transfer process occurs. The dissolved material at the hot zone is

deposited at the cold zone, and the elements concentration in the liquid metal represents a steady–state balance between the rates of solution and precipitation in different zones of corroding systems [3].

For austenitic stainless steels, it is well documented (for example, Gorynin *et al.* [2]) that corrosion resistance is determined by oxygen thermodynamic activity in lead and lead alloys. For oxygen concentrations lower than the concentration at which the dissolved oxygen is in equilibrium with the spinel formation on the steel surface materials, dissolution occurs. This equilibrium value is about 5×10^{-8} wt% at 550ºC. For concentrations higher than this value, materials oxidation appears. Steel composition has also a significant influence in the corrosion/protection of structural materials. In general, it is accepted that in absence of oxygen, carbon steels present a higher corrosion resistance than high chromium steels, which suffer attack [4]. However, results obtained by Gorynin [13] point out that at 460ºC, in flowing Pb-Bi with oxygen concentration less than 10^{-7} wt%, 1Cr-MoV alloy presents higher corrosion rate than 18Cr-10Ni-Ti alloy, whereas 1Cr-2Si-Mo is more resistant to corrosion than both the previous ones. For high oxygen activity the corrosion of iron–chromium alloys is higher than for iron whereas for low oxygen activity the alloy presents higher resistance corrosion. Formation of oxide layer on the structural materials can prevent alloy dissolution.

A general consideration of the results seems to point out that the oxygen content in the loop is not enough to form, in general, protective oxide layers on the specimens placed in the hot zone of the loop. In fact, specimens B, C (F82H) and Q, R (2¼ Cr-Mo) present material dissolution and no oxide layers. However, in the type A (F82H) and P (2¼ Cr-Mo) specimens tested from the beginning of the operation, an appreciable growth of the oxide layer was detected. It seems that A and P samples are in oxidation condition whereas the rest of the specimens would be in dissolution conditions. This observation would mean that, although the gas is bubbling during all the operation time with the same flow rate and the same oxygen content (10 ppm), the oxygen concentration in the liquid lead-bismuth varies along the operation time and so does the corrosion behaviour of the samples.

Type A specimens (F82H) inserted into the loop at the beginning of the operation are covered by an homogeneous double oxide layer. The thickness of this oxide layer reaches 20 μm after 3 022 hours. The growth of this oxide layer is almost inappreciable between 340 and 1 030 hours, and then it grows significantly up to 3 022 hours. These results seem to be in accordance with the general behaviour accepted for the oxidation of iron-chromium alloys and stainless steels [5]. After an initial protective period, a sudden rate increase occurs once the break-away time has been reached. This stage is often followed by a further rate reduction by a self-healing process. This last step has not been observed in our tests, probably due to their short duration. The oxide layers of type A specimens show similar characteristics. The inner oxide layer, Fe $(Fe_{2-x})Cr_xO_4$, seems to be protective enough to prevent lead-bismuth penetration. No eutectic is incorporated to this layer contrary to the observed in iron oxide outer layer. Eutectic concentration in the outer layer decreases and disappears in the interface outer/inner oxide layer.

Type P specimens (2¼ Cr-Mo) inserted into the loop at the beginning of the operation are covered by a non-adherent oxide layer with a wrinkled aspect. Labun *et al.* [6] describe a layer with these characteristics for a 3Cr-Fe steel oxidised in dry oxygen at 700-800 ºC. They say that the wrinkling is due to a substantial growth of this layer in the lateral direction relative to the underlying layers. In our case, lead-bismuth penetrates through the external oxide layer and is place between it and the steel. The layer formed on 2¼ Cr-Mo specimens is much thicker in all the cases that the formed on type A specimens. Fedirko *et al.* [7] tested Armco iron, Fe-16Cr and Fe-16Cr-1Al in stagnant liquid lead at 600ºC with some amount of lead oxide to get a concentration of 10^{-5} wt% oxygen and they mention in this work that the formed oxide layer is thicker for the Armco iron. The information on the oxidation behaviour of stainless steels in liquid lead-bismuth is very scarce. However, it is accepted than the available information on stainless steels oxidation in molten lead can be useful to analyse the materials behaviour in lead-bismuth.

For high oxygen activity, alloys with a high chromium content present a better behaviour than low chromium alloys. This is due to the different characteristics of the protective oxide layer based on formation of oxide rich in chromium, which is hindered for the low chromium alloys. At the same time, free and low chromium alloys are able to form thicker oxide layers, which are accepted to be less protective [14]. For low oxygen activity in the melt, alloys with low chromium content present a higher corrosion resistance [4], since chromium has a higher solubility than iron in lead-bismuth. This seems to be the case of Q, R (2¼ Cr-Mo) specimens comparatively to B, C (F82H) specimens although the behaviour of both steels is not conclusively different.

Fedirko *et al.* [8] also found that spinel rich in chromium can protect iron-chromium alloys in molten lead. After 1 000 hours of testing, four different zones could be observed on the transverse micro-sections of Fe-16Cr-1Al. The first zone was a porous oxide layer with a high concentration of iron and lead and a low concentration of chromium and aluminium. This zone was formed by magnetite and lead. Lead concentration decreased with distance from the surface, but on the interface of the first and the second zone lead was present. The second zone was a continuous oxide film enriched with chromium and aluminium. The composition of this film was a Fe_3O_4-$FeCr_2O_4$ solid solution with the spinel structure. Lead was not present in the interface between the second and third zone. A process of internal oxidation with chromium and aluminium oxides mainly along grain boundaries was detected in the third zone. Finally, the fourth zone had the matrix composition but grain boundaries also contained oxide compounds. On the contrary to the observed in oxygen saturated melts, spinel rich in chromium is not permeable to lead in solutions with low oxygen activity.

In addition, in static tests performed in oxygen saturated molten lead at 520ºC, Benamati *et al.* [9] observed the formation of continuous layers of reaction products with an average thickness of 20 μm after 2 000 hours and of 40 μm after 3 700 hours in martensitic steel F82H mod. specimens. The reaction product layers were formed by two distinct sub-layers of Me_3O_4. Only the inner one contained chromium in addition to iron. Lead was detected in the outer sub-layer of all the product layers. These authors point out that oxide layers formed in oxygen saturated liquid lead containing an additional source of oxygen in the form of lead oxide are not protective, since the oxide layer thickness increases along with the exposure time.

On the other hand, Müller *et al*. [10] found oxide layers of similar characteristics to the observed in type A specimens in samples of a martensitic steel with 9.99 Cr (OPTIFER) tested in stagnant liquid lead at 550ºC under controlled Ar-H_2/H_2O atmosphere containing 8×10^{-6} at% oxygen. Müller observed a corrosion attack with three different zones. The outer layer consisted of magnetite without appreciable chromium concentration. The middle layer was formed by Cr-Fe spinel, with a chromium concentration lower than the detected in the A_3 specimens. Finally, an internal oxygen diffusion zone in which oxides precipitate along the grain boundaries could be observed. After 3 000 hours, the thickness of magnetite and spinel were 20 and 15 μm respectively whereas the depth of diffusion zone was 10 μm.

According to Fedirko *et al.* [7], in liquid lead with low activity of oxygen the formation of the external oxide layer based on Fe_3O_4 is very low and significant amounts of active alloying elements are accumulated in more internal layers. The lack of mobility of chromium through the magnetite lattice explains the formation of the spinel layer. Faster diffusing elements like manganese and iron will pass through to the outer layer, while slower diffusing elements like chromium will be oxidised without movement and remain in the inner layer. Both magnetite and spinels M_3O_4 are based in a close-packed cubic sub-lattice of oxygen ions in which the metals ions are the faster moving species and determine the oxidation rates. Thus, in martensitic steels, chromium moves more slowly than iron. The outer layer is formed by magnetite and the inner layer consists of iron, chromium spinels. The

inner layer grows inward from the original metal surface. The oxygen transport through this layer can take place via pores within the inner layer, since solid state diffusion of oxygen through the magnetite lattice is too low [11]. The Auger analysis results on F82H specimens point out that the composition of the outer oxide layer fits well with magnetite composition, and the inner oxide layer corresponds to a spinel $Fe(Fe_{2-x})Cr_xO_4$. Spinel rich in chromium is the typical oxide layer on stainless steels with Cr concentration lower than 13% when they are oxidised at high temperature. Müller *et al*. [10] consider that no main differences exist between the oxide layers formed in lead and in an oxidation process in a controlled furnace atmosphere at the same temperature.

The thin oxide layers detected on sample D (F82Hmod.) and S (2¼ Cr-Mo) are formed by oxygen and chromium with a minor amount of iron. No chromium depletion was observed in the underlying alloy. In spite of having a high chromium concentration, these layers allow the eutectic penetration, whose concentration is maximum in the oxide/alloy interface and that apparently penetrates in the base alloy underneath the oxide/alloy interface. No external iron oxide was detected in these samples. The lack of an external iron oxide layer can be a consequence of two causes, not necessarily exclusive. On the one hand, oxygen activity in lead-bismuth may be lower than the necessary to form magnetite but high enough to form oxide of more noble elements like chromium. The low oxygen activity is supported by the dissolution process observed in the specimens inserted into the loop at intermediate times (B, Q and C, R specimens) and by the loop structural material dissolution and is questioned by the growth of oxide in type A and P specimens placed into the loop at the beginning of the test. On the other hand, an iron concentration higher than its solubility in lead-bismuth was measured in an eutectic sample taken out during the loop operation. This high iron concentration can hinder iron diffusion and prevent magnetite formation.

Regarding loop operation, nickel, chromium and iron dissolved in the hot area and deposited at the cold zone play an important role in the loop operation and may also be of significant importance with respect to changes of oxygen concentration in lead-bismuth along the loop life. Horsley *et al*. [11] point out that if the concentration of iron in the melt is higher than the solubility of iron in bismuth at the maximum temperature of the loop, then the rate of mass transfer is controlled by the precipitation rate in the cold region. On the one hand, the dissolution of these steel elements into the melt provokes the beginning of a plug formation at the coldest zones of the loop and explains the decreases of temperatures in these areas. On the other hand, these elements take the oxygen dissolved in the melt, since the particles found at the cold corners of the loop are formed by iron, chromium and oxygen. This would explain the behaviour of samples at intermediate times, which present attack, due to a insufficient oxygen concentration to form a protective oxide layer. As it was shown in Figure 3, at certain times of loop operation, especially after 2 000 hours, a sudden increase of temperatures of the cold zone is observed. This may be due to slag dissolution and may provoke oxygen liberation, which could explain the formation of a thin oxide layer on D and S specimens. In spite of this hypothesis, at present we do not have a plausible explanation for the observed behaviour of similar specimens tested for the same period at different loop operation times. However, the growth of oxide layer in A and P specimens simultaneously with the dissolution in B, Q and C, R specimens point out that lower oxygen activity is necessary for oxide layer growth than for oxide layer formation.

6. Conclusions

The results obtained in this experimental work point out that oxide layer protection of martensitic steels in lead-bismuth under temperature gradient is possible in determined conditions. A double oxide layer composed by a magnetite outer layer and a spinel $Fe(Fe_{2-x})Cr_xO_4$ inner layer, very rich in chromium, is formed. The spinel is non-permeable to lead-bismuth and constitutes a barrier between base material and liquid metal. Higher oxygen activity seems to be necessary for oxide formation than for oxide layer growth.

In the tested conditions the corrosion resistance of martensitic steel F82Hmod. and of low alloy steel 2 ¼ Cr-Mo have been very similar, in spite of the lower chromium concentration of the later. However, the oxide layers formed on F82Hmod. seem to be no-permeable to lead-bismuth whereas the ones formed on 2 ¼ Cr-Mo are thicker and permeable to the eutectic

It is possible to operate a natural convection loop for long times up to 3 000 hours. However, impurities in the melt, coming from structural material dissolution, interfere with oxide layer formation on the samples tested, and lead to a difficult interpretation of the obtained results.

REFERENCES

[1] J.J. Park *et al.*, *Review of Liquid Metal Corrosion Issues for Potential Containment for Liquid Lead and Lead-bismuth Eutectic Spallation Targets as a Neutron Source*, Nuclear Engineering and Design, 2000, 196, pp. 315-325.

[2] I.V. Gorynin, G.P. Karzov, V.G. Markov, V.A. Yakovlev, *Structural Materials for Atomic Reactors with Liquid Metal Heat-transfer Agents in the Form of Lead or Lead-bismuth Alloy*, Metal Science and Heat Treatment, 1999, Vol. 41, No. 9-10.

[3] J.R. Weeks and C.J. Klamut, *Liquid Metal Corrosion Mechanisms*, Proceedings of the Conference on Corrosion of Reactor Materials International Atomic Energy Agency, Vienna 1962.

[4] Ning Li, *Active Control of Oxygen in Molten Lead-bismuth Eutectic Systems to Prevent Steel Corrosion and Coolant Contamination*, 1999, Report from Los Alamos National Laboratory.

[5] G.C. Woods, *The Oxidation of Iron-chromium Alloys and Stainless Steel at High Temperature*, Corrosion Science, 1961, Vol. 2, pp. 173-196.

[6] P.A. Labun *et al.*, *Micro-structural Investigation of the Oxidation of an Fe-3 Pct Cr Alloy*, Metallurgical Transactions A, 1982, Vol. 13ª, pp. 2103-2112.

[7] V.M. Fedirko, O.I. Eliseeva, V.L. Kalyandruk and V.A. Lopushans'kyi, *Effect of Admixtures of Oxygen on the Oxidation of Iron and Fe-Cr Alloys in Lead Melts*, Materials Science, 1977, Vol. 33, No. 3.

[8] V.M. Fedirko, O.I. Eliseeva, V.L. Kalyandruk, V.A. Lopushans'kyi, *Corrosion of Armco Iron and Model Fe-Cr-Al Alloys in Oxygen- Containing Lead Melts,* 1977, Materials Science, Vol. 33, No. 2.

[9] G. Benamati, P. Buttol, V. Imbeni, C. Martini and G. Palombarini, *Behaviour of Materials for Accelerator Driven Systems in Stagnant Molten Lead,* Journal of Nuclear materials 279, 2000, pp. 308-316.

[10] G. Muller, G. Schumacher and F. Zimmermann, *Investigation on Oxygen Controlled Liquid Lead Corrosion of Surface Treated Steels,* Journal of Nuclear Materials, 2000, 278 pp. 85-95.

[11] J. Robertson, *High T Corrosion of Stainless Steel,* Corrosion Science, 1991, Vol. 32, No. 4, pp. 443-465.

[12] G.A. Horsley and J.T. Maskrey, *The Corrosion of 21/4% Cr-1%Mo Steel by Liquid Bismuth,* Journal of the Iron and Steel Institute, 1958, pp. 139-148.

[13] I.V. Gorynin, G.P. Karzov, V.G. Markov, V.S. Lavrukhin,V.A. Yakovlev, *Structural Materials for Power Plants with Heavy Liquid Metals as Coolants,* Conference on Heavy liquid Metals Coolants in Nuclear Technology, HLMC-98, Obninsk 1998.

[14] G.C. Wood, *The Oxidation of Iron-chromium Alloys and Stainless Steels at High Temperatures,* Corrosion science, 1961, Vol. 2, pp. 173-196.

ACCUMULATION OF ACTIVATION PRODUCTS IN PB-BI, TANTALUM, AND TUNGSTEN TARGETS OF ADS

A.S. Gerasimov, G.V. Kiselev, A.I. Volovik
State Scientific Centre of the Russian Federation
Institute of Theoretical and Experimental Physics (RF SSC ITEP)
25, B. Cheremushkinskaya, 117259 Moscow, Russian Federation

Abstract

Data on new radionuclide production in three types of target, Pb-Bi, tantalum, and tungsten target of ADS are presented in this paper. The irradiation by neutrons produced in blanket and in the target itself do not take into account proton irradiation. The change of isotopic composition, accumulation of new radionuclides, and radiation characteristics (activity, radiotoxicity is water, and radiation dose power) are calculated.

1. Introduction

One of the main parts of the accelerator driven system (ADS) is the neutron-producing target. It can be made of solid heavy metal such as tantalum or tungsten or liquid metal such as lead-bismuth. All these materials are typical for a neutron-producing target. ADS target is irradiated by accelerated protons, by high-energy neutrons from the target itself, and by low energy neutrons from the sub-critical blanket surrounding the target. The average energy of neutrons from the target itself is about several MeV. A flux density of neutrons from the blanket on the target is of the order of 10^{13} $cm^{-2}s^{-1}$ for common-type power blanket with thermal neutrons and can reach several units times 10^{15} $cm^{-2}s^{-1}$ for high flux blanket. Under influence of target irradiation, there are nuclide conversions causing the change of target isotopic composition and radioactive nuclei production.

The change of isotopic composition, accumulation of new radionuclides, and radiation characteristics (activity, radiotoxicity by water, and radiation dose power) caused by external neutrons from blanket and by internal neutrons from the target itself are calculated. The influence of protons on side nuclide production should be calculated separately and is not considered in the paper.

In calculating nuclide conversions by thermal neutrons, reaction rates A_i are taken using values of thermal neutron cross-sections σ_i and resonance integrals I_i of nuclides [1], $A_i = (\sigma_i+\gamma I_i)\Phi$, where Φ is neutron flux density, γ is neutron spectrum hardness showing a ratio of epithermal to thermal neutrons. Value $\gamma = 0.4$ (spectrum typical for light-water thermal-neutron blanket) is considered. For irradiation by internal neutrons from target, monoenergetic neutrons with energies 10 MeV are considered [2,3]. The average high-energy neutron flux density is over the volume of a target about 10^{15} $cm^{-2}s^{-1}$ at energy of protons from accelerator 1 GeV and beam current 10 mA. Corresponding thermal neutron flux from blanket is about 10^{14} $cm^{-2}s^{-1}$. It was accepted that the target has the form of a continuous cylinder with a diameter of 50 cm. Specific activity Q (Ci/g), radiotoxicity RT (litre/g) and radiation dose power $Q\Gamma$ ($R\cdot cm^2/g\cdot hr$) are defined by sums on all radioactive nuclides included in a target:

$$Q = \Sigma\, Q_i$$
$$RT = \Sigma\, RT_i,\ RT_i = Q_i / MPA_i,$$
$$Q\Gamma = \Sigma\, Q\Gamma_i$$

where MPA_i – maximum permissible activity of the given nuclide i in water determined by the modern Russian radiation safety standard [4], Γ_i – gamma-constant of the nuclide i. They are referred to 1 gram of a target.

2. Pb-Bi target irradiation

The initial target is Pb-Bi eutectic containing 44.5% Pb and 55.5% Bi with natural isotopic composition. In Tables 1 and 2, nuclide concentration and radiation characteristics of a target are presented. For low energy neutrons, three Φ values and $\gamma = 0.4$ are considered. Concentrations of nuclides are normalised by 0.445 nuclei of lead and 0.555 nuclei of bismuth in initial target. Only the most important nuclides are submitted in the tables. Radiation characteristics – activity *Q*, radiotoxicity RT and radiation doze power $Q\Gamma$ are referred to 1 gram of a target. Irradiation time T = 1 year.

In irradiation by thermal neutrons, capture cross sections of nuclides in target are very small. So, effects of thermal self-blocking of Pb-Bi target are not essential. Initial nuclide burning is negligible.

An important radionuclide determining the radiation characteristics of a target is ^{210}Po. Because of alpha-decay of this nuclide, radiotoxicity is high. However, radiation doze power is not so great as for other target materials because of low gamma-radiation of ^{210}Po. In high-energy neutron irradiation, ^{210}Po is the main radioactive nuclide, and ^{204}Tl gives also small contribution to radiation characteristics.

Table 1. **Nuclide concentration and radiation characteristics of Pb-Bi target irradiated by external low energy neutrons from blanket**

Nuclide	Initial concentrations	T = 1 yr		
		$\Phi=10^{13}$ cm^{-2}s^{-1}	$\Phi=10^{14}$ cm^{-2}s^{-1}	$\Phi=10^{15}$ cm^{-2}s^{-1}
^{204}Pb	0.0064	6.4-3	6.4-3	6.1-3
^{205}Pb	0	2.95-6	2.94-5	2.88-4
^{206}Pb	0.107	0.107	0.107	0.107
^{207}Pb	0.0983	0.0983	0.0981	0.0959
^{208}Pb	0.233	0.233	0.233	0.235
^{209}Bi	0.555	0.555	0.555	0.553
^{210}Po	0	6.32-6	6.31-5	6.30-4
Q, Ci/g	–	0.0289	0.289	2.88
RT, litre/g	–	8.90 + 9	8.90 + 10	8.88 + 11
QГ, (R cm^2/g hr)	–	1.54-3	0.0154	0.153

Table 2. **Nuclide concentrations and radiation characteristics of a target irradiated by 10 MeV neutrons**

Nuclide	Initial concentrations	T = 1 yr	
		$\varphi = 10^{15}$ cm^{-2}s^{-1}	$\varphi = 10^{16}$ cm^{-2}s^{-1}
^{204}Hg	0	2.38-10	2.38-9
^{204}Pb	0.0064	0.0064	0.0064
^{204}Tl	0	1.11-7	1.11-6
^{206}Pb	0.107	0.107	0.107
^{207}Pb	0.0983	0.0983	0.0983
^{208}Pb	0.233	0.233	0.233
^{209}Bi	0.555	0.555	0.555
^{210}Po	0	1.61-5	1.61-4
Q, Ci/g	–	0.0735	0.753
RT, litre/g	–	2.27 + 10	2.27 + 11
QГ, (R cm^2/g hr)	–	4.19-3	4.19-2

The comparison of radiation characteristics caused by neutrons from the target itself and neutrons from external blanket is based on the assumption that a high energy neutron flux density of 10^{15} cm^{-2}s^{-1} corresponds to a neutron flux from external blanket of 10^{14} cm^{-2}s^{-1}. The radiotoxicity caused by neutrons from the target itself is about 3 times less, and radiation dose power is 4 times less than the same characteristics caused by neutrons from an external blanket. This result is important as it shows a rather high role of neutrons from the target itself in the process of accumulation of those radionuclides which define the main radiation characteristics of the irradiated target.

3. Tantalum target irradiation

The initial target is made of natural tantalum. In Table 3, nuclide concentration and radiation characteristics are presented for low energy neutron irradiation. For $\Phi = 10^{14}$ $cm^{-2}s^{-1}$, value $\gamma = 0.1$ and for $\Phi = 10^{15}$ $cm^{-2}s^{-1}$ value $\gamma = 0$ are considered with thin target, so effects of self-blocking are weak. Radiation characteristics are determined by ^{182}Ta and, at some extend, by ^{185}W.

Table 3. **Nuclide concentration and radiation characteristics of tantalum target irradiated by external low energy neutrons from blanket**

Nuclide	Initial concentrations	T = 1 yr	T = 0.5 yr
		$\Phi = 10^{14}$ $cm^{-2}s^{-1}$	$\Phi = 10^{15}$ $cm^{-2}s^{-1}$
^{181}Ta	1.0	0.761	0.724
^{182}Ta	0	4.40-3	1.04-3
^{182}W	0	9.56-3	1.13-3
^{183}W	0	0.210	0.252
^{184}W	0	0.015	0.021
^{185}W	0	2.62-5	1.37-4
Q, Ci/g	–	27.8	7.84
RT, litre/g	–	1.1+10	2.7+10
QΓ, (R cm^2/g hr)	–	1.85+5	4.37+4

4. Tungsten target irradiation

In Table 3, partial nuclide introduction to radiation characteristics is shown for $\Phi = 10^{14}$ $cm^{-2}s^{-1}$. In Table 4, concentration of nuclides and radiation characteristics of a target are presented for low energy neutron irradiation. Concentrations of nuclides are normalised by one nucleus of natural tungsten, radiation characteristics by 1 gram of a target. For neutron flux $\Phi = 10^{14}$ $cm^{-2}s^{-1}$, value $\gamma = 0.4$ is considered, and for $\Phi = 10^{15}$ $cm^{-2}s^{-1}$, $\gamma = 0$ and T = 0.5 years is taken. Target diameter 50 cm. Only the most important nuclides are submitted.

Table 3. **Radiation characteristics of tungsten target irradiated by low energy neutrons from blanket with $\Phi = 10^{14}$ $cm^{-2}s^{-1}$**

Nuclide	Q, Ci/g	RT, litre/g	QΓ, (R cm^2/g hr)
^{181}W	0.703	1.4 + 7	150
^{185}W	5.68	6.5 + 8	1.6
^{187}W	21.9	–	5.3 + 4
^{188}W	0.297	1.7 + 8	3.3
^{182}Ta	0.703	2.8 + 8	470
^{183}Ta	0.0486	1.6 + 7	80
^{186}Re	1.46	5.8 + 8	140
^{188}Re	2.30	–	730
Total	32.4	1.7 + 9	5.5 + 4

Table 4. **Nuclide concentration and radiation characteristics of tungsten target irradiated by external neutrons from blanket**

Nuclide	Initial concentrations	T = 1 yr	T = 0.5 yr
		$\Phi = 10^{14}$ cm^{-2}s^{-1}	$\Phi = 10^{15}$ cm^{-2}s^{-1}
^{180}W	0.126-2	9.6-4	1.3-3
^{181}W	0	1.2-4	6.6-6
^{182}W	0.263	0.26	0.26
^{183}W	0.143	0.14	0.14
^{184}W	0.306	0.31	0.31
^{185}W	0	6.0-4	7.1-5
^{186}W	0.286	0.28	0.28
^{187}W	0	3.1-5	2.4-5
^{188}W	0	2.9-5	2.0-7
^{182}Ta	0	1.1-5	4.0-9
^{183}Ta	0	3.5-7	3.6-10
^{186}Re	0	7.8-6	6.7-8
^{188}Re	0	2.3-6	3.5-7
Q, Ci/g	–	32.4	18.1
RT, litre/g	–	1.7 + 9	8.5 + 7
QГ, (R cm^2/g hr)	–	5.5 + 4	4.1 + 4

Table 5. **Nuclide concentrations and radiation characteristics of a tungsten target irradiated by 10 MeV neutrons**

Nuclide	Initial concentrations	T = 1 yr	T = 0.5 yr
		$\varphi = 10^{15}$ cm^{-2}s^{-1}	$\varphi = 10^{16}$ cm^{-2}s^{-1}
^{180}W	1.3-3	1.4-3	2.6-3
^{181}W	0	4.2-3	0.030
^{182}W	0.263	0.26	0.25
^{183}W	0.143	0.15	0.17
^{184}W	0.306	0.29	0.24
^{185}W	0	4.0-3	0.03
^{186}W	0.286	0.27	0.22
^{187}W	0	3.0-8	2.5-7
^{182}Ta	0	1.0-7	1.9-6
^{186}Re	0	3.2-7	1.0-6
^{188}Re	0	4.7-12	2.0-10
Q, Ci/g	–	62.2	486
RT, litre/g	–	5.1 + 9	4.1 + 10
QГ (R cm^2/g hr)	–	3.9 + 3	9.9 + 4

In low energy irradiation, self-blocking effects are very high. For this reason, production of new nuclides is low in purely thermal spectrum even in high flux 10^{13} cm^{-2}s^{-1}. For neutron spectrum typical for light water blanket, with $\gamma = 0.4$, nuclide production is higher because of epithermal neutrons. Radiotoxicity at $\gamma = 0.4$ is determined by all radioactive nuclides. At $\gamma = 0$, ^{185}W gives a major part to radiotoxicity. Radiation doze power is determined by short-lived ^{188}W.

At 10-MeV neutron irradiation, radiotoxicity is determined by ^{181}W, ^{185}W, ^{184}Re, and radiation dose power by ^{184}Re.

Comparison of these data shows that a radiotoxicity caused by neutrons born in a target is 3 times greater and radiation dose power is 14 times less than the same characteristics caused by low energy neutrons from external blanket. However, it is necessary to mention that radiation characteristics caused by neutrons from an external blanket are defined by short-lived nuclides ^{187}W, ^{188}Re with half-life periods about 1 day, whereas at irradiation by neutrons born in target, main contribution come from nuclides ^{185}W, ^{181}W, and ^{184}Re with half-life periods from 38 up to 121 days. If we consider only radionuclides with half-life periods not less than several tenths of days, then it appears that high-energy neutrons born in a target make radiation dose power 6 times greater than neutrons from an external blanket.

5. Conclusion

Comparison of radiation characteristics produced in irradiation by low energy neutrons from surrounding blanket and high energy neutrons from a target shows a rather high role of neutrons from the target itself in the process of accumulation of those radionuclide which define the main radiation characteristics of the irradiated target.

Absolute values of radiation characteristics allow estimating necessary modes of irradiated target management. For tantalum and tungsten targets, radiation dose power is rather high and decreases slowly at cooling. Radiotoxicity value for all considered targets is close to that of radioactive waste of nuclear reactors. It should be recommended to store irradiated targets after some cooling while taking measures as for middle and high radioactive waste management.

REFERENCES

[1] S. Mughabghab, *Neutron Cross-sections*. Vol. 1, Part B. Academic Press, N.Y.-London, 1984.

[2] V. McLane *et al.*, *Neutron Cross-sections*, Vol. 2, Neutron Cross-section Curves, National Neutron Data Centre, BNL. N.Y., Acad. Press, 1988.

[3] ENDF/B-VI, Revision 2.

[4] *Radiation Safety Standards (NRB-99)*, Minzdrav of Russia, Moscow, 1999.

THERMAL AND STRESS ANALYSIS OF HYPER TARGET SYSTEM*

T.Y. Song, N.I. Tak, W.S. Park
Korea Atomic Energy Research Institute
P.O. Box 105 Yusung, Taejon, 305-600, Republic of Korea

J.S. Cho, Y.S. Lee
Department of Nuclear Engineering, Seoul National University
Shinlim-dong 56-1, Kwanak-gu, Seoul, 151-742, Republic of Korea

J.H. Choi, M.K. Song
Department of Mechanical Engineering, Gyeongsang National University
Kajoa-dong 900, Chinju, Kyongnam, 660-701, Republic of Korea

Abstract

HYPER (*HY*brid *P*ower *E*xtraction *R*eactor) is the accelerator driven transmutation system which is being developed by KAERI (Korea Atomic Energy Research Institute). We plan to finish the preliminary design of HYPER by 2001. Pb-Bi is used as the coolant and target material of HYPER. One of the issues related to the HYPER target system is the thermal and mechanical loads imposed on the Pb-Bi and the beam window. We used LCS (LAHET Code System) to calculate heat generation. FLUENT was used for thermal-hydraulic calculation, and finally stress calculation was performed by ANSYS. A beam condition such as current varied. The initial velocity of Pb-Bi also varied.

* This work has been supported by the Korea Ministry of Science and Technology (MOST).

1. Introduction

HYPER (*HY*brid *P*ower *E*xtraction *R*eactor) is the accelerator driven transmutation system designed by KAERI (Korea Atomic Energy Research Institute) [1]. An accelerator driven system provides the possibility of reducing plutonium, minor actinides, and environmentally hazardous fission products from the nuclear waste coming from the conventional nuclear power plant. In addition, it can be used to produce electricity. HYPER is designed to transmute TRU and fission products such as ^{99}Tc and ^{129}I.

Because an accelerator driven system is a sub-critical reactor, external neutrons should be provided by a target system inside the reactor. HYPER adopts Pb-Bi as the coolant and target material, which are not separated. Some key issues related to developing target system are window and Pb-Bi cooling, corrosion, radiation damage etc. Corrosion and radiation damage degrade the performance of the beam window, and an experimental study is necessary to understand the change due to those damages. In this paper, we use simulation codes to determine the target geometry and beam conditions under which HYPER target system can be operated with stability before corrosion and radiation damage affect the beam window.

We studied the basic thermal hydraulic characteristics of the target system using FLUENT code, and we also used ANSYS code [2] to calculate the stress of the beam window. The heat generation inside beam window and Pb-Bi was calculated using LCS (LAHET Code System) [3].

2. Double window target

Figure 1 shows the structure of the target area and beam window geometry. HYPER beam channel is cylindrical and located at the centre of the reactor with a 50-cm diameter. The window is designed to have 2-mm thick steel layers, and Pb-Bi coolant flows between the two layers for window cooling. The gap width of the coolant channel is about 4 mm. The cross-section of the beam tube is 30×30 cm^2 and the window has a cylindrically curved profile.

Figure 1. **Target area and beam window geometry**

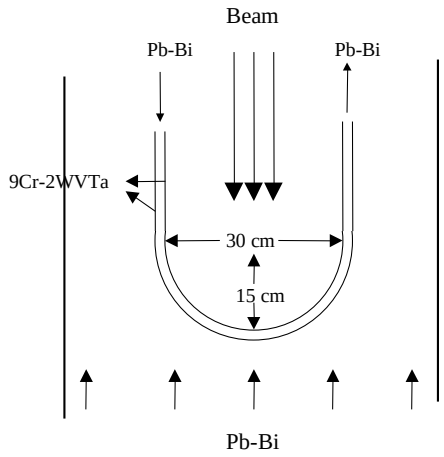

The target Pb-Bi is coming from the bottom of the beam channel and the beam is injected from the top. The Pb-Bi flow is slowed just below the centre of the beam window. Therefore Pb-Bi is forced to flow from left to right between windows.

For the beam window material, 9Cr-2WVTa was chosen since advanced martensitic/ferritic steels are better in Pb-Bi corrosion than austenitic steels and do not show a DBTT problem [4]. The yield strength of 9Cr-2WVTa is about 600 MPa at 400°C.

3. Calculation conditions

The cylindrical forced convection target system is set to be 50 cm in diameter and 100 cm in height. The bottom of the beam window is located 25 cm below the top. The initial temperature of Pb-Bi is set to be 340°C for both target and window cooling Pb-Bi. The initial velocity of window cooling Pb-Bi is 6 m/s. We separated the double window calculation from the single window calculation to simplify the calculation geometry.

The heat deposition in Pb-Bi and window is calculated using the LAHET Code System. The beam is assumed to have a circular shape with a diameter of 10 cm and a parabolic density distribution. The result shows that about 52% of the total beam energy are deposited as heat in the target zone. Figure 2 shows the heat deposition as a function of the radius from the beam centre and distance from the target surface for Pb-Bi and the window in the case of a 20 mA beam.

Figure 2. **Heat deposition rate for a 20mA beam**

Proton Beam Injection

($\times 10^9$ W/m^3)

	10cm	9cm	8cm	7cm	6cm	5cm	4cm	3cm	2cm	1cm
10cm	0.02	0.03	0.06	0.12	0.26	1.94	4.86	7.14	8.73	9.64
10cm	0.05	0.07	0.12	0.19	0.42	1.39	3.01	4.30	5.23	5.68
10cm	0.05	0.07	0.10	0.19	0.39	0.92	1.63	2.26	2.71	2.98
10cm	0.04	0.06	0.10	0.18	0.31	0.55	0.82	1.08	1.29	1.36
10cm	0.04	0.06	0.09	0.14	0.22	0.32	0.42	0.50	0.60	0.64

Proton Beam Injection

($\times 10^9$ W/m^3)

	10cm	9cm	8cm	7cm	6cm	5cm	4cm	3cm	2cm	1cm
2mm	0.004	0.006	0.009	0.019	0.071	1.90	5.29	7.20	9.09	9.64

4. 2-D calculation

The general CFD code FLUENT was used to simulate the two-dimensional thermal and flow distribution of the liquid target. Calculation analyses are performed in two-dimensional axi-symmetry cylindrical geometry. The calculation parameter is the liquid Pb-Bi inlet velocity which vary from 1.1 m/s to 2.0 m/s. The beam current and velocity of cooling Pb-Bi are fixed to 20 mA and 6 m/s respectively. In this calculation, the surfaces are set to be adiabatic boundaries. For the calculation of

this study, we used an orthogonal co-ordinate transformation. This transformation is performed using the grid generation components of the FLUENT code.

Figure 3 shows the calculation geometry of the FLUENT code. The centre of the Pb-Bi beam channel is narrowed to increase the velocity of up-coming Pb-Bi so that the efficiency of window cooling is maximised.

In the single window calculation, the maximum temperature of the window is 2 277°C for an inlet velocity of 1.1 m/s and 1 808°C for an inlet velocity of 2.0 m/s in the steel beam window region. These temperatures exceed the beam window melting temperature. Therefore, this is not allowable for the steel window. Figure 4 shows the temperature distribution and the velocity vector profile of the target and the window region for an inlet velocity of 2.0 m/s. Table 1 shows the calculation result of the maximum temperature for each case. Based on these calculations, the beam window can be damaged by high temperature and thermal stress. So, the independent cooling system for the beam window must be considered.

Figure 3. **FLUENT calculation geometry for the single and double window**

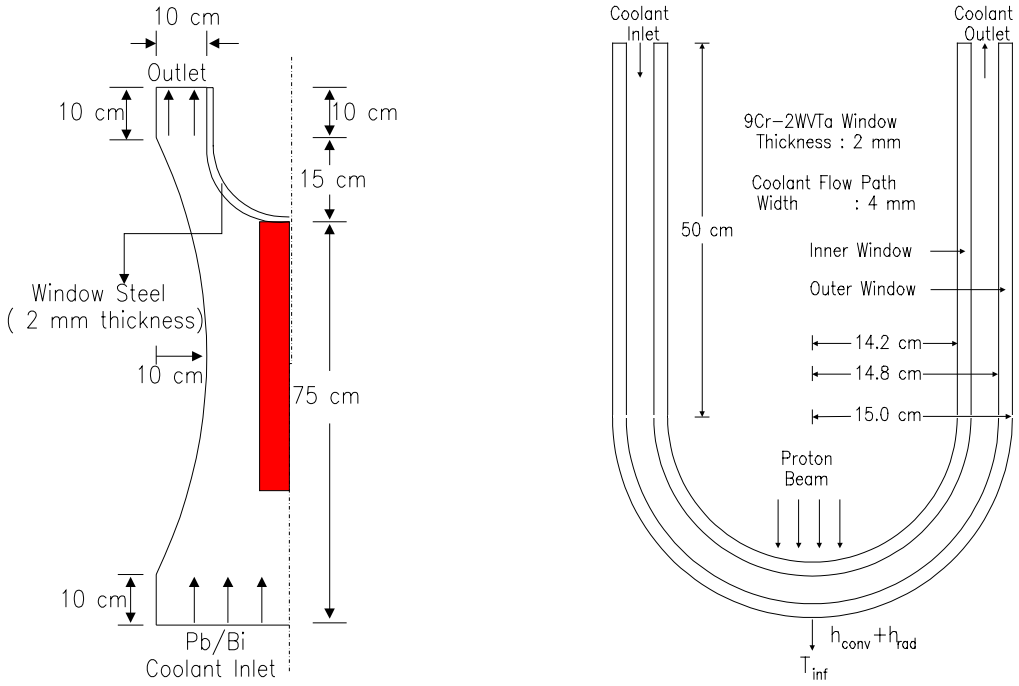

Figure 4. **Temperature and velocity distribution of the single window**

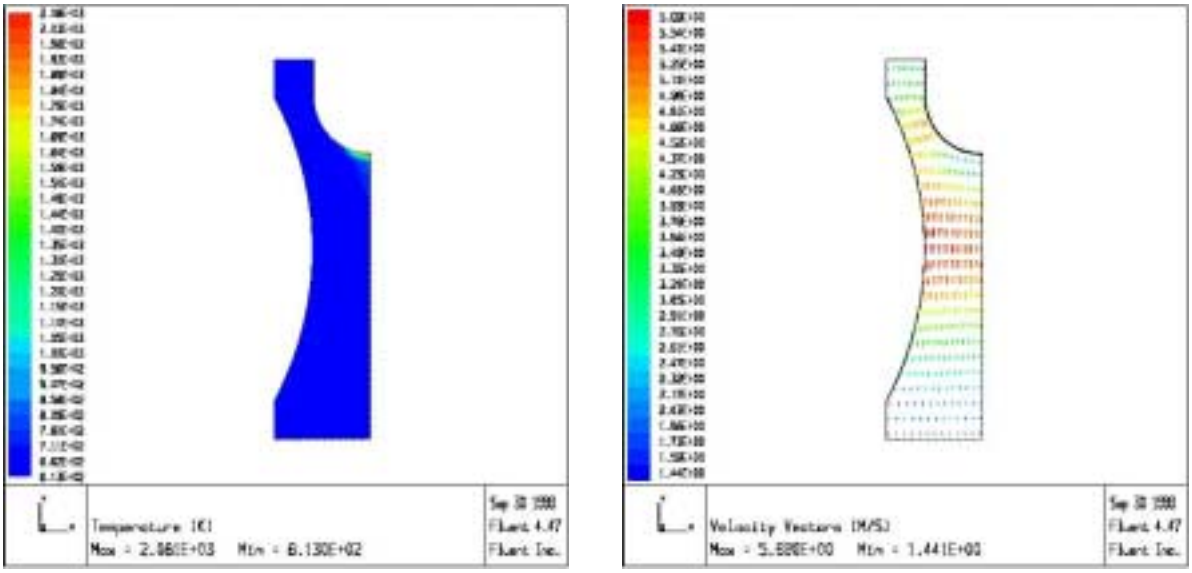

Table 1. **Maximum temperature for the single window**

Bottom inlet velocity (m/s)	1.1	1.35	1.5	2.0
Max. temp. (°C)	2 277	2 086	2 003	1 808

The coolant flowing direction is x-directional co-ordinate and the vertical direction of the coolant flowing is the y-directional co-ordinate. The spacing of the y-directional cells is 1 mm. We used the same heat generation rates for the inner and outer windows as shown in Figure 2. The heat transfer of the lower surface of lower window is treated by the heat transfer coefficient obtained by the calculation of the single window.

Maximum temperatures in the double windows are presented in Table 2. The maximum temperature in the inner window reaches 1 580°C. This value is higher than the window melting temperature. The inlet velocity of the Pb-Bi coolant flowing in the narrow channel must be larger than 6 m/s. As a result, the maximum temperature in the lower window reaches 1 077 °C for a 1.1 m/sec bottom inlet velocity of the single window and 927 °C for a 2.0 m/s bottom inlet velocity.

Table 2. **Maximum temperature for the double window**

Bottom inlet velocity (m/s)	1.1	1.35	1.5	2.0
Upper window (°C)	1 580	1 580	1 580	1 580
Lower window (°C)	1 077	1 027	997	927

Figure 5. **Temperature distribution of the double window case**

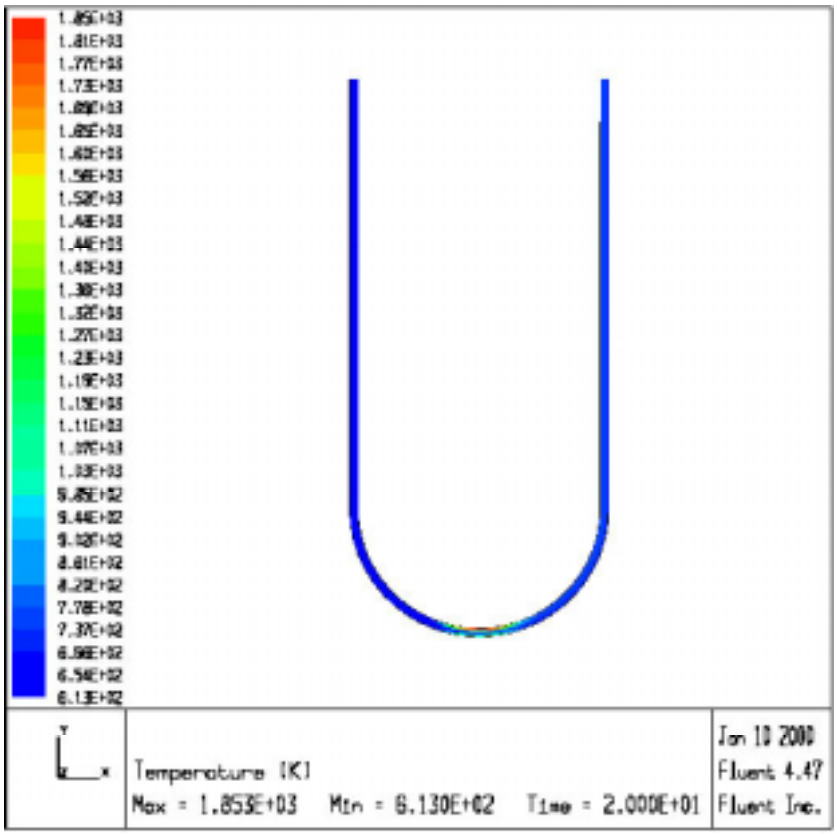

5. 3-D calculation

Figure 6 shows target geometry for FLUENT 3-D calculations. The beam channel is assumed to be rectangular to simplify the calculation. We first calculated the temperature of the bottom Pb-Bi and the single window part and then we calculated the double window part separately. In 3-D calculations, the velocity of up-coming Pb-Bi is fixed to be 2 m/s and 3 different beam currents are used, which are 2 mA, 10 mA and 20 mA. The velocity of Pb-Bi flowing between windows is 6 m/s.

Figure 6. **Target geometry for 3-D calculation**

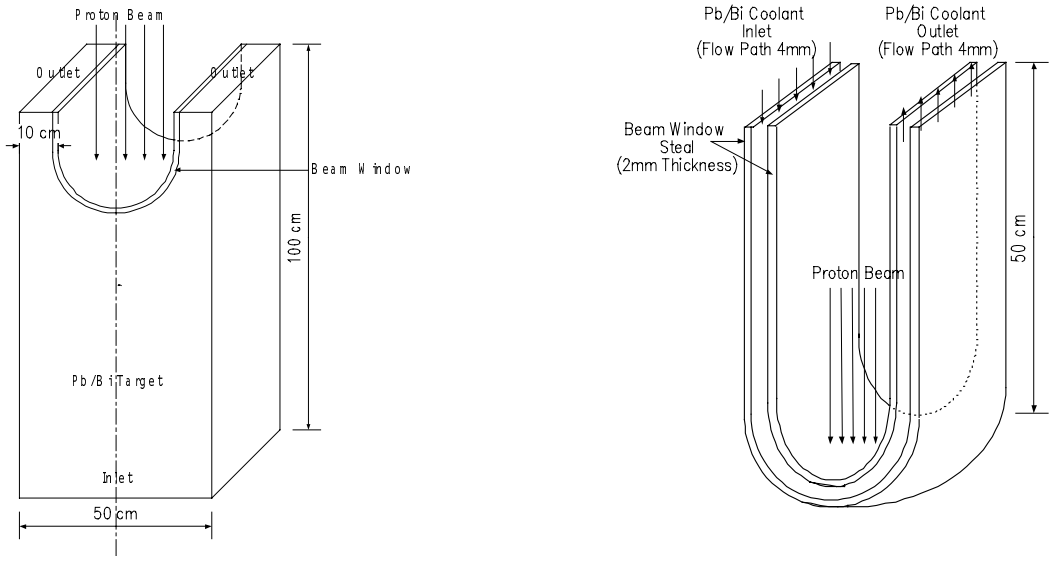

The maximum temperature of the single window was calculated to be 571°C in the case of a 2 mA beam. In the same case, the maximum temperature of the upper and lower window are found to be 464 and 429°C, respectively. Tables 3 and 4 show the maximum temperatures of the single and double window for 3 different beam currents.

Table 3. **Maximum temperature for the single window**

Beam current (mA)	2	10	20
Max. temp (°C)	571	1 497	2 657

Table 4. **Maximum temperature for the double window**

Beam current (mA)	2	10	20
Upper window (°C)	464	958	1576
Lower window (°C)	429	767	1187

After using FLUENT to produce a 3-D temperature distribution for the window, the result is transferred to ANSYS to calculate the thermal stress of the upper and lower window. Figure 7 shows the results of the ANSYS calculation. The maximum Von Mises thermal stresses are respectively about 185 and 97 MPa for the upper and lower beam window. In the stress calculation, the beam shape is assumed to be rectangular for the simplicity of calculation.

Figure 7. **Thermal stress distribution of the upper window for a 2 mA beam**

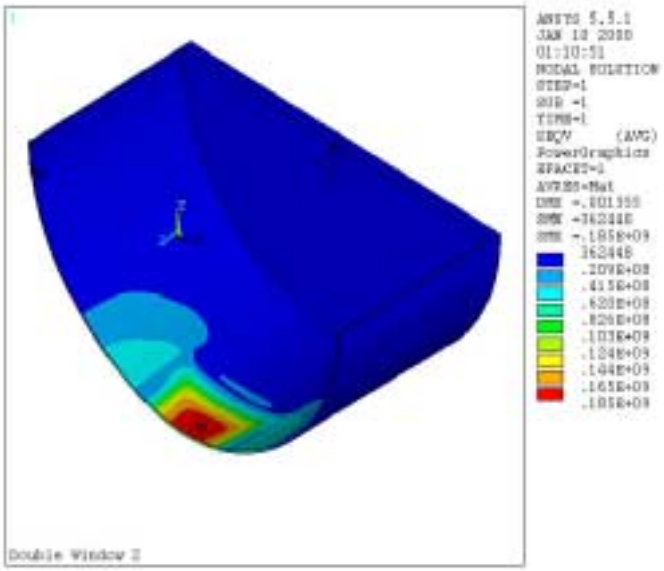

6. Conclusion

The thermal hydraulic and stress analysis of the liquid Pb-Bi target and beam window have been presented in this paper. Based on 2-D and 3-D analysis, temperature and velocity distributions were studied using FLUENT. We used ANSYS to calculate the stress of the beam window. A double window system was introduced to enhance the window cooling. The velocity of Pb-Bi flowing between two windows is set to be 6 m/s. When the beam current and velocity of up-coming Pb-Bi are 2 mA and 2 m/s respectively, the maximum temperature and thermal stress of the beam window were calculated to be 464°C and 185 MPa. Our target system is not a separate system, but a part of the whole sub-critical reactor. Therefore, the environment of the target should be considered to finalise the temperature and stress distribution. We are also considering the case of single window with a shape of hemisphere.

REFERENCES

[1] W.S. Park *et al.*, *Development of Nuclear Transmutation Technology*, KAERI/RR-1702/96, 1996.

[2] ANSYS User's Manual for Revision 5.0.

[3] R.E. Prael *et al.*, *User Guide to LCS: The LAHET Code System*, LA-UR-89-3014, 1989.

[4] Y. Dai, Proceedings of the International Workshop on the Technology and Thermal Hydraulics of Heavy Liquid Metal, 6.27-6.39, 1996.

SESSION IV
BASIC PHYSICS, MATERIALS AND FUELS

SUB-SESSION IV-C:
FUELS & TARGETS

FUEL/TARGET CONCEPTS FOR TRANSMUTATION OF ACTINIDES

A. Fernández, D. Haas, R.J.M. Konings, J. Somers
European Commission, Joint Research Centre, Institute for Transuranium Elements
P.O. Box 2340, 76125 Karlsruhe, Germany

Abstract

Four different concepts for fuels and targets for transmutation of (minor) actinides are discussed in the present paper. These include thorium-based mixed oxides, inert matrix mixed oxide, and composites based on mixtures oxide powders (CERCER) or mixtures of oxide and metal powders (CERMET). Fabrication methods have been investigated, especially taking account of the specific requirements for handling significant quantities of minor actinides (dust-free processes, remote handling). The processes tested at ITU are based on sol-gel and infiltration (INRAM) techniques or combination thereof. The processes are being validated first using cerium and then plutonium as simulants for the minor actinides, before the actual fabrication of Am- and Cm-containing materials begins in earnest following the completion of the construction of specially designed shielded cells (the MA-lab).

1. Introduction

Various fuel cycle concepts for partitioning and transmutation (P&T) of actinides are under discussion at present. In an evolutionary strategy, fast reactors are introduced in which the minor actinides are mixed with the plutonium in a mixed oxide, either uranium-based or eventually thorium-based. In such a multiple recycle scenario, the possibility to reprocess the fuel is of key importance. In a radial strategy, dedicated "transmuters" such as accelerator driven systems are introduced, with the aim to eliminate plutonium and minor actinide in a separate "second stratum" [1]. Dedicated fuel types are considered for this second stratum, which are characterised by a high minor actinide content and a high extent of transmutation. The latter can be achieved best if uranium is omitted from the fuel, as breeding of transuranium elements is avoided. This is especially important when the second stratum is a once-through process.

For the uranium-free fuels a wide variety of alternative matrix materials are considered, true inert material and "quasi" inert materials based on thorium. The actinide phase and the matrix can be combined in a homogeneous fuel form in which the actinides form a solid solution with the matrix, well known from the uranium-plutonium mixed oxide fuels. However, most inert-matrix mixed oxides of this type are generally characterised by a relatively low thermal conductivity. To overcome this, composite fuel forms are considered in which the matrix (a ceramic or a metal) improves the thermal properties of the fuel.

At the Institute for Transuranium Elements (ITU) some of these fuel and target options for transmutation of actinides are being studied, with emphasis on clean and, thus, dust-free fabrication methods for minor actinides (specifically americium and curium). A process consisting of a combination of SOL-GEL and infiltration techniques [2,3] is being developed and used for the fabrication of the following oxide-based fuel/target forms in a pellet-type fuel packing:

- Thorium-based mixed oxide (THOMOX), with the actinides incorporated as a solid solution in a ThO_2 matrix.
- Inert-matrix mixed oxide (IMMOX), where the actinides are incorporated in an yttria-stabilised zirconia (YSZ) solid solution.
- Ceramic-ceramic composite (CERCER), in which the actinides are in (near) spherical YSZ particles which are dispersed in a MgO matrix.
- Ceramic metal composite (CERMET), again with the actinides in spherical YSZ particles, which are dispersed in Mo, Fe or Zr matrices.

Currently these processes are being tested and validated with cerium and plutonium. The actual fabrication of Am- and Cm-containing materials will be performed in shielded cells, which are under construction at present. These cells, which form a complete fabrication chain (the MA-Lab), are equipped with gamma- and neutron shielding in the form of lead (50 mm) and water (500 mm).

2. Thorium-based mixed oxide

The fabrication of thorium based mixed oxide fuels and targets for transmutation can be achieved directly using the sol-gel method to give the $(Th,MA)O_2$ product. This process has been validated at the ITU for the Uranium analogues in the SUPERFACT and TRABANT irradiation experiments in Phénix and HFR Petten, respectively [4,5]. The particular advantage of the process lies in the wide range of actinide content, which can be obtained. In the SUPERFACT experiment, for example, $(U_{0.55}Np_{0.45})O_2$ and $(U_{0.6}Np_{0.2}Am_{0.2})O_2$ targets were prepared, while in the TRABANT1 experiment

$(U_{0.55}Pu_{0.4}Np_{0.05})O_2$ fuels were prepared. The main disadvantage of the sol-gel method lies in the aqueous liquid wastes produced.

If only relatively small quantities of minor actinide are required (up to 20 mol %), the infiltration (INRAM) procedure, described in detail below for yttria-stabilised zirconia (YSZ) targets, offers an interesting alternative to the sol-gel technique. Due to its partial solubility in weak acid solutions, UO_2 does not readily satisfy one of the basic requirements of the INRAM process. In contrast, ThO_2 is ideally suited, and, given its low activity, microspheres thereof can be produced with limited operator shielding. In a further variation of the process, $(Th,Pu)O_2$ spheres can be manufactured in conventional glove boxes and infiltrated with minor actinide nitrate solutions to give $(Th,Pu,MA)O_2$ products. At the ITU initial investigations have been performed on the production of such $(Th,Pu)O_2$ microspheres. These investigations will be continued and the process tested with the infiltration of uranyl or cerium nitrate solutions, before being validated in the minor actinide laboratory.

3. Inert-matrix mixed oxide

The fabrication process for the inert-matrix mixed oxide fuel/targets is shown schematically in Figure 1. Yttria-stabilised zirconia spheres are produced by a sol-gel process. Feed solutions with a determined Zr/Y ratio are prepared from Zr and Y oxychloride salts. Following addition of a surface active agent and an organic thickener, the solution is dispersed into droplets by a rotating cup atomiser. The droplets are collected in an ammonia bath, where gelation occurs. After ageing, the resulting spheres are washed, dried using azeotropic distillation procedure, and calcined at 1 123 K. These spheres have a polydisperse size distribution in the 40 and 150 µm range, and their porosity is about 80%. X-ray diffraction indicates that they have a cubic crystal structure with a measured lattice parameter of 514.0 ± 0.3 pm, which is in agreement with the published value for $(Zr_{0.85}Y_{0.15})O_{1.93}$ (513.9 ± 0.1 pm) [6].

Figure 1. **Schematic representation of the fabrication process of the inert-matrix mixed oxide fuels/targets using the infiltration method. A photograph of the polydisperse spheres is shown on the left.**

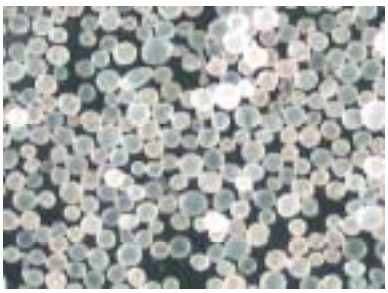

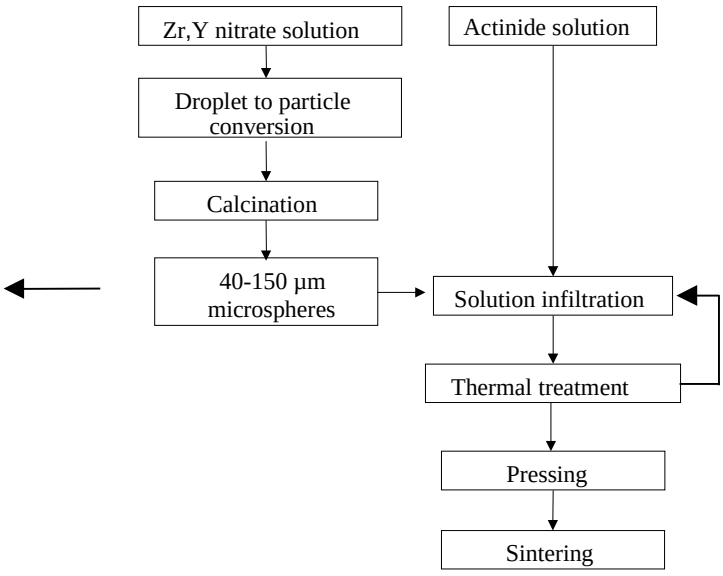

Once calcined the spheres are then infiltrated with a lanthanide (as simulant) or actinide solution. They are thermally treated to convert the infiltrated phase to the corresponding oxide. If higher

quantities of lanthanide/actinide are required this sequence of infiltration – calcination steps can be repeated. The metal content can be determined simply by gravimetric analysis of the beads before infiltration and after the calcination step. The resulting beads are free-flowing (at least for metal contents up to 40 wt%), and can be pressed directly into pellets, following addition of zinc stearate as lubricant. First tests have been made with Ce-nitrate solutions with concentrations of 200 and 400 $g \cdot l^{-1}$, and second tests with Pu-nitrate solutions with a concentration of 200 $g \cdot l^{-1}$, which for Pu is the maximum obtainable without risk of polymerisation and precipitation. In the case of Am, however, concentrations of up to 400 $g \cdot l^{-1}$ can be obtained also.

The results of the studies with cerium nitrate (200 $g \cdot l^{-1}$) indicate that about 40 wt% cerium can be infiltrated into the beads if 5 consecutive infiltration steps are used. X-ray diffraction measurements of the materials after sintering at 1923K for 6 hours in air showed that they have a cubic crystal structure, with the lattice parameter increasing with increasing CeO_2 content as described by Vegard's law (Figure 2).

Figure 2. **Left: lattice parameter of the $(Zr,Y,Ce)O_{2-x}$ spheres as a function of the Ce content; the solid line represent the Vegard's law for the $(Zr,Y)O_{2-x}$-CeO_2 solid solution. Right: geometric density of the pellets as a function of the infiltrated metal concentration.**

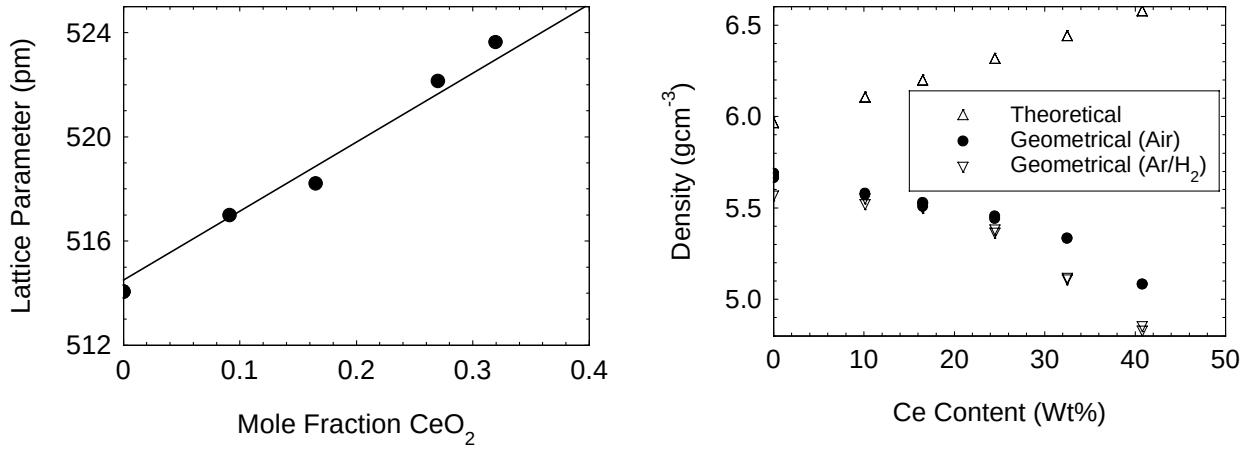

The density of the pellets manufactured in this way decreases with increasing CeO_2 content (for constant compaction pressure), whereas the theoretical density increases (Figure 2). A ceramograph of a $(Zr,Y,Ce)O_{2-x}$ pellet with 10wt% Ce (Figure 3) indicates it is devoid of cracks or other defects. The experiments with Pu, which are presently in progress, show comparable results. The density decrease may be related to the known change in mechanical properties of stabilised zirconia with increasing extent of stabilisation. It might be overcome by modifying the compaction pressure and the sintering atmosphere; such studies have been initiated.

Figure 3. **Left: Ceramograph of a $(Zr,Y,Ce)O_2$ pellet with 10% Ce. Right: Ceramograph of a $(Zr,Y,Ce)O_{2-x}$-MgO composite; the volume fraction of $(Zr,Y,Ce)O_{2-x}$ is 20%.**

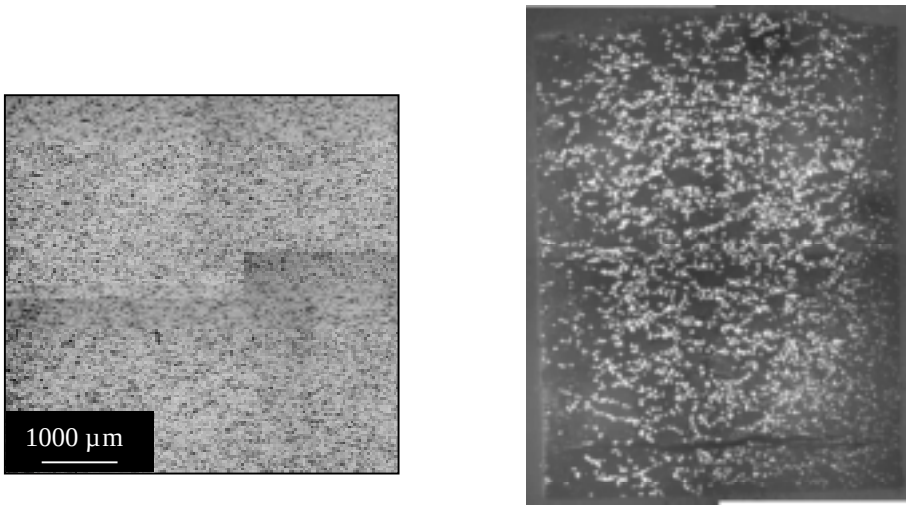

4. Ceramic-ceramic composite

CERCER composite pellets of $(Zr,Y,Ce)O_2$-MgO were fabricated by mixing $(Zr,Y,Ce)O_2$ spheres with MgO granules, using Zinc stearate as lubricant. The pellets were sintered at 1923K for 6 hours in air. The $(Zr,Y)O_2$ spheres were fabricated by the rotating cup, as described above, and the 80-90 µm and 125-140 µm fractions were selected, by sieving, for infiltration with a Ce-nitrate solution with a concentration of 400 $g \cdot l^{-1}$. A commercial MgO powder (CERAC M-1017) was granulated (size fraction 50200 – 80 µm) and either used directly or mixed with the original fine powder. Tests on MgO pellets without YSZ macrospheres showed that by pressing the different mixtures of granules, densities of greater than 95% of the theoretical value were obtained in all cases.

The resulting products in these experiments did not prove satisfactory, which is in contrast to previous work on $(Zr,Y,Ce)O_2$- $MgAl_2O_4$ composite pellets [7]. The $(Zr,Y,Ce)O_2$-MgO CERCERs always exhibit many cracks in the pellets, predominantly between the spheres (Figure 3). To understand this behaviour, dilatometer (Netsch DIL 402) measurements of the sintering behaviour of on $(Zr,Y)O_2$, $(Zr,Y,Ce)O_2$ spheres, MgO and $MgAl_2O_4$ were performed. The results shown in Figure 4 indicate distinct differences in the densification of the various materials. It is clear that MgO densifies much more (DL/L = 22.0%) than the $(Zr,Y,Ce)O_{2-x}$ spheres (DL/L = 14.7%) and, moreover, the densification starts at a somewhat lower temperature. In contrast, the extent of densification of $MgAl_2O_4$ is significantly less (DL/L = 18.0%) and starts at temperatures above that of the $(Zr,Y,Ce)O_{2-x}$ spheres. This implies that the sintering behaviour of the two powders in the $(Zr,Y,Ce)O_2$-MgO CERCER are so distinct so that cracks are difficult to avoid. This would require an extensive investigation to manipulate the properties of both powders to match another one. Tests on calcining the $(Zr,Y,Ce)O_2$ at lower temperature proved unsuccessful, as it appeared that the organic additives were not sufficiently removed from the spheres. Preliminary tests on calcining the MgO granules at higher temperatures (up to 1273 K) were also unsuccessful as the sintered pellets show multiple cracks. A solution thus must be found by modification of the sintering properties of the MgO powder. Alternatively, one could consider the reduction of the size of the beads, which will reduce the stresses during sintering also. This will, however, have a penalty with respect to the undamaged volume fraction in the composite during its irradiation in a nuclear reactor.

Figure 4. **Densification of $MgAl_2O_4$, $(Zr,Y,Ce)O_{2-x}$, $(Zr,Y)O_{2-x}$, and MgO as a function of temperature.**

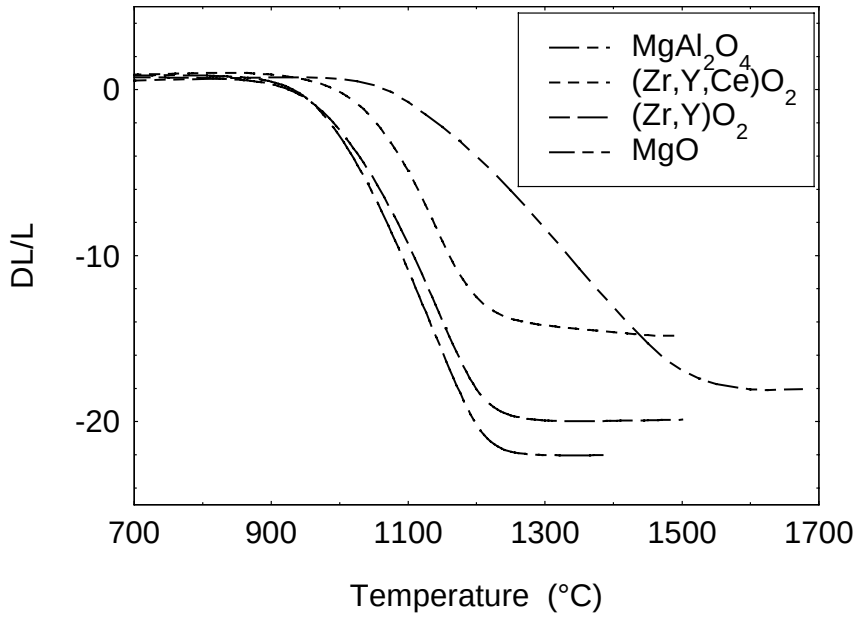

5. Ceramic-metal composite

CERMET composite pellets of $(Zr,Y,Ce)O_2$-Mo were fabricated by compaction of a mixture of the cerium infiltrated sieved fraction (112 – 125 μm) of the beads and commercial Mo powder (Merck) with addition of zinc stearate as lubricant. The pellets were sintered at 1923K in Ar/H_2.

The densities of the $(Zr,Y,Ce)O_2$-Mo CERMETS were typically in the order of 90-92% of the theoretical value. Visual inspection of the pellet surface and the ceramographs of sectioned samples show that they have perfect cylindrical geometry and excellent integrity without macro or micro cracks (see Figure 6). Nevertheless due to the fact that there is a very distinct difference in hardness of the two materials, many spheres were pulled out of the matrix during polishing, resulting in "apparent" porosity in the pellet. A typical ceramograph of a $(Zr,Y,Ce)O_2$-Mo is shown in Figure 6. It should also be noted that there is excellent physical contact between the Mo matrix and the macrospheres so that the maximum benefit of the high thermal conductivity of the Mo is achieved.

Figure 6. **Left: ceramograph of a(Zr,Y,Ce)O_{2-x}-Mo CERMET; the amount of (Zr,Y,Ce)O_{2-x} is about 20 vol%. Right: Detailed image of the sphere-matric interface in a (Zr,Y,Ce)O_{2-x}-Mo CERMET.**

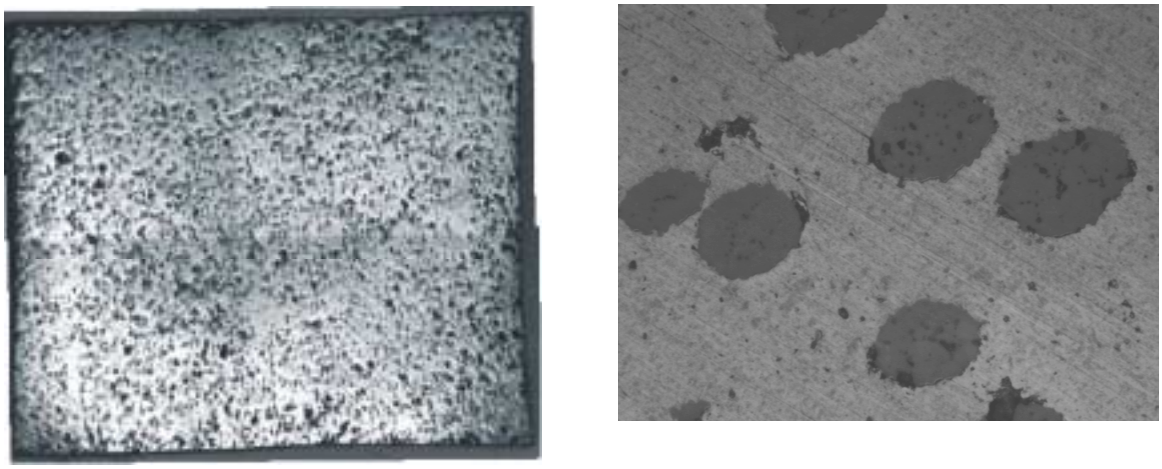

6. Conclusions and outlook

The results presented in this paper have demonstrated the feasibility of the fabrication of homogeneous zirconia- and thoria-based fuels for transmutation of minor actinides, using liquid processes such as sol-gel and infiltration. Though our experiments have been made with cerium and plutonium as simulants of americium, the previous experience with these techniques obtained in the SUPERFACT and EFTTRA experiments [2,4] gives confidence that they can be extended to americium without difficulties. The sol-gel technique offers the highest flexibility with respect to the actinide content in the material, but it produces significant amount of active liquid waste, which could be recycled in an industrial process. The active liquid waste is minimal when the infiltration technique is used, but the actinide content that can be obtained is limited. Moreover, the properties of the infiltrated YSZ powder change with increasing amount of infiltrant, resulting in an increase of the porosity with increasing infiltrated metal content. Though this is favourable to manage the helium accumulation typical for MA fuels [8], it will lead to a decrease of the thermal conductivity. Especially for ZrO_2-based material, where the thermal conductivity is already a limiting factor for its application, this may be unacceptable. Experiments to investigate the cause of these low densities have therefore been started.

The results presented in this paper for the (Zr,Y,An)O_2-MgO composite fuels are not promising. It seems technically difficult, if not impossible, to obtain fault-free composite pellets when the dispersed phase consists of spherical particles with a size of greater than 100 µm, which is required, if the radiation damage to the matrix is to be minimised [9]. The effect of reducing the size of the dispersed particles on the fabrication process will be tested. Smaller particles would lead to greater damage of the matrix during irradiation, but this penalty could be tolerated, if the improvement of the thermal behaviour is the decisive requirement.

Promising results have been obtained for (Zr,Y,An)O_2-Mo composite fuels, but the Mo matrix is not the prime candidate for CERMET fuel. Therefore the study of steel-based CERMET fuels will be initiated.

REFERENCES

[1] R.J.M. Konings and J.L. Kloosterman, *A View of Strategies for Transmutation of Actinides.* Progr. Nucl. Energy, in press (IMF'6 Special Issue).

[2] A. Fernandez, K. Richter, J. Somers. *Preparation of Spinel ($MgAl_2O_4$) Spheres by a Hybrid Sol-gel Technique*. 9th Cimtec- World Ceramics Congress. Advanced in Science and Technology 15. Ceramics: Getting into the 2000's. Part C (1999).

[3] K. Richter, A. Fernandez, J. Somers, *Infiltration of Highly Radioactive Materials: A Novel Approach to the Fabrication of Transmutation and Incineration Targets.* J. Nucl. Mater., 1997, 249, 121.

[4] N. Chauvin and J.-F. Babelot, *Rapport de synthèse commun CEA/ITU sur l'expérience SUPERFACT 1*, CEA Cadarache, Note Technique SDC/LEMC 96-2028 (1996).

[5] J. Somers, J.P. Glatz, D. Haas, D.H. Wegen, S. Fourcaudot, C. Fuchs, A. Stalios, D. Plancq, G. Mühling, *Status of the TRABANT Irradiation Experiments*, in Proceedings of the International Conference on Future Nuclear Systems, Global'99, Jackson Hole, Wyoming, 1999.

[6] JCPDS, International Centre for Diffraction Data, 30-1468, (1996).

[7] N. Boucharat, A. Fernández, J. Somers, R.J.M. Konings, D. Haas, *Fabrication of Zirconia-based Targets for Transmutation,* Progr. Nucl. Energy, in press (IMF'6 Special Issue).

[8] R.J.M. Konings, R. Conrad, G. Dassel, B. Pijlgroms, J. Somers, E. Toscano, J. Nucl. Mat., in press (also published as EUR Report 19138 EN (2000)).

[9] N. Chauvin, R.J.M. Konings, H.J. Matzke, *Optimization of Inert Matrix Fuel Concepts for Americium Transmutation.* J. Nucl. Mat., 1999, 274, 105-111.

AMERICIUM TARGETS IN FAST REACTORS

S. Pilate[1], A.F. Renard[1], H. Mouney[2], G. Vambenèpe[2]
[1]Belgonucléaire, Brussels
[2]Électricité de France, Paris & Lyon

Abstract

It would be advantageous to irradiate americium targets up to very large burn-ups, so as to throw them away to waste without any further reprocessing. Former studies considered the recycling of americium in conventional LWRs. But even after long irradiation times the incineration rate of americium, of the order of 50%, was not sufficient to avoid reprocessing and re-fabrication of targets.

In fast reactors, americium targets could be placed in special assemblies filled with a neutron moderator material which enhances Am incineration. Recent calculations show that a burn-up of 90% in the targets could be reached upon affordable irradiation times.

A major problem remains the choice of the inert support material of the targets. So far, the support materials currently envisaged have exhibited too large swelling rates. A type of support material virtually non swelling would be in the form of coated particles, like those irradiated without damage up to very high burn-ups in high temperature reactors. Studies are being launched on the feasibility of such Am targets with coated particles in fast reactors.

1. Introduction

It is a hard challenge in the nuclear fuel cycle to simultaneously insure a sustainable energy supply, and reduce the long-term toxicity of nuclear waste.

The first goal implies to reprocess the spent fuel and to recycle it to obtain the maximum energy generation. This leads to recycle plutonium up to a high burn-up, many successive times. The reactor system has to be (at least) self-sustaining in plutonium.

But the irradiation of plutonium gives rise to a build-up of americium, which in turn produces curium, which will later partly decay to plutonium again. The long-term toxicity of nuclear waste is dominated, for storage times ranging from 300 years to 100 000 years, by Pu, Am and Cm isotopes. In first approximation, the sum of the quantities of Pu, Am and Cm discharged from the reactor, related to the electrical energy produced, may be taken as an indicator of the long-term radio-toxicity.

The reactor type which allows best to extract energy from plutonium is the fast neutron reactor; it also limits to a large extent the Pu isotopic degradation and the formation of Am and Cm. However some minor actinides are still created and should be minimised. In particular, curium is an intense alpha and neutron emitter, so that its presence is a heavy burden in fuel cycle operations (reprocessing, transport, re-fabrication, handling).

In this paper, the following approach is favoured:

- Preference is given to a heterogeneous recycling of minor actinides, separated from plutonium and embedded in special target pins, with a support material inert to neutrons; in comparison, the homogeneous admixing of these actinides in the basic MOX fuel is more cumbersome and penalising.
- It would be an advantage to recycle americium only, leaving curium to the waste, provided however that a long once-through irradiation of these Am targets makes sense, with the aim to avoid if possible any spent target reprocessing.

This paper presents in part 2 the types of fuels and reactors considered. In part 3, different scenarios of energy generation either by PWRs or by LMFRs are considered for recycling, Pu, Am and Cm; a “double-strata” scenario with the introduction of accelerator driven systems (ADS) is also included for comparison.

Part 4 shows how a mixed scenario (PWRs+LMFRs) can be adapted to recycle Pu in the basic fuel, and incinerate Am and Cm, or Am only, in targets. A discussion of all these scenarios is conducted in part 5, with an hint at the penalties incurred in fuel cycle costs and electricity generation costs. Conclusions are drawn in part 6.

The paper makes use of calculations run at Belgonucléaire [1,2] and at CEA [3,4]. The results were sometimes normalised to improve their consistency.

2. Types of fuels and reactors

The paper is centred on oxide fuels, either in thermal or fast reactors.

The reference case for all comparisons is a 1 500-MWe PWR loaded with UO_2, irradiated to an average discharge burn-up of 60 GWd/t, which is the burn-up target for the years to come.

Pu recycling is being practised in PWRs nowadays. But so far, Pu was rarely recycled more than once, because of its important isotopic degradation and production of minor actinides under irradiation with thermal neutrons.

A way to allow Pu multi-recycling in PWR is the so-called MIX concept, in which the MOX Pu content is stabilised by adding enriched UO_2 to the MOX. In this way, Pu multi-recycling can proceed further in PWRs and reach an equilibrium in which Pu consumption equals Pu production. According to calculations, about 10 successive recycles are necessary to reach the equilibrium. Nevertheless, such a solution is costly, as nearly the same UO_2 enrichment is needed as in the reference UO_2 case.

The fast reactor concept considered is the EFR of 1 500 MWe, which was extensively studied by the EFR Associates as a successor to Superphenix [5]. The EFR cores retained, (140 GWd/t average burn-up with the design limit of 200 dpa damage in steel), are either self-sustaining in Pu with a thin fertile blanket, or moderately burning Pu when all fertile blankets are removed. The average Pu enrichment is about 20% in the first case and 23% in the second one.

CAPRA-type EFR cores with very high Pu enrichments of about 40% are not considered here: these strong Pu burners are producing a too large amount of minor actinides.

Table 1 gives the main fuel cycle characteristics and the types of reactors retained. The equilibrium is reached between production and consumption of Pu, or of Pu+Am+Cm.

Table 1. **Fuel characteristics and reactor types (Equilibrium cores)**

Reactor type	**Main fuel enrichment %**	**Fuel mass in reactor** (t/GWe)	**Residence time** (efp days)	**Actinides created (+) or destroyed (-) (kg/TWhe)**		
				Pu	**Am**	**Cm**
PWR (UO_2), 60 GWd/t	4.9 (U5)	86	1 780	+26	+1.65	+0.25
PWR (MIX), 60 GWd/t						
- Pu recycling only	4.5 (U5), 2.1 (Pu)	76	1 560	0	**+4.5**	**+2.24**
- Pu, Am, Cm recycling	4.5 (U5), 2.7 (Pu)	76	1 560	0	**0**	**0**
LMFR: EFR, 140 GWd/t						
- Pu recycling only	20 (Pu)	28.5	1 700	0	+3.5	**+0.28**
- Pu, Am, Cm recycling	20	28.5	1 700	0	0	**0**
- Pu burner	23	28.5	1 700	-20	0	**0**

3. Scenarios of Pu, Am and Cm homogeneous recycling

Calculations were first done with Pu only being recycled in these reactors, while Am and Cm are thrown to waste. Plutonium is supposed to be recovered at reprocessing up to 99.9%, a performance already achieved today. The quantities of Pu, Am and Cm, related to the electricity generation, in kg/TWhe, going to wastes, give an indicator of waste toxicity over storage times varying from 1 000 to 100 000 years.

When recycling Pu but not the minor actinides, PWR and LMFR reactors allow reducing the actinide waste by a factor of 4 or 7, respectively. To reduce them further requires to also recycle minor actinides.

Calculations were thus mainly run for the simultaneous recycling, in the form of a homogeneous MOX fuel, of Pu, Am and Cm. One assumes that, while 99.9% of Pu is recovered at reprocessing, 99% of Am and Cm can be recovered. The respective losses of 0.1 and 1% are coherent targets; as Am + Cm represent less than 10% of Pu in the reference case, it makes sense to assume 1% losses.

The core variants of PWR and FR have slightly larger enrichments than when recycling Pu alone, as they need to be self-sustaining in Pu, Am and Cm.

An interesting mixed scenario is built, combining PWRs, and LMFRs; the exact share results from mass balance calculations. The PWRs fuelled with UO_2 produce the actinides while the LMFRs incinerate them. The LMFR reactor type is an EFR without blankets, with an enrichment of about 23% Pu.

A further scenario is added for the sake of comparison. It follows the double strata principle. The major electricity generation is still provided by a mixed reactor system, PWR / EFR, but the latter recycles Pu only, while special dedicated reactors are assumed to burn minor actinides (they need some plutonium, too). Being fuelled mostly with minor actinides in a dedicated U-free fuel, they will have deteriorated safety coefficients (lower Doppler, larger coolant void reactivity), and this is the reason why they would preferably be accelerator driven systems (ADS), i.e. fast reactors with Keff ~ 0.95, and a neutron spallation source.

Calculations showed that it was possible to minimise the (expensive) second stratum to some 5% of the electricity production.

Table 2 gives the actinide throughputs, in kg/TWhe, for all these scenarios of homogeneous recycling of Pu+Am+Cm.

The first observation is that both all-PWR (MIX) and all-LMFR (EFR) scenarii offer equivalent actinide waste reduction factors, about 130. One noticeable difference is that the all-LMFR strategy recycles more Pu, but 5 to 6 times less Cm.

A mixed scenario with about 34% PWRs fuelled with UO_2 and 66% LMFRs of the EFR type without blankets can give a larger reduction factor, mainly because the recycled Pu quantities are lower. According to the EFR studies [5], the kWhe production cost is about 10% larger for EFR than for a PWR, so that a mixed reactor park is better from the economical point of view.

Surprisingly enough, a double strata strategy with 5% ADS is not better to reduce the actinide wastes. This is explained by the relative accumulation of minor actinides: on multiple recycling the quantities of minor actinides to be loaded remain relatively important. Of course the uncertainty on such quantities at equilibrium is quite large, so that the efficiency could be quoted roughly comparable.

It should be underlined that this conclusion depends on the assumptions made on the recovery rates at reprocessing: 0.1% for Pu and 1% for Am and Cm. If they were taken to be 0.1% for Pu and all Am and Cm isotopes (as many scientists do assume), the comparison would give different results, like:

- A factor 180 for the all-FR scenario.
- A factor 290 for the mixed PWR/EFR scenario.
- A factor 250 for the introduction of 5% ADS in a double strata strategy.

Nevertheless the trends observed above remain the same, with a slight advantage to the mixed scenario.

Table 2.**Homogeneous recycling of Pu, Am, Cm.**
Actinides throughputs (kg/TWhe).

Scenarii	**Core throughputs (kg/TWhe)**					**Actinide waste (kg/TWhe)**				**Waste reduction factors**
	Pu	**Am**	**Cm**	**TRU**	**U+ TRU**	**Pu**	**Am**	**Cm**	**Total**	
100% PWR UO_2	0	0	0	0	0	26	1.65	0.25	27.9	**Ref.**
All-PWR:	56	6.5	8.9	71	2 050	0.056	0.065	0.089	0.210	**130**
All-EFR:	143	5.7	1.6	150	705	0.143	0.057	0.016	0.216	**130**
Mixed PWR(UO_2)-EFR:	98	5.9	2.1	106	463	0.098	0.059	0.021	0.178	**160**
Double strata: Mixed PWR(UO_2)-EFR(Pu) + 5% ADS	99	10.5	3.65	113	381	0.099	0.105	0.036	0.24	**120**

4. Scenarios with minor actinide targets (heterogeneous)

Instead of polluting all MOX fabrication plants with Am and especially Cm, strong emitter of neutrons and of alphas (heating), it is preferable to handle the minor actinides in a distinct fabrication chain with reinforced shielding where minor actinides could be embedded in targets with a support material inert to neutrons.

Further simplifications and cost savings could be obtained:

a) By incinerating the targets in a single long irradiation, up to say, 90% burn-up, and by rejecting the spent targets to waste without reprocessing, so as to avoid the target reprocessing costs (target reprocessing has not been demonstrated so far).

b) By incinerating americium only, and rejecting curium at all stages.

To judge the pros and cons, cost savings are to be put in regard of the actinide waste reduction factors. It is clear that a) and b) lead to an imperfect incineration.

A priori, actinide targets could be inserted in thermal reactors. Calculations were done [2] with the following assumptions about the target pins:

- Loading onto corner positions of MOX assemblies in PWR reactors with the MIX concept (use of enriched ^{235}U to stabilise the Pu enrichment).
- Irradiation time 3 times longer than for the basic fuel pins.

But even with such prolonged irradiations, the results were disappointing, as 50% of the minor actinides loaded had not yet been fissioned at discharge.

For that reason, actinide targets are better loaded in fast reactors; they would be placed in special assemblies of the core, filled with a moderator material (B^{11}_4C, ZrH_2 and CaH_2 have been considered). The presence of moderator improves the efficiency of actinide transmutation. More details on these calculations are given in [4].

Table 3 gives, for the mixed PWR/EFR scenario, the actinide mass balances with the use of targets in EFR, for three different assumptions:

a) Multiple irradiation with intermediate reprocessing of Am+Cm targets, for which a 1% loss will be assumed, in coherence with the homogeneous cases above.

b) One irradiation only of Am+Cm targets up to a 90% burn-up; the spent targets are thrown to waste without reprocessing.

c) One irradiation of Am targets up to a 90% burn-up.

The second case was explicitly calculated [4]. Reaching 90% burn-up was shown to be possible by the insertion of 42 target assemblies in the EFR core which normally contains 388 fissile positions, and by the addition of a complete outer row of 78 target assemblies replacing the radial blanket. The residence time of the 42 inner target assemblies would reach 10 years, to be compared with the 6 years residence time of the EFR fissile assemblies.

Thanks to the introduction of these target assemblies, some important safety parameters are improved, like the Doppler effect (increased) and the coolant void reactivity (decreased); simultaneously, the limit in terms of steel damage (200 dpa) can still be guaranteed.

The results of Table 3 refer to a mixed PWR(UO_2)/EFR scenario: according to the calculations, 44% of the energy would be supplied by PWRs and 56% by FRs of the EFR type without blanket (These are preliminary results, the respective shares of the reactors could still slightly change).

It can be observed that a mixed PWR(UO_2)/EFR scenario with reprocessing gives about the same actinide waste reduction factor (160) in the homogeneous or in the heterogeneous option.

An imperfect target recycling leads to smaller reduction factors of, about respectively:

- 50 if (Am,Cm) targets are incinerated to 90% and not reprocessed anymore.
- 30 if targets loaded with Am only are incinerated to 90% and not reprocessed anymore.

Table 3. **Heterogeneous recycling of Am, Cm in targets. Actinide streams (kg/TWhe).**

Cases	In-core streams (kg/TWhe)					Actinide wastes (kg/TWhe)				Wastes reduction factor
	Pu	Am	Cm	TRU	U + TRU	Pu	Am	Cm[1)]	Total	
Scenario 44% REP UO_2 and 56% EFR[2)]	89			89	394	0.089 +	0.035 +	0.005 +		
Targets: a) Am, Cm reprocessed and recycled		***3.5***	***0.8***			*0.014*	–	*0.029*	0.172	**160**
b) Am + Cm up to 90% burn-up		***3.5***	***0.5***			*0.125*	*0.038*	*0.235*	0.527	**50**
c) Am alone to 90% burn-up		***3.5***	**–**			*0.086*	*0.032*	*0.690*	0.937	**30**

1) In case a, for Cm: 0.465 are rejected from the fuel and 0.230 from the targets.
2) Figures on this line correspond to the core basic fuel; figures of the following lines to the targets.

6. Discussion

The discussion will concern successively: the envisaged scenario, the heterogeneous option, the reduction of waste toxicity, the flexibility of target irradiation and the way to effectively reach 90% burn-up in targets.

6.1 The envisaged scenario

The mixed PWR/FR scenario envisaged above obviously relies on a revival of the fast reactor option. This assumes that fast reactors will be largely deployed, at the time uranium resources will become scarce, and thus more expensive. This was the subject of many studies in the past, and will not be discussed here again.

It will simply be recalled that for the introduction of fast reactors of the EFR type, cost estimates were published by the EFR associates [5]. They essentially set the EFR kWhe cost at a level about 10% higher than for the PWR, and the part of the EFR kWhe cost due to the fuel cycle was estimated to be also about 10%. Such estimates were supposed to apply when EFR type reactors would have largely been deployed.

6.2 Homogeneous or heterogeneous option

Inserting Am or Am + Cm into the MOX fuel itself of the FR in the homogeneous option brings additional difficulties in the re-fabrication plant, so that the fuel cycle cost will increase.

The deliberate insertion of Am in the MOX is an extrapolation from the present fabrication conditions of MOX fuel from an aged Pu. On this effect a comparison of dose rates was made in [6]. But the presence of Cm in the fuel would bring a severe penalty, which can hardly be estimated at present.

The heterogeneous option has the clear advantage to disconnect the fabrication routes of Pu (treated in MOX fuel as presently) and Am + Cm, which would be placed in target rods in a separate smaller fabrication facility. Being smaller, it is easier to shield.

According to the figures of Tables 2 and 3, the streams of minor actinides (in kg/Twhe) are reduced from:

	Am = 5.9	Cm = 2.1	in the homogeneous case
to	Am = 3.5	Cm = 0.8	in the heterogeneous case.

The cumbersome Cm streams have been significantly reduced.

It is clear that two sources of extra-costs can be avoided by, first, renouncing to target reprocessing, and especially by recycling Am only and not Cm. Does it make sense?

6.3 The associated reductions of waste toxicity

Is it useful to reduce the waste toxicity due to actinides by a factor of 30 or 50?

The recent studies on partitioning and transmutation were often setting a waste toxicity reduction factor of 100 as a good target. While the toxicity of the spent LWR fuel comes back to the “natural level”, i.e. that of the uranium ore initially used, after about 200 000 years, a reduction by a factor 100 means that this would be after about 2 000 years. The risk associated with human intrusion is obviously minimised.

A reduction by a factor 30 to 50 means that the doses associated with a human intrusion in the waste storage become comparable to those of a human intrusion into a uranium ore layer, not after 2 000 years, but after some 10 000 years.

Reduction factors by 30 to 50 thus appear to make sense.

On the other hand, such reductions would also be favourable for what concerns the heat release of the waste storage. This aspect deserves further studies.

6.4 The flexibility of target irradiation

The great flexibility of target irradiation in moderated assemblies of the fast reactor can be underlined. Indeed this option could be deployed progressively:

- In a first step, the targets would contain Am only, irradiated in one run, and thrown to waste after discharge: the actinide masses in wastes could be reduced by a factor 30, in a mixed PWR(UO_2)/EFR strategy, for a moderate increase of the kWhe cost only.

- A later step could be to add Cm to the Am targets, and burn them in the same way; the waste reduction factor would somewhat increase to 50, but the cost would also increase.
- Later on, and if the need is recognised, the reduction factor might be improved progressively up to about 160, provided that the targets of minor actinides are reprocessed and recycled.

Such versatility is attractive. The needed R&D programme in support, engaged step by step, remains at a moderate level.

6.5 Ways to reach 90% burn-up in targets

Research has been engaged on Am targets. Many European laboratories have started fabrication and irradiation of such targets. In particular, the EFFTRA-T4 experiment with fabrication made at ITU and irradiation in the HFR reactor at Petten, supported by other partners, has reached an Am burn-up of 28% [7]. A problem was however raised by the large swelling of the spinel matrix, which would not allow much longer irradiation. The EFFTRA partners are searching for improvements.

Among the possible solutions, a promising one is offered by the technology of Pu coated particle fuel, as successfully experienced in the DRAGON experimental reactor [8]: this particle fuel did not swell even after a 60% burn-up corresponding to almost complete depletion of the Pu. The adaptation of this process to Am targets deserves therefore careful feasibility verifications.

Studies have just been started at BELGONUCLEAIRE and EDF to assess the possibility of an adaptation of this type of fuel to Am targets, to make them resistant to the important build-up of gas pressure related to helium and fission products, the goal being to effectively burn 90% of the Am loaded.

7. Conclusions

This paper has underlined how attractive is the concept of putting Am, or Am + Cm targets on special moderated positions of an EFR core. Their irradiation up to 90% burn-up seems feasible in a long but still affordable irradiation.

It was shown by calculations that, if reprocessed and recycled, this target concept in a fast reactor could lead, in a reactor park made of a mix of PWRs (UO_2) and LMFRs, to an actinide waste mass reduction factor of 100 or more.

If the targets can reach a 90% burn-up and are not further reprocessed, this factor decreases to about 50 (for the case of Am + Cm targets) or 30 (targets loaded with Am alone). Such reduction factors, though moderate, already represent sensible improvements of the waste storage conditions.

The flexibility of the concept is an advantage. The research might be first focused on Am target irradiation without reprocessing. It could progressively encompass the addition of Cm, and later the target reprocessing.

A problem remains the integrity of targets with a burn-up as high as 90%. Inert support materials irradiated so far exhibited a large swelling rate. The concept of particle coated fuel, virtually non-swelling, deserves to be examined for application to Am targets. Studies on this concept are starting.

REFERENCES

[1] Th. Maldague *et al*., *Core Physics Aspects and Possible Loading for Actinide Recycling in Light Water Reactors*, Global'95 Conf., Versailles, Sept. 1995.

[2] Th. Maldague *et al*., *Recycling Schemes of Americium Targets in PWR/MOX Cores*, 5th Information Exchange Meeting on Actinide and Fission Product Partitioning and Transmutation, Mol, Belgium, Nov. 1998, EUR 18898 EN, OECD/NEA (Nuclear Energy Agency), Paris, France, 1999.

[3] J.Y. Doriath *et al*., *Scenario with Inert Matrix Fuel: a Specific Study*, 6th Inert Matrix Fuel Workshop, Strasbourg, May 2000.

[4] C. De Saint Jean *et al*., *Optimisation of Moderated Targets for the Incineration of Minor Actinides in a Fast Reactor in the Framework of Scenario Studies*, to be submitted to Global 2001 Conf., Paris.

[5] J.C. Lefevre *et al.*, (EFR Associates): *European Fast Reactor: Outcome of Design Studies*, 1998.

[6] A. Renard *et al.*, *Fuel Fabrication Constraints when Recycling Americium*, Global'97 Conf., Yokohoma, Oct. 1997.

[7] R. Konings *et al.*, *Transmutation of Americium and Technetium: Recent Results of EFFTRA*, 5th Information Exchange Meeting on Actinide and Fission Product Partitioning and Transmutation, Mol, Belgium, Nov. 1998, EUR 18898 EN, OECD/NEA (Nuclear Energy Agency), Paris, France, 1999.

[8] H. Bairiot *et al*., *Plutonium Coated Particles Development*, Nuclear Technology, Vol. 23, Sept. 1974.

RESEARCH ON NITRIDE FUEL AND PYROCHEMICAL PROCESS FOR MA TRANSMUTATION

Y. Arai, T. Ogawa
Japan Atomic Energy Research Institute
Tokai-mura, Naka-gun, Ibaraki-ken, 319-1195, Japan

Abstract

Research on nitride fuel and pyrochemical process for transmutation of long-lived minor actinides (MAs) in JAERI is summarised, focusing on the recent results following those presented at the last conference in Mol. Fabrication of MAs nitride, irradiation tests of nitride fuel and development of nitride/pyrochemical process have been carried out in JAERI based on the double-strata fuel cycle concept, in which MAs are transmuted to short-lived or stable nuclides by sub-critical accelerator driven system (ADS) with nitride fuel.

1. Introduction

The partitioning and transmutation (P&T) study in Japan, so-called OMEGA programme, is entering the second phase after the C&R by Atomic Energy Committee (AEC) conducted in 1999. Japan Atomic Energy Research Institute (JAERI) has proposed the transmutation of long-lived MAs such as Np, Am and Cm using sub-critical ADS with nitride fuel based on the double-strata fuel cycle concept. Besides the construction of high-energy proton accelerator and design study of transmutation plant, the technological development of separation of MAs from high-level waste (HLW), fabrication of MAs nitride fuel and reprocessing of the spent fuel is the important subject investigated hereafter.

In the double-strata fuel cycle concept, commercial fuel cycle and MAs transmutation fuel cycle are designed and operated independently. The former insists on economy and reasonable utilisation of Pu in both LWR and FBR cycles, while the latter focuses on effective transmutation of hazardous MAs. Nitride is suitable for the fuel material for MAs transmutation from the viewpoint of supporting hard neutron spectrum and heat conduction ability. In addition, actinide mononitride with NaCl-type structure will have a mutual solubility leading to the flexibility of accommodating variable composition in the fuel. Pyrochemical process is used for the reprocessing of spent fuel, since it has several advantages over the wet process in case of treating MAs concentrated with large decay heat and fast neutron emission. One of the drawbacks of nitride fuel is that we must use nitride fuel with ^{15}N enriched nitrogen in this case. But the pyrochemical reprocessing has the practical feasibility of recycling expensive ^{15}N.

In this paper the research on nitride fuel and pyrochemical process for MAs transmutation in JAERI is summarised, focusing on the recent results following those presented at the last conference in Mol [1]. Fabrication of MAs and Pu bearing nitride is described next. The present status of the irradiation programme of nitride fuel in JAERI is introduced in the third part. The fourth part concerns the subjects related to pyrochemical reprocessing of nitride fuel. Finally, summary and future subjects are given in concluding remarks.

2. Fabrication of MA nitride

2.1 AmN and (Cm,Pu)N

Carbothermic reduction was applied to the preparation of AmN and (Cm,Pu)N for the first time [2,3]. The experiments were carried out in JAERI's hot cells of Waste Safety Testing Facility (WASTEF). Starting materials were $^{243}AmO_2$ and $^{244}CmO_2$ powders obtained from Federal Science Centre of Russia and Oak Ridge National Laboratory, respectively. For the latter oxide, however, a considerable amount of ^{240}Pu has accumulated by the decay of ^{244}Cm during storage for about 30 years. The present composition of the oxide was determined to be $(Cm_{0.40}Pu_{0.60})O_2$ by alpha spectrometry.

The molar mixing ratios of C/Am for carbothermic reduction were chosen at 4.65 and 1.59, while those of C/(Cm+Pu) were 3.2 and 1.6. The mixtures of AmO_2+C and $(Cm,Pu)O_2$+C were heated in a molybdenum crucible at 1 573 and 1 773 K in N_2 gas stream, respectively. The CO gas release was monitored continuously by an infrared spectroscope. After the release of CO gas subsided, the flowing gas was changed to N_2-4%H_2 mixed gas. The reason that we lowered the heating temperature for AmN than for (Cm,Pu)N by 200 K is to avoid the loss of Am by vaporisation [4,5]. On the other hand, heating

temperature for (Cm,Pu)N followed the case for PuN since metallic Pu and Cm almost have the same vapour pressures. Characteristics of the products of carbothermic reduction were examined by X-ray diffraction analysis.

The formation of AmN and (Cm,Pu)N with NaCl-type structure was confirmed in all cases after carbothermic reduction. However, oxide phases were also identified in case the initial mixing C/M ratios (M = Am or Cm + Pu) were smaller than 2.0 as anticipated. The remaining oxides were monoclinic Am_2O_3, and the mixtures of monoclinic Cm_2O_3 and hyperstoichiometric bcc Pu_2O_3 in the respective cases. This result might be related to thermodynamic stability of sesquioxide in transplutonium elements compared with their dioxide. Conditions of the carbothermic reduction and results of X-ray diffraction analysis are summarised in Table 1.

The lattice parameter of AmN with initial C/Am ratio of 4.65, 499.8 pm, almost agreed with the value of AmN prepared by metal or hydride route. On the other hand, the lattice parameter of $(Cm_{0.40}Pu_{0.60})N$ with initial C/(Cm + Pu) ratio of 3.2 almost agreed with the value estimated from Vegard's law between CmN and PuN. This result confirmed the mutual solubility of CmN and PuN, which is one of the advantages of nitride fuel for transmutation of MAs. Apparatus for chemical analysis are under installation in the hot cell for examining chemical purity of the nitrides.

Table 1. **Conditions of carbothermic reduction and results of X-ray diffraction analysis for AmN and (Cm,Pu)N**

Starting composition	**Temperature (K)**	**Flowing gas (Time)**	**Phases identified**	**Lattice parameter (pm)**
AmO_2 + 4.65C	1 573	N (1.7 h) + N -4%H (1.7 h)	AmN	499.8 ± 0.1
AmO_2 + 1.59C	1 573	N_2 (5 h)	AmN Am_2O_3	500.3 ± 0.1
$(Cm,Pu)O_2$ + 3.2C	1 773	N_2 (4 h) +N_2 - 4%H_2 (4 h)	(Cm,Pu)N	494.8 ± 0.1
$(Cm,Pu)O_2$ + 1.6C	1 743	N_2 (5 h)	(Cm,Pu)N Cm_2O_3, bcc Pu_2O	497.4 ± 0.2

2.2 Np(C,N)

Carbonitride is an intermediate product of carbothermic reduction for synthesising mononitride. In carbothermic reduction, an excess amount of carbon is usually added to dioxide and the residual carbon is removed by subsequent heating in N_2-H_2 mixed gas stream as in the above case. It is known that the residual carbon exists in carbonitride solid solution or as free carbon, depending on nitrogen partial pressure and temperature. Here, a thermodynamic consideration is given to Np(C,N) in order to investigate the reasonable condition for synthesising high-purity mononitrides.

Starting materials were $^{237}NpO_2$ and reactor-grade graphite powders obtained from Harwell laboratory of UK and Graphitwerk Kropmühl of Germany, respectively [6]. At first, two-phase specimen of <Np(C,N)> + <C> was prepared by heating $^{237}NpO_2$ + 2.8C mixtures in N_2 stream at 1 773 K. Then it was heated to equilibrium in different temperatures and nitrogen partial pressures; at

1 723, 1 823 and 1 923 K in N_2, N_2/Ar = 1/1 and N_2/Ar = 1/99 streams. X-ray diffraction analysis was carried out in order to determine the lattice parameter of Np(C,N) and to confirm that the products were still constituted by the two phases of <Np(C,N)> + <C>. The composition of Np(C,N) was calculated from the lattice parameter assuming Vegard's law between NpC and NpN. The reasonableness of the present experimental manner was confirmed by the preceding tests using U(C,N) and Pu(C,N) solid solutions, for which the thermodynamic properties were reported previously [7,8].

The equilibrium compositions of Np(C,N) determined from the present experiments were plotted in Figure 1. Since the specimen heated at 1 923 K in N_2/Ar = 1/99 stream deviated from the two-phase region, it was excluded in the analysis. It is seen in Figure 1 that the equilibrium composition of Np(C,N) shifts to nitride rich side as decreasing heating temperature and increasing nitrogen partial pressure during heating. On the other hand, the equilibrium composition was evaluated from thermodynamic calculation based on the following equilibrium:

$$[NpN]_{NpC} + \langle C \rangle = [NpC]_{NpN} + 0.5(N_2) \quad (1)$$

where $[NpN]_{NpC}$ and $[NpC]_{NpN}$ indicate one mole of NpN and NpC dissolved in Np(C,N), and free carbon and nitrogen gas are indicated as <C> and (N_2), respectively. At first an ideal solid solution model was applied to Np(C,N) and the solid lines in Figure 1 shows the calculation results based on this assumption. In calculation, Gibbs energy of formation of NpN was cited from a recent vaporisation experiment [9] and that for NpC from the table recommended by IAEA [10].

It is shown in Figure 1 that the results of experiments and thermodynamic calculation agree with each other within an experimental error in the present case. This agreement suggests that Np(C,N) solid solution could be treated as ideal one as is the case of Pu(C,N). Further, it was found from the present experiments that the soluble amount of carbide in mononitride decreases in order of UN, NpN and PuN; at 1 823 K under 1.05×10^5 Pa of nitrogen partial pressure, the equilibrium compositions of carbonitride coexisting with free carbon are U($C_{0.14}N_{0.86}$), Np($C_{0.05}N_{0.95}$) and Pu($C_{0.01}N_{0.99}$), for example [11]. This tendency was caused by relative thermodynamic instability of monocarbide in higher actinides. In the case of higher actinides, an increase in carbon to dioxide mixing ratio will not lead to increase of carbon impurity contents in the products, since excess carbon existing as free carbon is likely to be removed with relative ease compared with the case of carbonitride. The evolution of CO gas during the initial stage of carbothermic reduction is also promoted by increasing carbon to dioxide mixing ratio in general.

Figure 1. **Temperature dependence of equilibrium composition of $Np(C_{1-x}N_x)$ solid solution under N_2, N_2/Ar = 1/1 and N_2/Ar = 1/99 streams. Experimental results are compared with thermodynamic calculation assuming an ideal solution model.**

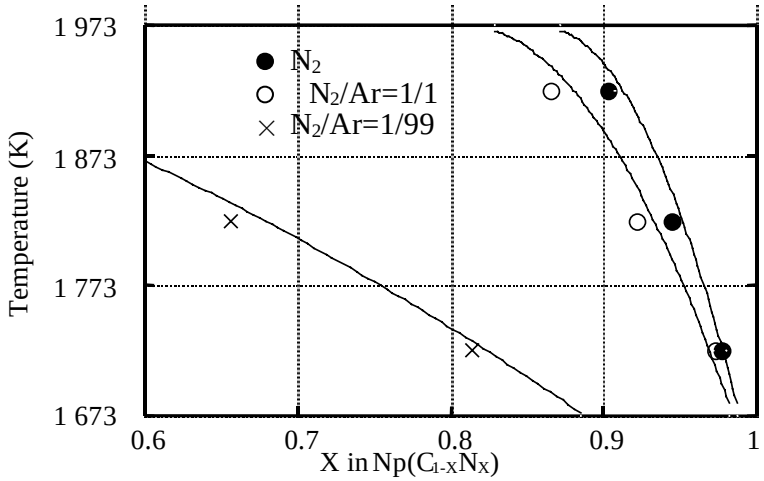

2.3 Nitride with inert matrix

Nitride fuel used in ADS will contain Pu besides MAs in order to control a core efficient multiplication coefficient nearly constant at ~0.95 during operation period. In addition, so-called inert matrix nitrides are added as a diluting material. From a material-science viewpoint, the requirement of the fuel for ADS is structural stability under operating temperature and high radiation fluence, high heat conduction ability, compatibility with cladding material and reprocessing technology and so on. But there has been little information on the behaviour of nitride fuel containing inert matrix for the moment. The purpose of the present study, fabrication of nitride containing inert matrix, is to provide basic information on the fabrication and feasibility of nitride fuel containing inert matrix. Here, ZrN, TiN and YN are arbitrarily chosen among the candidates of inert matrix. PuN pellets containing ZrN and TiN were fabricated by classical mechanical blending manner [12], while (Am,Y)N solid solution was prepared by carbothermic reduction of $AmO_2 + Y_2O_3$ mixture [13].

ZrN and TiN powders on the market and PuN prepared by carbothermic reduction of PuO_2 were used as starting materials. Classical mechanical blending manner was applied in this case, where Pu content was adjusted at 40 and 60 wt% for PuN + ZrN and 50 wt% for PuN + TiN pellets. The mixed powders were pressed into thin disk, heated in N_2-8%H_2 stream at 1 673 K and crushed into powders again. This procedure was repeated by three times, followed by pressing into green pellets and sintering in Ar stream at 2 003 K. The final heat treatment was carried out in N_2-8%H_2 stream at 1 673 K for control of stoichiometry.

X-ray diffraction pattern of PuN + ZrN pellets showed an almost single phase of NaCl-type structure. The lattice parameters almost agreed with the value estimated from Vegard's law between PuN and ZrN, which suggested the formation of (Pu,Zr)N solid solutions. On the other hand, two separate NaCl-type phases were identified for PuN + TiN pellet. The lattice parameters did not change from those of PuN and TiN, which suggested that the amount of PuN dissolved in TiN and that of TiN in PuN were negligibly small under the present experimental conditions. This contrast result between PuN + ZrN and PuN + TiN pellets could be explained by the relative lattice parameter difference (RLPD) speculated by Benedict [14].

A contrast result was also found for the density of the sintered pellets. PuN + ZrN pellets were sintered to higher density than 90% T.D. but only 76% T.D. was attained for PuN + TiN pellet under the same sintering condition. It is suggested that the formation of solid solution promotes sintering to high density and leads to toughness of pellets in this case. Microstructure of PuN + ZrN pellet (Pu, 40 wt%) is shown in Figure 2 compared with that of pure PuN pellet. It is seen that they have a similar grain size of 7-8 μm. The single phase is not a strict requirement for the fuel of ADS, but the control of microstructure becomes important if the fuel is the mixture of multi phases. Further, some consideration is needed to attain high density leading to toughness for PuN + TiN pellet.

On the other hand, $(Am_{0.1}Y_{0.9})N$ solid solution was prepared by direct carbothermic reduction of the mixture of $0.1^{243}AmO_2 + 0.45Y_2O_3$. The molar C/(Am+Y) ratio was chosen at 1.98, which was higher than the stoichiometric value of 1.55. The mixed powder was compacted into a disk and heated in N_2 stream at 1 573 K for reducing AmO_2 at first. Then temperature was raised to 1 773 K in N_2 stream for reducing Y_2O_3 and formation of (Am,Y)N, followed by removal of excess carbon in N_2-4%H_2 stream at 1 773 K. It was found from X-ray diffraction pattern that $(Am_{0.1}Y_{0.9})N$ solid solution without any oxide phases was prepared. The lattice parameter was 490.14 pm, which was close to the value assumed by Vegard's law between AmN and YN. No significant loss of Am by vaporisation was observed.

Figure 2. **Microstructure of (Pu,Zr)N pellet (Pu; 40 wt%) (right) compared with PuN pellet (left).**

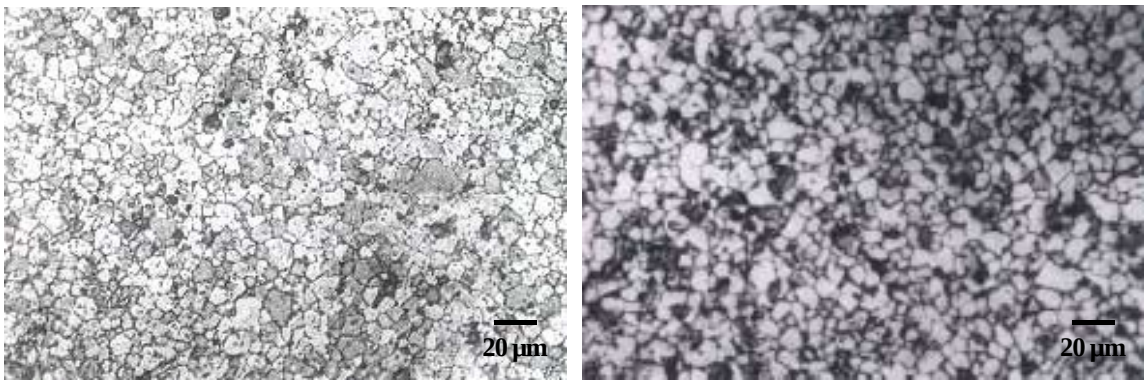

3. Irradiation test of nitride fuel

3.1 Irradiation of (U,Pu)N fuel

The irradiation test of (U,Pu)N fuel has been carried out in JAERI since 1990. For the moment, the post irradiation examinations (PIEs) of 4 He-bonded fuel pins irradiated at Japan Materials Testing Reactor (JMTR) have been completed and basic information on the fuel behaviour has been clarified [11]. On the other hand, the irradiation of two He-bonded (U,Pu)N fuel pins at fast test reactor JOYO was finished in 1999 based on the joint research JAERI and Japan Nuclear Cycle Development Institution (JNC). After cooling for a few months, PIEs were started in the end of last year.

As for the fuel pins irradiated at JOYO, some preliminary results have been obtained from the non-destructive PIEs carried out at JNC's hot cells. The maximum linear power and burn-up were evaluated at 78 kW/m and 39 000 MWd/t, respectively. Any failure of fuel pins was not observed.

The difference of two fuel pins exists in diametrical gap width between the (U,Pu)N fuel pellet and cladding tube of austenitic stainless steel, i.e. 0.17 and 0.32 mm, namely smear density of fuel pin, i.e. 82 and 78% T.D. According to the results of profilometry, a larger increase of diameter was observed for the higher smear-density fuel pin. However, the maximum increase was 0.04 mm ($\Delta d/d = 0.5\%$) at most, which would not affect the fuel performance. Fission gas release was evaluated at about 5 and 3% for the respective fuel pins, which were much smaller than those of MOX fuel irradiated under the similar condition. After the completion of non-destructive PIEs, destructive PIEs are carried out at both JAERI and JNC' hot cells.

3.2 Irradiation of U-free nitride

A candidate fuel for ADS is a mononitride solid solution containing MAs and Pu besides diluting inert matrix. However, there is little information on the irradiation behaviour of nitride fuel containing MAs or inert matrix. So a capsule irradiation test of U-free nitride fuel is planned in JAERI from 2002 at JMTR. According to a preliminary design, 2 He-bonded nitride fuel pins are encapsulated and possible fuel compositions are (Pu,Zr)N, (Pu,Y)N, PuN + TiN containing Pu of about 20 wt%. Cladding material is austenitic stainless steel and the linear power ranges from 30 to 50 kW/m according to the design study of ADS [15]. Following the detailed design of capsule and licensing procedure, the preparation of fuel pellets and fabrication of fuel pins are carried out in 2001. Acquiring new information on basic irradiation behaviour of U-free nitride fuel is expected. Further, irradiation tests of MAs nitride fuel are near-future subjects.

4. Pyrochemical reprocessing of nitride fuel

4.1 Preparation pyroprocess database

In the reprocessing stage of spent fuel, pyrochemical process based on the electrorefining in LiCl-KCl eutectic melt developed for metallic fuel [16] is applied to nitride fuel of ADS. In order to support the development of nitride/pyrochemical process, some basic research has been carried out in JAERI [17]. It includes high-temperature spectrophotometry, molecular dynamics and EXAFS for chloride systems besides electrochemical measurements in the LiCl-KCl eutectic melt. Thermodynamic calculation of LiCl-KCl-MCl_x-$CdCl_2$-MN-Cd-M-N-C-O system (M, actinide element) is also carried out using the free energy minimiser, Chemsage. The output should be consistent with reliable experimental data from electrochemical measurements. Further, JAERI is constructing "pyroprocess database" under the joint research with JNC. The user will be able to select data on free energy formation of super-cooled liquid chlorides, activity coefficients in the LiCl-KCl eutectic melt, stability diagram of M-N-Cl system and so on in the database.

4.2 Electrolysis of NpN and PuN

Anodic dissolution of NpN and PuN in W cage in the LiCl-KCl eutectic melt and subsequent recovery of Np and Pu metals at solid cathode were investigated [18,19]. Cyclic voltammograms of NpN and PuN were taken in the LiCl-KCl melt containing small amounts of $NpCl_3$ and $PuCl_3$. Typical result for NpN is shown in Figure 3. Anodic current caused by the following equation was observed in the voltammogram:

$$NpN = Np^{3+} + 3e^- + 0.5N_2 \quad (2)$$

Cathodic current was also observed in the reverse potential sweep of the voltammogram. Equation (2) was a slow reaction and considered as a rate-determining step of the electrodissolution of NpN, since the current did not increase in proportion to square root of the potential scanning rate, and the cathodic peak seemed to shift to more negative potential as increasing scanning rate.

On the other hand, the equilibrium potential of NpN in case of using Ag/AgCl electrode as a reference was determined as -0.779, -0.773 and -0.766 V at 723, 773 and 823 K, respectively, from electromotive force measurements. The equilibrium potential was interpreted by comparison with the theoretical redox potential of NpN. Since Ag/AgCl electrode was used as a reference electrode, the overall reaction could be expressed as:

$$NpN + 3AgCl = NpCl_3 + 0.5N_2 + 3Ag \quad (3)$$

So the theoretical redox potential of NpN, $E_{NpN\text{-}Ag/AgCl}$ could be derived from Gibbs energy of formation of $NpCl_3$, NpN and AgCl, activity of $NpCl_3$ in the LiCl-KCl eutectic melt and that of AgCl in the LiCl-KCl eutectic melt of the reference electrode and the partial pressure of N_2. For example at 773 K, by use of reported thermodynamic values and some assumptions, $E_{NpN\text{-}Ag/AgCl}$ can be expressed as:

$$E_{NpN\text{-}Ag/AgCl} = -0.730 + 0.0111 \ln p_{N2} \quad (4)$$

where p_{N2} denotes the partial pressure of N_2 gas in the LiCl-KCl eutectic melt. The first term of the right side of Equation (4), -0.730 V, corresponds to the standard redox potential of NpN at 773 K. This value is comparable with the equilibrium potential obtained by electromotive force measurement, -0.773V. Assuming that the difference between observed and theoretical potential is only caused by the nitrogen partial pressure in the LiCl-KCl eutectic melt, p_{N2} is calculated at 2.1 kPa. Although the measurement was carried out under high purity Ar gas atmosphere, N_2 gas generated by the electrodissolution of NpN would be present in the LiCl-KCl eutectic melt. However, the exact contribution of p_{N2} to the redox potential should be further investigated, since p_{N2} in the LiCl-KCl eutectic melt was not determined in the present study and the equilibrium potential might be influenced by the impurity and surface condition of NpN. The similar results were also obtained for the electrolysis of PuN.

Figure 3. **Cyclic voltammograms of NpN in the LiCl-KCl eutectic melt at 723, 773 and 823 K. Concentration of $NpCl_3$ and scan rate are 0.53 wt% and 0.01 V/s, respectively.**

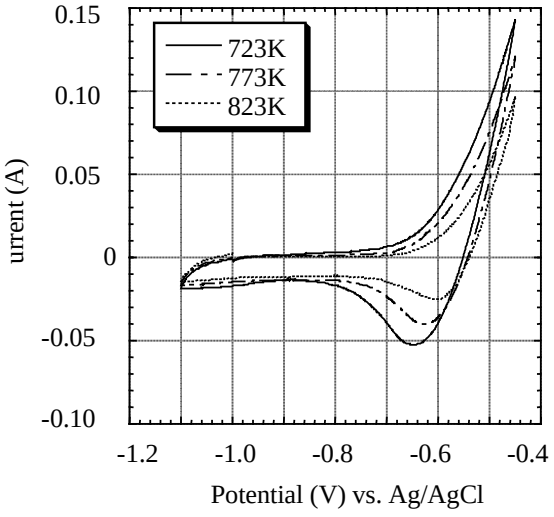

In addition to the voltammetric studies, the recovery of Np metal at solid cathode was carried out by the electrolysis of NpN by both potential-controlled and current-controlled method. In the potential-controlled method, the constant potential of -1.800 V was applied between Mo and reference electrodes with monitoring anode potential and flowing current. On the other hand, in the current-controlled method, the constant current of -0.020 A was applied during the electrolysis with monitoring cathode and anode potentials. It was suggested from the variation of the potentials that Np metal was successfully recovered at Mo cathode, while NpN being dissolved at anode.

The results of ICP-AES indicate that the concentration of $NpCl_3$ in the eutectic melt was kept constant during the electrolysis of NpN. Further, the amount of Np dissolved at anode was nearly equal to that of deposited Np at cathode estimated from the accumulated electric current. These results suggest that neptunium nitride chloride, NpNCl, would be scarcely formed unlike the formation of UNCl observed in the electrolysis of UN [20]. In the electrolysis of PuN, any formation of insoluble nitride chloride was not observed either. These results were possibly caused by relative high stability of trivalent ions of transuranium elements in the chloride eutectic melt.

Since the electrodeposites at cathode were the mixtures of Np metal and the eutectic melt, they were heated at 1 073 K for 3 600 s. in Ar gas stream in order to separate them. A fraction of the products was subjected to X-ray diffraction analysis. Some salt components such as LiCl, KCl and $NpCl_3$, however, were still identified in the diffraction pattern in addition to alpha-Np phase.

4.3 Electrode reaction of Np and Pu in liquid metal cathode

In the transmutation fuel cycle of double strata concept, Pu and MAs are recovered together at liquid Cd cathode. It is known that such recovery becomes possible since the free energy change of electrochemical reduction comes close at liquid Cd due to the decrease of activity coefficients of transuranium elements and rare earth metals. So it is inevitable that electrodeposites at liquid Cd are more or less contaminated by rare earth elements. On the other hand, Bi is another candidate of liquid cathode. The separation of transuranium elements from rare earth elements is easier at liquid Bi cathode than at liquid Cd. An advantage of Cd is that the recovered actinides would be easily separated by distillation of Cd. Here, the electrode reaction of Np and Pu at liquid Cd and Bi cathodes was investigated electrochemically [21].

Cyclic voltammograms of Np^{3+}/Np couple in the LiCl-KCl eutectic melt at liquid Cd and Bi electrodes are shown in Figure 4 compared with that at Mo electrode. The peaks corresponding to electrodissolution and electrodeposition can be found in the figure. The redox potential of Np^{3+}/Np couple at Mo electrode was obtained from electromotive force measurement. There is a difference between the redox potential of Np^{3+}/Np couple at Mo electrode and those at liquid Cd and Bi electrodes. The cathodic peaks at liquid Cd and Bi electrodes at 723 K appeared at more positive potential by about 0.2 and 0.5 V, respectively, compared with at Mo electrode. We have speculated that the potential shift was caused by thermodynamic stabilisation of actinides due to the formation of intermetallic compounds as mentioned below.

Redox potential of Np^{3+}/Np couple at solid electrode can be expressed as:

$$E_{Np3+/Np} = E_{Np3+/Np}^{0} + (RT/3F) \ln [Np^{3+}]/[Np] \quad (5)$$

where $E_{Np3+/Np}^{0}$ denotes standard potential vs. Ag/AgCl electrode, $[Np^{3+}]$ and [Np] their activities and F the Faraday constant.

On the other hand, the following equation for formation of intermetallic compound was assumed at liquid Cd cathode.

$$Np + n\ Cd = NpCd_n \tag{6}$$

Using Gibbs energy of formation of $NpCd_n$,ΔG_{NpCdn}, redox potential of Np^{3+}/Np couple at liquid Cd electrode can be written as:

$$E_{Np3+/Np-Cd} = E_{Np3+/Np} + \Delta G_{NpCdn}/3F - (RT/3F) \ln [NpCd_n] + (nRT/3F) \ln [Cd] \tag{7}$$

where $[NpCd_n]$ and [Cd] denote their activities. It seems reasonable to suppose activity coefficients of $NpCd_n$ and Cd at the liquid cathode and concentration of $NpCd_n$ are close to unity locally. Taking into the above assumptions, the potential difference between solid Mo and liquid Cd electrodes are written by:

$$\Delta E = -\Delta G_{NpCdn}/3F + (nRT/3F) \ln [Cd] \tag{8}$$

Experimental results agreed with the potential difference estimated from Equation (8) when the formation of $NpCd_{11}$ was assumed at 723 K and formation of $NpCd_6$ was assumed at 773 and 823 K. Using the same manner, it was suggested that the formation of $NpBi_2$ was most likely at the liquid Bi electrode.

Almost the similar results were obtained in the case of Pu^{3+}/Pu couple. In this case the formation of $PuCd_6$ was assumed and this speculation was also confirmed by the micro-probe analysis of the liquid Cd cathode after the recovery of Pu as mentioned below.

Figure 4. **Cyclic voltammograms of Np^{3+}/Np couple at Cd, Bi and Mo electrodes at 723 K. Concentration of $NpCl_3$ and scan rate are 0.465 wt% and 0.01 V/s, respectively.**

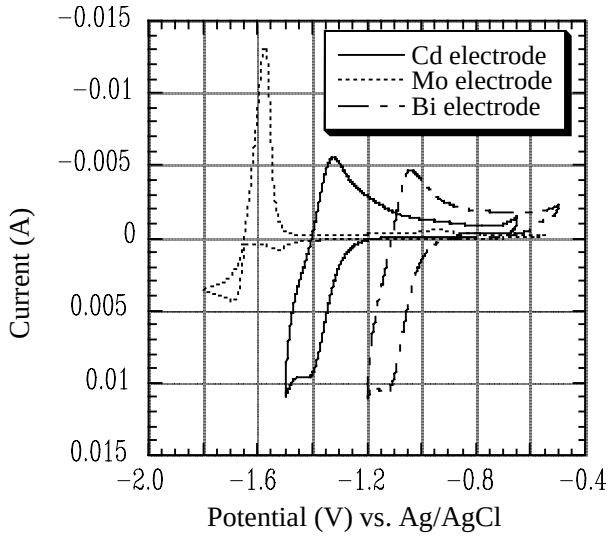

4.4 Recovery of Pu into liquid Cd cathode

This study was carried out under the joint research of JAERI and Central Research Institute of Electric Power Industry (CRIEPI) and the experimental details are described in another paper in this conference [22]. Electrorefining was carried out in the LiCl-KCl eutectic melt containing about

2 wt% of Pu at 773 K. For the moment, the recovery of ten-gram scale of Pu into liquid Cd cathode has been demonstrated with a concentration of Pu higher than 10 wt%, which is much higher than the solubility limit of Pu in liquid Cd at 773 K.

The surface of the liquid Cd after recovery of Pu was smooth and it was easily separated from the crucible. The crucible made of AlN seemed reusable under the present condition. After cutting and polishing, the liquid Cd cathode was subjected to electron probe microanalysis. It was confirmed that the recovered Pu seemed to have accumulated at the bottom of liquid Cd cathode. Further, the formation of $PuCd_6$ phase was confirmed as anticipated from the thermodynamic speculation mentioned above.

5. Concluding remarks

The recent results on nitride fuel and pyrochemical process development carried out in JAERI were presented. In addition to UN, NpN, PuN and their solid solutions, small amounts of AmN and (Cm,Pu)N were prepared by carbothermic reduction using ^{243}Am and ^{244}Cm nuclides. U-free nitride fuel diluted by inert matrix such as ZrN, TiN and YN was prepared and characterised for the first time. The physical and chemical property and irradiation behaviour shall be examined hereafter. The irradiation of 2 He-bonded (U,Pu)N fuel pins at fast test reactor JOYO was completed and PIEs are underway. As for pyrochemical reprocessing of nitride fuel, electrolysis of NpN and PuN, electrode reaction of Np and Pu at liquid Cd and Bi electrodes, and recovery performance of Pu into liquid Cd have been investigated.

The irradiation behaviour and physical and chemical properties of MA nitrides should be investigated hereafter. The irradiation test of U-free nitride is scheduled for 2002 at JMTR. Possible composition of the fuel is (Pu,Zr)N, (Pu,Y)N or PuN+TiN pellets. Electrorefining of burn-up simulated nitride fuel, nitride fuel fabrication from the liquid Cd cathode and its characterisation are the important subjects for the development of nitride/pyrochemical process.

In addition, a Module for TRU High Temperature Chemistry (TRU-HITECH) having three hot cells and one glovebox comes into construction stage under the joint research with the Japan Atomic Power Company (JAPC). Ten-gram order of ^{241}Am, hundred-milligram order of ^{243}Am and ten-milligram order of ^{244}Cm can be handled in TRU-HITECH besides U, Np and Pu. The research on Am and Cm in TRU-HITECH will start from 2002.

REFERENCES

[1] Y. Suzuki, T. Ogawa, Y. Arai, T. Mukaiyama, *Recent Progress of Research on Nitride Fuel Cycle in JAERI*, in Proc. 5th Information Exchange Meeting on Actinide and Fission Product P&T, Nov. 25-27, 1998, Mol, Belgium, EUR 18898 EN, pp. 213-221, OECD/NEA (Nuclear Energy Agency), Paris, France, 1999.

[2] M. Takano, A. Itoh, M. Akabori, T. Ogawa, S. Kikkawa, H. Okamoto, *Synthesis of Americium Mononitride by Carbothermic Reduction Method*, in Proc. Global'99: Nuclear Technology – Bridging the Millennia (Jackson Hole, Wyoming, Aug. 29-Sept. 3, 1999) (CD-ROM).

[3] M. Takano, A. Itoh, M. Akabori, T. Ogawa, M. Numata, H. Okamoto, *Carbothermic Synthesis of (Cm,Pu)N*, 10th International Symposium on Thermodynamics of Nuclear Materials (STNM-10) (Halifax, Nova Scotia, Aug. 6-11, 2000), to be published in J. Nucl. Mater.

[4] T. Ogawa, T. Ohmichi, A. Maeda, Y. Arai, Y. Suzuki, *Vaporisation Behaviour of (Pu,Am)N*, J. Alloys and Compounds, 224 (1995) 55-59.

[5] T. Ogawa, Y. Shirasu, K. Minato, H. Serizawa, *Thermodynamic of Carbothermic Synthesis of Actinide Mononitride*, J. Nucl. Mater., 247 (1997) 151-157.

[6] Y. Suzuki, Y. Arai, K. Okamoto, T. Ohmichi, *Preparation of Neptunium Mononitride by Carbothermic Reduction*, J. Nucl. Sci. Technol., 31 (1994) 677-680.

[7] M. Katsura, T. Sano, *The Uranium-carbon-nitrogen System*, J. Nucl. Sci. Technol., 3 (1996) 194-199.

[8] P.E. Potter, *A Note on the Plutonium-carbon-nitrogen System*, UK Report, AERE–M2156 (1969).

[9] K. Nakajima, Y. Arai, Y. Suzuki, *Vaporisation Behaviour of Neptunium Mononitride*, J. Nucl. Mater., 247 (1997) 33-36.

[10] C.E. Holley, Jr., M.H. Rand, E.K. Storms, in: *The Chemical Thermodynamics of Actinide Elements and Compounds, Part 6: The Actinide Carbides*, International Atomic Energy Agency, Vienna (1984) p.49.

[11] Y. Arai, T. Iwai, K. Nakajima, O. Shirai, Y. Suzuki, *Experimental Research on Nitride Fuel Cycle in JAERI*, in Proc. Global'99: Nuclear Technology – Bridging the Millennia (Jackson Hole, Wyoming, Aug. 29-Sept. 3, 1999) (CD-ROM).

[12] Y. Arai, K. Nakajima, *Preparation and Characterisation of PuN Pellets Containing ZrN and TiN*, J. Nucl. Mater., 281 (2000) 244-247.

[13] M. Akabori, M. Takano, A. Itoh, T. Ogawa, M. Numata, M. Shindo, *Fabrication of Americium Nitride Targets/Fuels for MA Transmutation*, 30iemes Journées des Actinides (Dresden, May 4-6, 2000).

[14] U. Benedict, *The Solubility of Solid Fission Products in Carbides and Nitrides of Uranium and Plutonium, Part II: Solubility Rules Based on Lattice Parameter Differences*, EUR 5766 EN (1977).

[15] T. Takizuka, T. Sasa, H. Tsujimoto, H. Takano, H. Takano, *Studies on Accelerator Driven Transmutation Systems*, in Proc. 5th Information Exchange Meeting on Actinide and Fission Product P&T, Nov. 25-27, 1998, Mol, Belgium, EUR 18898 EN, pp.383-392, OECD/NEA (Nuclear Energy Agency), Paris, France, 1999.

[16] Y.I. Chang, *The Integral Fast Reactor*, Nucl. Technol., 88 (1989) 129-138.

[17] T. Ogawa and Y. Arai, *Nitride/Pyroprocess for MA Transmutation and Fundamental Database*, OECD/NEA Workshop on Pyrochemical Separation, Avignon, France, March 14-15, 2000.

[18] O. Shirai, T. Iwai, K. Shiozawa, Y. Suzuki, Y. Sakamura, T. Inoue, *Electrolysis of Plutonium Nitride in LiCl-KCl Eutectic Melts*, J. Nucl. Mater., 277 (2000) 226-230.

[19] O. Shirai, M. Iizuka, T. Iwai, Y. Suzuki, Y. Arai, *Recovery of Neptunium by Electrolysis of NpN in LiCl-KCl Eutectic Melts*, J. Nucl. Sci. Technol., 37 (2000) 676-681.

[20] F. Kobayashi, T. Ogawa, M. Akabori, Y. Kato, *Anodic Dissolution of Uranium Mononitride in Lithium Chloride-Potassium Chloride Eutectic Melt*, J. Am. Ceram. Soc., 78 (1995) 2279-2281.

[21] O. Shirai, M. Iizuka, T. Iwai, Y. Suzuki, Y. Arai, *Electrode Reaction of Plutonium at Liquid Cadmium in LiCl-KCl Eutectic Melts*, J. Electroanalytical Chem., 490 (2000) 31-36.

[22] M. Iizuka, K. Uozumi, T. Inoue, T. Iwai, O. Shirai, Y. Arai, *Development of Plutonium Recovery Process by Molten Salt Electrorefining with Liquid Cadmium Cathode*, 6th Information Exchange Meeting on Actinide and Fission Product P&T, Madrid, Spain, Dec. 11-13, 2000, EUR 19783 EN, OECD/NEA (Nuclear Energy Agency), Paris, France, 2001.

TRANSMUTATION STUDIES IN FRANCE, R&D PROGRAMME ON FUELS AND TARGETS

M. Boidron[1], N. Chauvin[1], J.C. Garnier[1], S Pillon[1], G. Vambenepe[2]
[1]Direction des Réacteurs Nucléaires, CEA, Cadarache 13108 Saint Paul Lez Durance Cedex, France
[2]EdF, 12-14 Av. Dutrievoz, 69628 Villeurbanne Cedex, France

Abstract

For the management of high level and long-lived radioactive waste, a large and continuous research and development effort is carried out in France, to provide a wide range of scientific and technical alternatives along three lines, partitioning and transmutation, disposal in deep geological formations and long term interim surface or subsurface storage.

For the line one, and in close link with the partitioning studies, research is carried out to evaluate the transmutation potential of long-lived waste in appropriate reactors configurations (scenarios) relying on current technologies as well as innovative reactors. Performed to evaluate the theoretical feasibility of the Pu consumption and waste transmutation from the point of view of the reactor cores physics to reach the equilibrium of the material fluxes (i.e. consumption = production) and of the isotopic compositions of the fuels, these studies insure the "scientific" part of the transmutation feasibility.

For the technological part of the feasibility of waste transmutation in reactors, a large programme on fuel development is underway. This includes solutions based on the advanced concepts for plutonium fuels in PWR and the development of specific fuels and targets for transmutation in fast reactors in the critical or sub-critical state.

For the waste transmutation in fast reactors, an important programme has been launched to develop specific fuels and targets with experiments at various stages of preparation in different experimental reactors including Phénix. Composite fuels as well as particle fuels are considered. This programme is presented and recent results concerning the preparation of the experiments, the characterisation of the compounds properties, the thermal and mechanical modelling and the behaviour of U free fuels are given.

1. Introduction

For the management of high level and long live radioactive waste and in the frame of the first line of research identified in the French Law of December 91, the potential of a partitioning and transmutation strategy to reduce the quantity and the toxicity of the waste is to be evaluated (along with the other alternatives that are disposal in deep geological formations and long term interim surface or subsurface storage [1]). The research is centred on minor actinides (americium, curium, neptunium) which represent the majority of the long-term radiotoxic elements in the waste, once plutonium has been extracted, and certain fission products with a very long-lived isotope, relatively abundant and potentially mobile (technetium, iodine and caesium). The objective of the partitioning studies is to develop chemical processes to obtain advanced partitioning of radionuclides to complete the partitioning of uranium and plutonium. The development of extracting molecules and the validation of the basic concepts, which corresponds to the stage of scientific feasibility of this research, is currently underway, and the process validation (technical feasibility) is to be achieved for 2006.

Within the same time, the objectives of the transmutation programme are to evaluate the transmutation potential of long lived waste in appropriate reactor configurations (scenarios) relying on current technologies (Pressurised Water Reactor and Fast neutrons Reactors) as well as innovative reactors (with dedicated systems such as the accelerator driven systems) and also to study the materials to be used for the new type of fuels suitable for transmutation in order to define the first elements of adequate solutions.

After a general presentation of what is considered in the R&D programmes on transmutation and a short review of the scenarios studies, emphasis is led on the presentation of the research carried out on the materials needed for the future fuels necessary for a transmutation strategy.

2. Strategy for a long-term work programme

Three steps can be identified before a possible industrial development of the transmutation strategy, the first being the stage of scientific feasibility in which the possibility of transmutation is evaluated on the basis of the reactor cores physics, the second including detailed studies to obtain elements of technical feasibility in terms of fuel cycle impacts, safety and economic considerations and fuel development, and the third dealing with the industrial feasibility with a stage of demonstration in representative conditions of the chosen technologies.

Studies on transmutation deal with the two first steps with a special emphasis on the fuels studies, the development of fuels being one of the key points to reach the objectives of waste transmutation.

Feasibility of the transmutation have been considered in different parks of reactors taking into account in the first part of the scenarios the reactors of current technology (PWR and FR) ensuring electricity production as well as incineration of waste, and in the second part, the reactors dedicated to transmutation with high content of waste that can be either critical or ADS. The third part to be considered are the other innovative technologies and cycles like molten salt reactors and pyrochemistry that can be alternatives to the other ways. A first review of the results including scientific and technological feasibility is planned in 2001 for the scenarios dealing with reactors of current technology, in 2003 for the innovative reactors and in 2005 for the alternative ones.

Since plutonium is both a recyclable energy material and the main contributor to potential long-term radio toxicity, the start point of all the scenarios is the management of plutonium in the fleet of reactors and the research on transmutation is connected to the studies linked to the plutonium consumption (links identified in the Capra Cadra programme [2]), the development of advanced

concepts for plutonium consumption [3,4], and particle fuels [5] and the research on new nuclear technologies for the future. In addition to competitiveness, the new types of reactors will have to present marked progresses in terms of minimisation of natural resources, safety and reduction of waste production. These requirements induce research to develop fuels with good thermal characteristics, able to sustain high temperatures, to reach high specific power and high burn ups. The solutions to be found for the transmutation have to be connected to these developments

3. Transmutation scenarios

The scenario studies were performed to insure the theoretical (or "scientific") feasibility of the Pu consumption and waste transmutation from the point of view of the reactor core physics to reach the equilibrium of the material fluxes (i.e. consumption = production) and of the isotopic compositions of the fuels.

Taking the open cycle as a reference (Reference case in Table 1), five families of scenarios have been considered in agreement with the French National Commission of Evaluation; three scenarios rely on existing technology (PWR of the Franco-German European Pressurised Reactor–EPR type) using plutonium and optionally ensuring the incineration of minor actinides (Case 1); fast neutron reactors of the European Fast Reactor-EFR type ensuring the multirecycling of plutonium and minor actinides (Case 2) (optionally the mono-recycling of minor actinides); a combination of PWR (UOX and MOX) and fast neutron reactors (Case 3) to burn the plutonium and incinerate, according to the variety, the minor actinides and some long-lived fission products). The other two cases use innovative technologies (combination of PWR [UOX] reactors and dedicated systems such as the ADS); a double component park considers PWR and dedicated fast reactors (Case 4), and in the "double strata" system (Case 5), the first stratum contains PWR and fast neutron reactors that multirecycle the plutonium, and in the second stratum, the hybrids transmute the minor actinides and long-lived fission products.

The characteristics of the various reactor fleets considered are summarised in Table 1.

Table 1. **Description of scenarios**

Scenario	**PWR UO_2**	**PWR MIX**	**EFR**	**EFR**	**Dedicated FR U free Pu+Am+Cm (double component)**	**ADS (U free) (Mainly Am-Cm recycling) (double strata scenario)**
Ref.	100%					
1		100%				
2			100%			
3	44%			56%(1)		
4	79%				21%	
5	46%			49%(2)		5%

(1) Incineration in moderated targets.
(2) Pu recycling only.

The scientific feasibility of plutonium management and waste transmutation have been established for the different cases [2,6]:

- With homogeneous recycling of Pu and MA in the EPR reactors (Case 1), in the case of the homogeneous multirecycling with a ^{235}U enriched fuel (MIX) and in the EFR reactors (Case 2) that allow additional transmutation of LLFP in moderated targets.
- In the EPR – EFR park (Case 3) with homogeneous recycling of Pu and Np, and transmutation of Am and Cm in targets placed in a moderated neutron spectrum in the fast core.
- In the double component hypothesis (Case 4), around 20% of dedicated systems are needed to ensure Pu and MA consumption.
- In the double strata (Case 5), around 50% of the first stratum are EFR reactors burning Pu, 5% of dedicated systems assuming MA transmutation.

In terms of reduction of the radio toxicity of the ultimate waste in the case of ingestion, the results are roughly of the same order for the different scenarios, depending on the elements considered, with a reduction factor of 3 to 10 for Pu consumption alone, and a reduction factor of 100 for Pu and Minor Actinides management, by comparison to the open cycle (reduction factor of one).

Nevertheless, the scenarios are not equivalent if one considers the amount of recycled masses, Scenario 1 leading for example to large amounts of Pu and MA and especially of curium which have to be taken into account when considering the technical feasibility and especially the impact on the cycle.

These results lead to consider the development of MA fuels for PWR (with multi-recycling of Pu), for fast reactors (with either mono-recycling of MA and LLFP in moderated targets or multi-recycling in quasi standard fuels) and also for dedicated reactors. The R&D programme is presented below according to these three items, after a review of the available results.

4. R&D programme on materials for transmutation

The aim of the R&D programme is to obtain elements of technical feasibility for the fuels to be used in the different strategies to contribute to the evaluation of the scenarios in 2006.

Aside the homogeneous recycling (in PWR and FR) which requires standard fuels with a low content in minor actinides, the heterogeneous recycling (in FR and ADS) leads to consider fuel with a high content of minor actinides but without uranium to prevent the formation of “new” actinides. This type of fuels can be either solid solutions of actinides or composite fuels with an actinide compound in a matrix support that must be as inert as possible towards neutrons to be stable under irradiation and able to reach very high fission rates up to 90%, far above the standard ones (see Table 2).

Table 2. **Objectives for transmutation in fast neutron spectrum**

	Targets	**Standard fuel in FR**
Composition	Inert matrix ~1-7g.cm^{-3} MA	(U, Pu)O_2
Fast fluence (n.m^{-2})	10-40 10^{26} (moderated or fast spectrum)	20 10^{26}
Linear power (W/cm)	Min.: 10, max: 400	400
Temperature range	500-2 000	2 200
Fission rate (%)	30% ->>90%	17.5%
Prod. helium (cm^3.g^{-1} of fissile phase)	36 (FR = 85%, AM~1g/cm^3)	0.15
Prod. fission gases (cm^3.g^{-1} of fissile phase)	20.6 (FR = 85%, AM~1g/cm^3)	3.6
Dose on the cladding in dpa	200	150

For these U free fuels, that represent a technological discontinuity with regards to U and Pu oxides, development is needed in different areas, first with the characterisation of the basic properties of the fuels components, and for the elaboration of the fabrication process, then with the realisation of experimental irradiations and post irradiation examinations to obtain elements of the behaviour under irradiation and also in term of simulation to prospect the behaviour of new concepts.

As the different phases require the use of shielded nuclear installations, the time needed to define a solution usable for the industrial level, will be around 15 years and more. For the specific case of fast neutron reactors, a first step will be reached before 2010 with the identification of the performance potential of the tested solutions. This will allow the definition of a second step for 5 to 10 years to reach the ultimate objectives fixed to the selected concepts.

This leads to privileged generic and basic research and, along with the present experimental programme, to develop the simulation of irradiated elements and fuels (including specific irradiation tools) and to share this development in international collaborations.

The programme detailed below covers a large fields of applications and is presented according to the technology considered with in first, the hypothesis of transmutation in PWR for which the R&D is to be connected to the projects under consideration to burn plutonium, and in second the actions linked to the use of fast neutrons reactors which offer determinate advantages for a transmutation strategy (ratios of fission to capture more favourable than in thermal flux, availability of neutrons) and have proven their capacity to use plutonium. Before the presentation of the experimental programme in FR, a status of the knowledge of the behaviour of the composite fuels is made, to point out the fields of research. In third the research for the fuels to be used in ADS is starting with work beginning on the characterisation of the elements of interest.

5. Fuels studies for transmutation in pressurised reactors

The solution considered in the calculations is the homogeneous mode on the basis of the MIX fuel [4], with a fuel composition of 2.7% plutonium, 0.3% americium, 0.4% curium and a uranium enrichment of 4.5%, in a standard UO_2 EPR fuel rod geometry.

Another option using a basis of standard fuel rod geometry and UO_2 fuel is the Corail concept [3] in which around 30% of MOX type rods are set with enriched UO_2 rods in a standard PWR assembly.

To prevent the formation of ^{239}Pu from ^{238}U captures, two other options are under investigations using an inert matrix in which the plutonium and actinides can be dispersed. This concept is investigated considering:

- Standard geometry for the rods that are of two kinds, one including UO_2 fuel and others containing composite fuel (Duplex concept).
- A modified geometry with annular rods and composite fuel.

This last concept is studied to develop an Advanced Plutonium Fuel Assembly (APA) [4] and recent developments [7] have shown the possibility to integrate actinides in the fuel. The objective of stabilising the plutonium inventory is reached assuming 29% of APA EPR, 36% APA EPR being needed to stabilise the plutonium inventory together with Am and Cm transmutation.

The R&D work is concentrated on the development of the appropriate concept for Pu consumption in PWR, the fuel to be developed for this purpose will have to take into account the possibility to burn also minor actinides. Boiling water reactors that constitute a growing part of the reactors in the world and that have the capacity to use plutonium will also be considered in order to assess their ability to recycle plutonium and to transmute the waste when compared to the EPR one.

The high temperature reactors characterised by high thermal efficiency and the capacity to offer inherent safety may be used to burn plutonium in a complementary way. Their possibilities are under investigation [5] and their contribution regarding the objectives of the fuel cycle will be assessed.

6. Fuel for transmutation in fast reactors – elements of behaviour under irradiation

In conventional reactors (PWR, FR) the addition of limited amounts of Am, Np, Cm in the standard fuel in the whole core (homogeneous mode) is not supposed to affect deeply the fuel behaviour. For the UPu type of fuel of fast reactors, the fuel behaviour is not too much affected by less than 2 wt% of minor actinide (MA) addition as was confirmed by the SuperFact [8] experiment in the fast reactor Phénix where (U, Pu, Np)O_2 and (U, Pu, Am)O_2 were successfully irradiated until a fission rate of 7% (32% transmutation rate).

The main problems are concentrated in the “heterogeneous recycling”, in which MA targets are loaded with a high content of actinides in some areas of the core. These so called targets are U-free fuels in order to reduce waste production and the support of the MA compound is a matrix such as a ceramic or a metal as inert as possible regarding neutron interaction.

6.1 Requirement and design of MA targets

The aim of such inert matrix fuels (IMF) is to be efficient for the transmutation and to allow a good level of safety in case of incident or accident the requirement for a transmutation strategy being fission rate up to 90% with a MA content of ~1-2 g cm^{-3} (low part of the range compared to the requirement of 7-8 g cm^{-3} for ADS fuels with fission rate around 30%).

The fissile atoms and the support matrix can either form a solid solution or be integrated in a composite fuel like ceramic inclusion in ceramic matrices (Cercer) or ceramic inclusions in metal (Cermet), the respective composition and concentration of the different parts of these composites

being adjusted to take into account the different effects induced by irradiation. The main requirements are good thermal and mechanical properties for the matrix and chemical stability in the course of its evolution for the actinide phase. Possible ceramic or metal candidate materials have been selected with criteria concerning their basic properties (thermal and mechanical properties, activation with neutrons, chemical compatibility with neighbouring materials,…) and their behaviour under irradiation.

The criteria prevailing for the selection have been initially considered on the basis of the available data [9] that concern essentially out of pile behaviour, data being rather scarce in the field of the behaviour under irradiation in the adequate neutron energies and fluxes.

Under irradiation in reactor, three main sources of damage have to be considered for the IMF: fast neutrons interaction, effects of fission fragments and alpha decay products (alpha particle + heavy recoil atom). These energetic particles produce damage through electronic and atomic interactions and the consequences, that depend on the material, may affect significantly bulk properties: changes of lattice parameter, phase changes, amorphization, swelling, evolution of thermal and mechanical properties.

Furthermore, MA fuels for transmutation will have a specific behaviour under irradiation when compared to standard fuels: the power evolution history will not be constant and will vary with a factor of 10 (or more), the total quantity of gases (fission gases + helium) will be higher of factors of some hundreds, and the maximum burn-up level to be reached is above 90% of the Fissile Initial Metal Atoms which is far above the usual levels of standard fuels (see Table 2 for comparison).

In order to design specific IMF concepts adapted to the objectives of transmutation, the R&D programme must cover first the basic materials qualification (properties, fabricability, behaviour under irradiation) and also the in pile test of the concept itself. For the material qualification under irradiation, the experiments are designed to study the different effects:

- Fast neutron fluence with experiment like Matina (see below).
- Fission products with ion irradiations in accelerators, this part must be developed after the first experiments on the spinel [10].
- Alpha interaction with helium implantation experiments started in the frame of the Efttra programme.
- Effect of fast neutrons and fission products in irradiations like Matina and Efttra T3, T4 ter.

Global experiments are then performed to test the in pile behaviour of the concept i.e. the evolution of the different elements and of the composite itself.

6.2 Irradiation results and qualification of the concepts

The main results in this field come from the irradiation programme that was conducted in the frame of the European collaboration Efttra (where three main field were identified, materials for transmutation, either matrices and actinides compounds, and test of target concepts) [11] and also from experiments performed in the Siloe and Phénix reactors. The main results are synthesised below.

6.2.1 Inert matrices

6.2.1.1 $MgAl_2O_4$

If spinel behaves very well under high fast neutron fluence [12,13] (more than 22 10^{26} $n.m^{-2}$), fission products recoil or alpha decays product severe damage in the matrix. The large programme on this material has given results for different irradiation conditions. The Efttra T4 (effect of alpha decay due to Am + fission) [14] and Tanox and Thermhet irradiations [15,16] (effects of fission only) illustrate the swelling and the modification of the material (Figures 1a and 1b). This quite unsatisfactory behaviour have not been observed in the case of fuels based on macromasses concept (Thermhet fuel with fissile inclusions of 100 to 300 µm in diameter, Figure 1c) and operating in a different temperature range (above 1 000°C) like Thermhet and Matina [17].

Due to the complexity of the different effects and of their respective interactions, behaviour of spinel under irradiation is not fully understood up to now. Nevertheless, the use of the spinel matrix for transmutation may still be a solution in the case of a concept of macro dispersed fuel tailored to take into account the irradiation damage and fuel swelling therefore operating at a sufficiently high temperature to favour defects recovery and gas diffusion.

Figure 1a. **Clad diameter change of Efttra T4**

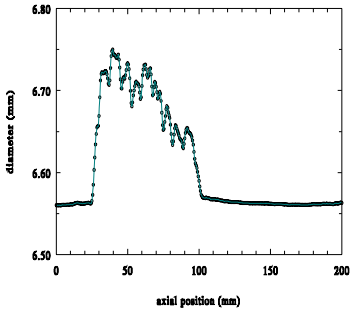

Figure 1b. **Micro dispersed fuel of Thermhet**

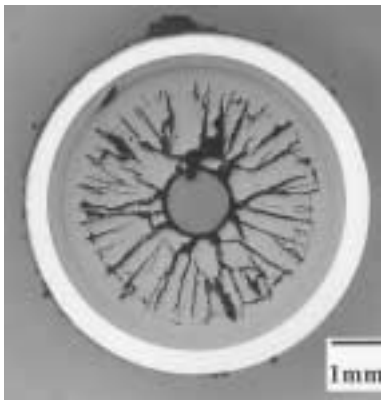

Figure 1c**. Macro masses of Thermhet**

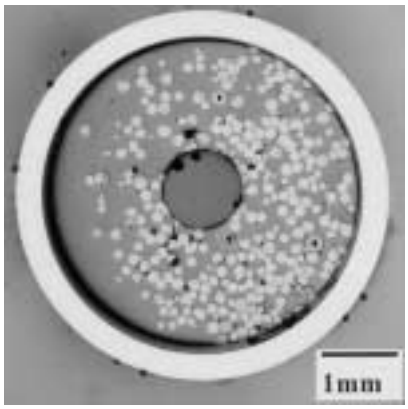

6.2.1.2 MgO

The Matina experiment allowed also to test magnesia up to 1.4% FIMA and 2 10^{26} $n.m^{-2}$ [17] of fast fluence (effect of neutrons without fissions) and the pellets appearance was very closed to the fresh ones. This lead to consider MgO as a good candidate for fast reactors conditions. Its behaviour will be tested in the future Ecrix experiment in the micro dispersed form and also in the Camix experiment with macro dispersed americium oxide.

6.2.1.3 Al_2O_3

The average swelling of 1.9% in volume measured in the Efttra T2bis irradiation for only 0.46 10^{26} n/m^2 of fast neutron fluence and the one of 28% for a fast fluence of 17 10^{26} n/m^2 in Santenay in Phenix confirm the poor interest of alumina for transmutation since fast neutrons induce extensive dislocation-loop formation and swelling.

6.2.1.4 ZrO_2

Due to its low heat conductivity, the element was not identified at the start as a reference, but its fairly good structure stability under irradiation (in its stabilised form), makes it a possible candidate that will be tested in the Camix experiment (see below).

6.1.2.5 Other matrices, CeO_2, $Y_3Al_5O_{12}$, Y_2O_3, TiN, W, Nb, V, Cr

Most of these materials have been tested under neutron irradiation [11,15,17] but the examination being still underway, their potential as matrices remain to appreciate.

6.2.2 Actinide compounds

6.2.2.1 NpO_x

For the experiments planned in the Super Phénix reactor, pellets have been successfully fabricated under the form of standard fuel loaded with some 2 wt% of Np to test the homogeneous way and NpO_2 inclusions were dispersed in $MgAl_2O_4$, Al_2O_3 and MgO for the heterogeneous recycling. The decision to stop the Super Phenix operation brought the irradiation projects to an end in 97 and the new programme planned in Phénix have been concentrated on the main problems, the efforts being centred on americium compounds.

6.2.2.2 AmO_x

Americium oxide has a very complex phase diagram and the compound may show a high oxygen potential or a high chemical reactivity towards its environment (like the matrix in contact or other elements like sodium) [18], furthermore the thermal conductivity of AmO_x is very low. This simple oxide form has been considered in the first experiments (Efttra T4, Ecrix) and an alternative is now proposed with a solid solution of AmO_2 and ZrO_2.

6.2.2.3 (Am, Zr)O_x

Some zirconia based solid solutions present very attractive properties and analogy with $UZrO_2$ suggests a good behaviour towards radiation. $(Am_{0.5}, Zr_{0.5})O_2$ and the pyrochlore form, $(Am_2, Zr_2)O_7$, were both considered and characterised [19] in the Oak Ridge National Laboratory in the frame of the CEA/ORNL collaboration that may be extended to the same targets with curium in the place of americium. This type of compound will be tested in the Camix experiment.

6.2.3 Target concepts

The first targets were based on a concept of a micro dispersion of the actinide phase in the host matrix and a lot of experiments have been performed based on two types of matrices: MgO + AmO_x, $MgAl_2O_4$ + AmO_x.

Magnesia based targets have been fabricated for the Ecrix experiments in Phénix, and samples were used for properties measurements of the composite (thermal characteristics, oxygen potential, melting point, heat capacity, thermal expansion and diffusivity) as well as specific tests like compatibility with sodium in collaboration between ITU and CEA. The irradiation will give indication on the behaviour of the magnesia-based concept as a candidate for americium transmutation.

The first fabrication of this type of fuel was made by the impregnation process and then irradiated in the High Flux Reactor in Petten in two irradiations: Efttra T4 and T4bis [11,14] where fission rates

reached respectively 38.5% and 70% FIMA with a transmutation rate closed to 100%. This gives indication that technical feasibility of transmutation is possible but the pellet have swollen considerably, as a consequence of radiation damage and gases accumulation (Figure 1a).

Figure 2a. **Calculated effect of fission and alpha particles on the damaged volume of the matrix**

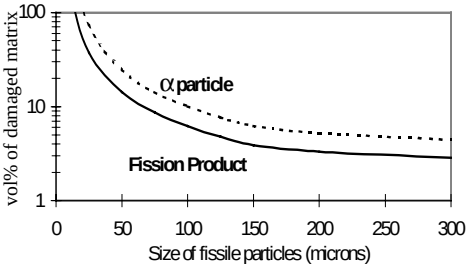

Figure 2b. **Macro particles of UO_2 dispersed in a spinel matrix**

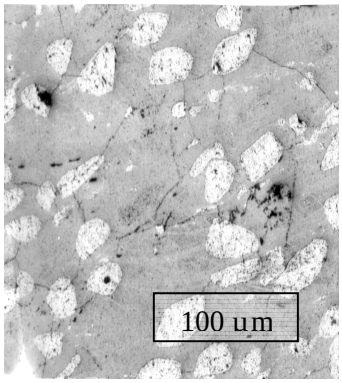

Figure 2c. **Macro particles of UO_2 dispersed in MgO**

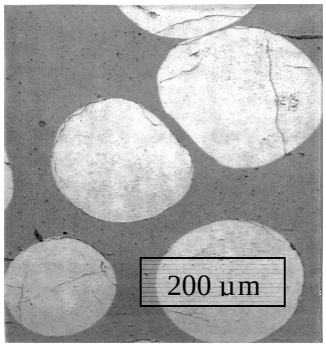

These results and data of other experiments indicate that the target concept is to be improved to reach the ambitious objectives for transmutation scenario (fission rate >90%) namely in taking into account the radiation damage and gas production. Improvement of the dispersion is researched with the introduction of macro masses (100-300 µm diameter) [20] to concentrate radiation effects due to fission fragments or alpha decay in a small shell (Figure 2a). On a spinel-based matrix the product answers the requirements (puerility and size of the particles, homogeneity of the target, absence of cracks) as shown in Figure 2b, but the process is still under development for magnesia to obtain an acceptable composite (see cracks in Figure 2c) with other innovative options of the fissile particles.

The experiments Thermhet and Efttra T3 were the first tests of this concept that will be introduced in the Camix experiment.

6.3 Modelling

The irradiation behaviour of fuels for homogeneous recycling is simulated with the usual code Germinal used for standard fuel, completed with specific models for helium production or evolution of minor actinide isotopes. For targets, a heterogeneous modelling (see Figures 3a and 3b) is used with a finite elements code (Castem) to calculate thermal and mechanical behaviour taking into account the fissile-bearing phase and the matrix.

The experiments Thermhet [21,22] and Efttra T4ter [23] were calculated with a good agreement measurement/calculation.

Figure 3a. **3D idealised meshing of a pellet with a periodic distribution of inclusions**

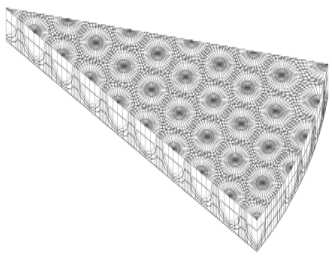

Figure 3b. **2D meshing deduced from a metallography**

6.4 Conclusion on the behaviour under irradiation

The work performed up to now, have brought numerous results in terms of fabrication of this new types of fuels, characterisation of the basic properties, behaviour under irradiation of the different components and of composite fuels.

With a start point based on simple chemical form of the fissile elements (AmO_2 particle) directly mixed with the matrix to obtain a micro dispersed composite, the different results obtained have lead to an optimisation of the concept with a greater complexity of the various parameters, the optimisation elements being [9,20]:

- The choice of a spherical host phase with size ranging between 50 to 300 µm in diameter.
- A MA compound in a stabilised phase of the type $AmZrYO_2$.
- A matrix material leading to a composite with acceptable thermal and mechanical characteristics and that can sustain a not too complex fabrication process. In this domain the possible choices rely on spinel, MgO and zirconia.
- The management of matrix damage and gas production, the later being still a matter of discussion the choice going from complete retention to complete release of fission gases. Calculations are still to be made to evaluate the possibilities of new ways of porosity repartition (porous matrix or “jingle” concept) and of coated particles.

In addition to the experimental programme described below, an important work remains to be done, in close relation with the reactor choice, in order to collect the necessary data. Figure 4 shows that after the present experimental phase will be completed and new designs are defined, a second phase will be necessary to reach the final objectives fixed to the fuels.

Figure 4. E**xperiments for MA transmutation**

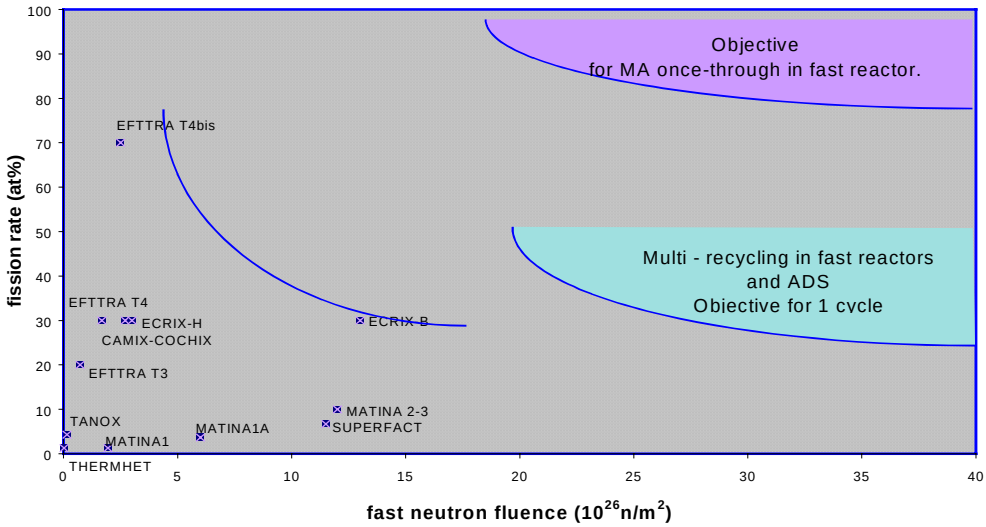

7. Irradiation programme for fuel development in Phénix

The irradiation programme is designed to cover various objectives related to the behaviour under irradiation of the fuel rod, and more generally of the different materials entering in the concept (actinide or long-life fission product targets, moderators...):

- For MA transmutation in the homogeneous mode and considering the major acquired knowledge on the fuel of fast neutron reactors, no major problem is expected and the objective of the experiments is to evaluate the performance of the fast neutron reactor fuel in the presence of a low percentage of minor actinides.

- For MA in heterogeneous mode, the developments of actinide target-fuels is at its beginning. The objectives of the first experiments are to test the various possible solutions for the elements (inert matrix, americium compound...) and for the composite (dispersion fraction and mode of the americium composite...).

- Similarly, for the LLFP and the solid moderating materials selected in the incineration concepts, the behaviour under irradiation of the composites with the most interesting physical and chemical properties is to be studied.

7.1 Incineration of MA in the homogeneous mode

For the homogeneous mode, in addition to the experience already acquired with SuperFact [8] based on a fast neutron reactor standard $UPuO_2$ fuel, the performances of a metallic fuel with a low percentage of minor actinides (neptunium + americium + curium) and rare earth, will be studied in the Metaphix experiments conducted in the scope of a contract with ITU on behalf of the Japanese CRIEPI. Metaphix 1,2,3 are three 19-rod type rigs capsules with three experimental rods. The target burn-up are 2, 7 and 11 at%, respectively. The rods are at Phénix dimensions, cladded in AIM1 with a fuel constituted of a metallic alloy UPuZr (+minor actinides) and a sodium bond. Each rig will contain a reference rod (without minor actinides), a rod with a MA content of 2% and a rod with a MA content

of 5% [24]. The target irradiation conditions for the metallic fuel rods at the beginning of their irradiation are a maximum heat rating of 350 W/cm, a nominal TNG cladding temperature of ca. 580°C. The 3 capsules will be introduced in the reactor in the year 2001.

7.2 Incineration of MA in the heterogeneous mode

For the heterogeneous mode and to optimise the irradiation possibilities of Phenix, several aspects will be studied simultaneously:

- Damage of the matrices by irradiation separating the effects of neutron effects, fission products and alpha particles.
- Behaviour under irradiation of the various americium composites and/or of the composite and matrix arrangement.

7.2.1 Selection of the matrix

Matina 1 allows the irradiation up to 2 10^{26} $n.m^{-2}$ (fast flux) of various matrices (MgO, $MgAl_2O_4$, Al_2O_3, $Y_3Al_5O_{12}$, TiN, W, V, Nb, Cr), some of them (MgO, $MgAl_2O_4$, Al_2O_3) with UO_2 micro inclusions to study the effects of fission products. Dismantled in 96 at the end of the 49th operating cycle, Matina 1 supplied 2 rods subjected to destructive examinations to provide elements for the selection of the matrix for the Ecrix H and B experiments.

The remaining rods were re-introduced in Phénix awaiting for the continuation of the irradiation Matina 1A up to 6 10^{26} $n.m^{2}$

In addition to Matina 1A, the experimental base on the reference matrix MgO will be broaden:

- On the one hand, by taking into account the microstructure of the composite as a parameter to be optimised (the “macrodispersed” concept).
- On the other hand, by irradiations up to more significant fast fluences.

Furthermore, the investigation field will be enlarge to include matrices that were not (or slightly) present in Matina 1.The matrices considered for this purpose are stabilised zirconia ZrO_2, tungsten as a metallic matrix, the manufacturing and characterisation work on these materials will possibly be shared with other R&D entities.

Both objectives are taken into account in the Matina 2-3 irradiation project i.e. a 19-rod rig with ca. a dozen experimental rods containing Cercer and Cermet composites planned to begin its irradiation in 2003 up to a fast fluence of ca. 10 10^{26} $n.m^{-2}$.

7.2.2 Selection of the americium composite – composite optimisation

The Ecrix programme includes two irradiations, identical as regards the material constituting the americium target but different as regards the target irradiation conditions: the irradiation neutron spectrum will be moderated by two different materials: $^{11}B_4C$ for Ecrix B and CaH_x for Ecrix H. The two experiments have required the development of two specific irradiation rigs planned to be available beginning of 2001 and specific calculations (Figures 5 and 6a) to take into account the flux modifications [25].

Figure 5a. **Ecrix B rig**

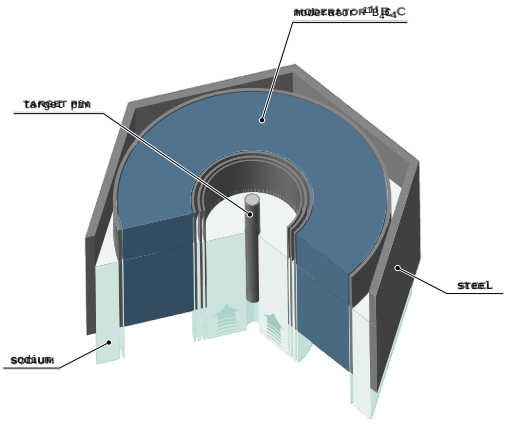

Figure 5b. **Ecrix H rig**

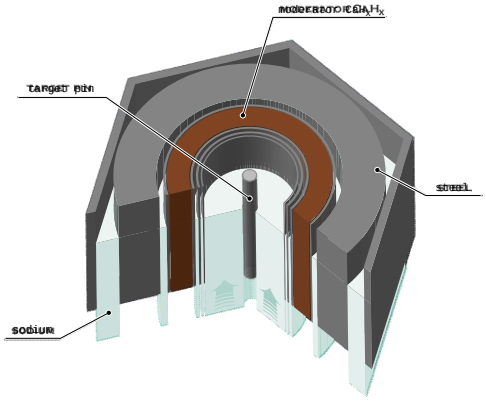

The fuel of the two Ecrix rods is a composite target with americium oxide “micro-dispersed” in the MgO matrix. The objective is to reach a fission rate of 30 at%. The required duration to reach this objective is 700 Effective Full Power Days for Ecrix B and 450 for Ecrix H with respective maximum linear power of ca. 50 and 70 W/cm without the uncertainty. The introduction in the reactor of the two experimental capsules is planned for the year 2001.

The manufacturing of the pellets has been completed in Atalante (Figure 6b) [26], and the two rods will be ready by end of 2000. Compared to the other experiments, the simultaneous implementation of a fast neutron reactor flux, a neutron spectrum converter and an americium target gives these experiments a prototypic aspect that goes beyond the sole objective of studying the behaviour of the target

Figure 6 a. **Evolution of the volumic power in Ecrix B and H (top)**

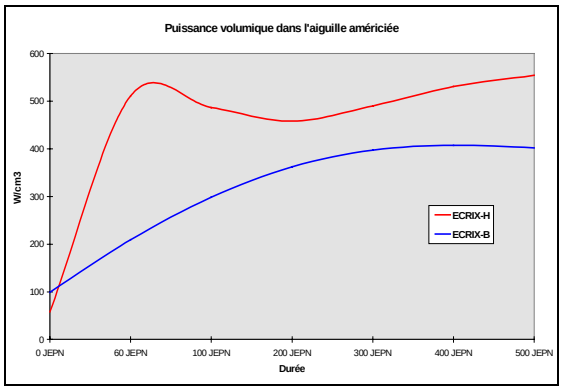

Figure6 b. **Micrograph of the Ecrix fuel**

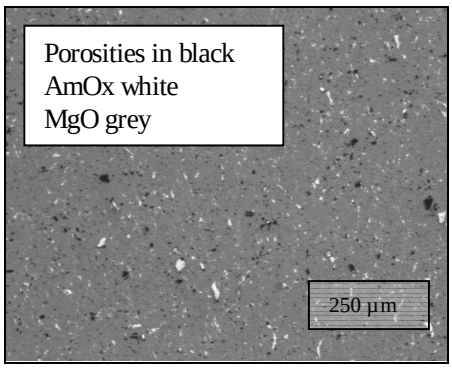

To open the field of investigation, a further irradiation is planned to select the optimised composite and the americium targets. A research axis will concern the stabilisation of the americium oxide in a cubic structure thanks to the addition of a stabilising element with composites of the $(Am,Zr,Y)O_{2-x}$ type. The Camix irradiation (Composites of AMericium in PHÉNIX) will cover the optimisation of the actinide compound. A second axis of the investigation will concern the dispersion mode of the americium compound in the inert matrix considering the macro dispersed concept (with $(Am,Zr,Y)O_{2-x}$ in $ZrYO_2$ and MgO). Such a process applied to different matrices is to be operational

for the Cochix irradiation (optimised target in Phénix) that should start in end 2002 with the objective of a fission rate equivalent to that of Ecrix i.e. ~30 at%.

7.3 Incineration of long life fission products

In this domain, and after the first results obtained in the Efttra T1 (Tc,I) and T2 (Tc) experiments [11], studies are concentrated on iodine and technetium (transmutation of caesium requiring both chemical and isotopic separation, the reference strategy is direct disposal).

Two experiments are planned in Phénix. The first experiment Anticorp 1 includes 3 rods containing technetium 99 in the metallic form, to study the behaviour of the material under irradiation for a transmutation atomic rate of 15% corresponding to an irradiation of 350 EFPD in a CaH_x moderated device planned to start its irradiation beginning of 2002.

A second LLFP transmutation experiment focused on iodine transmutation is planned in 2003 using the natural isotope (the use of ^{129}I is still considered) to study the behaviour under irradiation of various possible iodine compounds (effect of the neutron damage and chemical evolution of the compound). This programme will be conducted in close partnership with NRG.

7.4 Experiment on moderators

The need of a locally moderated spectrum in fast neutron reactors leads to the design of two specific devices for the Phénix irradiations using the first moderators of acquired fabrication and so easily available $^{11}B_4C$ and CaH_x. Research on other moderators will continue in the Modix irradiation (MODerator in PHÉNIX) planned in 2002, to test hydride-moderating materials (CaHx and possibly YHx) up to a significant fast fluence of 10 10^{26} $n.m^{-2}$.

The temperature stability of the compounds is the subject of an experimental out of pile programme (studies of the dissociation temperature in different atmospheres).

7.5 Experiments linked to nuclear data

In order to improve the knowledge of the cross-sections of the various nuclei involved in the corresponding transmutation chains, under neutron flux conditions representative of the considered recycling mode (fast or locally moderated spectrum), two specific experiments will be launched each containing rods with a large number of minor actinide and long-life fission product isotopes separated into small quantities of several milligrams: Profil R in an otherwise standard sub assembly in the fast flux of the internal core and Profil M using a moderated $^{11}B_4C$ device.

8. Experiments in other reactors

CEA is involved in several R&D international collaborations aimed to develop technologies for transmutation.

First of all, the Efttra collaboration including CEA and other European organisations (ITU, NRG, EDF, IAM, FZK) working jointly on P&T issues. A valuable set of data has already been gained from the experiments performed in the HFR reactor of Petten [11]. Various inert matrices have been tested with and without inclusions of fissile material together with experiments on LLFP.

A CEA/Minatom work programme is underway in Russia. The Bora Bora irradiation in Bor60 is designed to test various fuel concepts developed in the frame of Capra Pu management programme with the test of pelleted PuO_2-MgO that will bring data on the behaviour of this composite. The Amboine project – in its initiating phase - deals with the feasibility of the Vipac concept for Am transmutation based on AmO_2 MgO. The irradiation of such a target is planed in a second phase.

The determination of fundamental proprieties of zirconium pyrochlore as the host phase for Am-Cm in the composite target is underway with the contribution of Oak-Ridge National Laboratory [19].

On the mid-term, new realisation in Japan, in the frame of bilateral collaboration agreements with JNC and JAERI are under discussion, exchanges being considered on oxide compounds for the homogeneous mode and also on the properties of nitrides.

A general view of the various components of the experimental programme is given in Table 3.

Table 3

Homogeneous dispersion of MA	Matrices behaviour, effect of neutrons	Effect of neutrons and FP, composite study	Effect of n + FP + alpha particles, Am compound and composite study	PFVL studies	General data
SuperFact; Trabant 1 pin 2 (oxide); **Metaphix 123** (metal)	Santenay, T2,2bis, Matina 1, **1A,** T3	Matina 1,**1A,** Tanox,T3,T4ter, Thermhet, **Bora Bora**	**T5, Ecrix B H, Camix Cochix, AmO2Vipac**	T1,T2bis, **Anticorp 1 2**	**Profil R M** (cross-sections) **Modix** (moderators)

Done, **under preparation**

9. Transmutation in dedicated systems

The impact of the fuel design on the transmutation in dedicated reactors has been largely investigated firstly in the frame of the European Capra Cadra project [2], then in the frame of the "Fuel and Fuel Processing (FFP)" sub-group of the European Technical Working Group on ADS [27].

Taking into account the innovative specifications of such "dedicated" fuels, a systematic analysis of the different actinide compounds have been done, in order to select the most promising candidates with the current knowledge. Presently, an R&D programme proposal is being submitted to the European Commission in the frame of the 5th framework programme. It aims at extending the basic properties knowledge, assessing the synthesis and reprocessing processes and optimising the design of such innovative fuels.

9.1 Specifications

Compared to conventional fuels (UOX or MOX), dedicated fuels are distinguished by:

- The absence of fertile uranium (U-free fuels or Pu-based fuels) to enhance the transmutation efficiency (no new actinide formation). In that case, inert matrices may be considered as support of the actinide phase in replacement of uranium as in the case of transmutation in fast reactors. Considered in a strategy of multi recycling and reprocessing, these fuels may include plutonium which can be interesting for the choice of the compounds and that lead to more stable irradiation conditions than in FR.

- Their high minor actinides (Np, Am, Cm) content (3 to 4 times the one of composite fuels for FR) with the ratio Pu/MA varying from 1:5 to 5:1. That leads to enhance the radioactivity level of the virgin fuel compared to conventional fuels and to request for the fabrication step remote handling and special protection to shield gamma and neutron radiation.
- High burn-up to decrease the fuel cycle cost, but less than in the case of transmutation in FR (30% against up to 90%). As for the "once through" fuels, dedicated fuels must accommodate a large fission gas and helium production and a high level of radiation damage. The impact on fuel design and materials choice is thus very significant but to the difference of FR, the reactor parameters are not fixed and that leads to some additional possibility in the choice.

9.2 Actinide compounds selection

According to the fuel specifications above, a classification of the different fuel types, from the less promising to the most one, is proposed taking into account the current knowledge on minor actinide compounds, which is unfortunately very sparse and poor.

- Metallic fuels, based on metal actinide alloys, are considered as the less interesting candidates. because of the low melting point of the major constituents (Np and Pu melts at 640°C), the expected limited mutual solubility of the actinides and the risk of stainless steel clad-fuel eutectic reaction at low temperature (410°C). Even if some improvements may be put forward such as a large Zr addition to enhance the fuel margins to the melting, considerable uncertainties remain on the actinides alloys metallurgy and on the fabrication processes (because of the high volatility of Am and Pu).
- Carbide fuels are known to have good thermal and mechanical properties and have shown in the past relatively good performance. However, the complex phase relations, especially between the sesqui- and monocarbides and the highly pyrophoric nature of these compounds make them less interesting than the other classes of refractory compounds (nitrides and oxides).
- Nitride fuels are attractive because of their expected good thermal properties and their ability to form solid solution whatever the minor actinide content. The major uncertainties concern the risk of dissociation at high temperature, which could be a critical issue in case of severe accident and the americium nitride vaporisation, which could complicate the fabrication step and limit the running temperature in pile. Large swelling under irradiation is also a specific feature of the nitride fuels, which should involve technical developments to accommodate it. If improvements to meet all the requirements can be considered like operation at low temperature, the development of such fuels must have to overcome the problems of temperature stability and also the technical and economical problem of the nitrogen 15 enrichment to avoid the ^{14}C formation.
- Oxide fuels are probably the most promising candidates since they offer a logical extension of the current MOX fuel technology. Although the thermal properties of actinide oxides are not so favourable compared to nitrides, they should be improved by using support matrices (oxide or metal) with good thermal properties. The experience developed in Europe on composite targets could be directly applied to dedicated fuels. Other engineering solutions (e.g. annular pellets, annular pins with internal cooling, specific coated particles) could be also developed. Finally, in spite of thermal weakness, improved oxide fuels should be considered not only as the "safest" solution if we take into account all the basic knowledge accumulated for 30 years on MOX fuels and the great synergy with other programmes, but also the best compromise if one consider the entire fuel cycle (in terms of fabrication and reprocessing command, reactor safety approach,…).

9.3 Programme for dedicated fuels

From this analysis based on the current knowledge on actinide compounds, nitrides and oxides are thought to be the most attractive support to the transuranium elements in ADS. However a large R&D programme is needed to enlarge our knowledge on such compounds and to optimise the fuel design to make it sure and safe.

The "Confirm" programme [28], which started in September 2000 in the frame of the 5th PCRD, is the first one devoted to the nitride fuels. The (Pu/Am, Zr)N compounds will be synthesised and characterised and (Pu, Zr)N will be irradiated in the Stüdvisk reactor. In parallel, modelling development is performed to predict the performance of such fuels.

The "Future" programme, which will be proposed to the European Commission in January 2001, will be focused on the oxide fuels. The (Pu, Am; (Zr))O_2 will be synthesised and characterised and composite fuels based on (Pu, Am; (Zr))O_2 will be studied. Modelling codes for the homogeneous and heterogeneous fuels will be developed.

Both programmes should allow by 2004 to collect information enough to judge the feasibility of such fuels and to influence the next R&D programmes.

10. Conclusion

The efforts made since several years for the development of the fuels necessary to insure a transmutation strategy lead to acquire knowledge on the basic data for the different materials needed, the fabricability of the composites, and the first elements about their behaviour under irradiation for MA and FP compounds.

The experimental programme planned in Phenix have been consolidated and the preparation work have reached marked milestones like the irradiation devices fabrication, the realisation of the first experimental pins with AmO_2 MgO composite, the various calculations and safety files necessary for the start of the experiments planned in 2001 (Metaphix 1,2,3; Ecrix B,H; Profil R). The first experimental results together with the knowledge acquired during the preparation of this first phase allow the definition of an optimisation of the targets that will be introduced in a second phase in 2003. Results from this programme together with those coming from other irradiations and of international programmes will be use to elaborate the first elements of technical feasibility of the fuels for transmutation in 2006.

Definition of fuels answering all the needs will require an additional research of long duration integrating the choices made in the scenarios taking into account external parameters such as cost, industrial feasibility, reactor park evolution and public acceptance. In this context, the necessity to cover a large domain of parameters, will lead to favour international co-operation and to privilege analytical experiments owing a better understanding of the phenomena together with some technological ones. The identified concepts will need to be tested in experimental reactors before considering an industrial phase.

If the necessary developments for an homogeneous transmutation using the present fuels as a start, appear available in around ten years time, the development of composite fuels in technological discontinuity when compared to the present fuels, needs continuous efforts on matrices, actinide compound and fuel conception. The development of dedicated fuels will require specific characterisation of the potential fuels adapted to the working parameters of ADS and taking into account the evolution of the strategy in this domain. The use of different cycles like molten salts must be appreciated in the course of the other actions made in these domains on a long-term schedule.

REFERENCES

[1] P. Bernard, B. Barré, N. Camarcat, M. Boidron, B. Boullis, J.M. Cavedon, D. Iracane. *Progress in R&D Relative to High Level and Long-lived Radioactive Wastes Management: Lines 1 (Partitioning-Transmutation) and 3 (Conditioning, Long-term Interim Storage) of the 1991 French Law,* Global'99, Jackson Hole (USA).

[2] A. Vasile, G. Vambenepe, J.C. Lefèvre, K. Hesketh, W. Mashek, C. De Raedt, D. Haas. *The Capra – Cadra Programme,* Proceedings of Icone 8, 8th Conference on nuclear engineering, April 2-6, 2000, Baltimore, USA.

[3] S. Aniel, M. Rohart, A. Puill, J. Bergeron, G. Rouvière. *Plutonium Multi-recycling in PWR: the Corail Concept*, Proceedings of Icone 8, 8th Conference on Nuclear Engineering, April 2-6, 2000, Baltimore, USA

[4] A. Puill and J. Bergeron. *Advanced Plutonium Fuel Assembly: an Advanced Concept for Using Plutonium in Pressurised Water Reactors,* Nuclear Technology, Vol. 119, Aug. 1997.

[5] X. Raepsaet, F. Damian, R. Lenain and M. Lecompte, *Fuel Cycle Performances in High Temperature Reactor,* Global'99, Jackson Hole (USA).

[6] J.P. Grouiller, J.L. Guillet, H. Boussier, J.L. Girotto, *Nuclear Materials Recycling in Conventional or Advanced Reactors: a Scenario Study*, Global'99, Jackson Hole, USA.

[7] H. Golfier, J. Bergeron, A. Puill, M. Rohart, *Multi-recycling of Plutonium and Incineration of Americium, Curium, and Technetium in PWR,* Safewaste 2000, Montpellier, France.

[8] N. Chauvin, J.F. Babelot. *Joint CEA/ITU Synthesis Report of the Experiment SuperFact 1,* Rapport EURATOM 1999.

[9] N. Chauvin, R.J.M. Konings, H.J. Matzke, *Optimisation of Inert Matrix Fuel Concepts for Americium Transmutation,* Journal of Nuclear Materials, 1999, 274,105-111.

[10] R. Fromknecht, J.P. Hiernaut, H.J. Matzke, T. Wiss, *He-ion Damage and He-release from Spinel $MgAl_2O_4$ Radiation Effect in Insulators*, Proc. Nucl. Instrum., Method in Phys. Research. Jena, July 18-23, 1999, Paper P 03.28.

[11] D. Haas *et al., The EFTTRA European Collaboration for the Development of Fuels and Targets for Transmutation: Status of Recent Development,* Conference Global'99.

[12] E.A.C. Neeft *et al., Neutron Irradiation of Polycrystalline Yttrium Aluminate Garnet, Magnesium Aluminate Spinel and A-alumina.* Journal of Nuclear Materials, 1999, 274, 78-83.

[13] K. Fukumoto *et al.,* Journal of Nuclear Materials, 32 (1995) 773-778.

[14] R.J.M. Konings *et al.*, *The EFTTRA T4 Experiment on Americium Transmutation*, Technical Report EURATOM 1999.

[15] A. Mocellin, Ph. Dehaudt, *Composite Fuels Behaviour Under and After Irradiation*, Technical Committee Meeting AIEA Moscow, 1-4 oct.1996.

[16] V. Georgenthum *et al.*, *Influence of the Microstructure for Inert Matrix Fuel Behaviour. Experimental Results and Calculation*, Global'99.

[17] N. Chauvin, T. Albiol *et al.*, *In-pile Studies of Inert Matrices with Emphasis on Magnesia and Magnesium Aluminate Spinel.* Journal of Nuclear Materials, 1999, 274, 91-97.

[18] S. Casalta, H.J. Matzke, C. Prunier, *A Thermodynamic Properties Study of the Americium-oxygen System*, Global'95.

[19] Ph. Raison, D. Haire, T. Albiol, *Materials Relevant for Transmutation of Americium and Experimental Studies on the Pseudo-ternary System, AmO_2-ZrO_2-Y_2O_3,* Journal of Nuclear Materials, to be published.

[20] N. Chauvin, R.J.M. Konings, H.J. Matzke, *Optimisation of Minor Actinide Fuels for Transmutation in Conventional Reactors (PWR, FR),* Conference Global'99.

[21] V. Georgenthum *et al.*, *Experimental Study and Modelling of the Thermo-elastic Behaviour of Composite Fuel in Reactor – Emphasis on Spinel Based Composites*, Paper accepted for Progress in Nuclear Energy.

[22] V. Georgenthum, CEA/EDF PhD thesis, Université de Poitiers 2000.

[23] R.J.M. Konings, K. Bakker *et al.*, Journal of Nuclear Materials, 1998, 254, 84-90.

[24] *Fabrication of UPuZr Metallic Fuel Containing Minor Actinide*, Global'97 Conference, October 5-10, 1997, Yokohama, Japan.

[25] J.C. Garnier, N. Schmidt *et al.*, *The ECRIX Experiments*, Global'99 Conference, 29 Aug.-3 Nov. 1999, Jakson Hole, USA.

[26] Y. Croixmarie *et al.*, *The Ecrix Experiment*, Global'99.

[27] M. Salvatores, *Transmutation: a Decade of Revival. Issues, Relevant Experiments and Perspectives*, 6th Information Exchange Meeting on Actinide and Fission Product Partitioning and Transmutation, Madrid, Spain, 11-13 Dec. 2000, EUR 19783 EN, OECD/NEA, Paris, France (2001).

[28] J. Wallenius *et al.*, 6th Information Exchange Meeting on Actinide and Fission Product Partitioning and Transmutation, Madrid, Spain, 11-13 Dec. 2000, EUR 19783 EN, OECD/NEA, Paris, France (2001).

FISSION PRODUCT TARGET DESIGN FOR HYPER SYSTEM

Won S. Park, Yong H. Kim
Korea Atomic Energy Research Institute
P.O. Box 105, Yusong, Taejon 305-600, Republic of Korea
E-mail: wonpark@kaeri.re.kr

Jong Seong Jeong
Department of Nuclear Engineering
Seoul National University, Republic of Korea

Abstract

The design optimisation of FP Target is performed to maximise the transmutation of ^{99}Tc and ^{129}I in the HYPER system without causing any core safety concerns. The localised thermal flux is obtained by inserting some moderators such as CaH_2. Many types of target configurations are investigated. The configuration that ^{99}Tc is loaded as a plate type in the outer-most region and ^{129}I is loaded as NaI rods mixed with CaH_2 rods in the inner region is believed to be the most optimum in terms of transmutation rate and core power peaking. The designed FP target configuration is estimated to have the transmutation rate of 6.41%/yr and 13.88%/yr for ^{99}Tc and ^{129}I, respectively. The maximum pin power peaking is 1.232 that is within the acceptable range. In addition, the configuration is expected to make the core coolant void coefficient more negative but the Doppler coefficient less negative.

1. Introduction

An accelerator driven sub-critical system named HYPER (HYbrid Power Extraction Reactor) is being developed within the framework of the national long-term nuclear research plan. Many types of transmutation systems were investigated in terms of transmutation capability, safety, and the proliferation resistance of the related fuel cycles. A simple stratum shown in Figure 1 is supposed to be the most reasonable for transmutation in terms of the proliferation issues. The HYPER system utilising fast neutron spectrum is believed to have excellent compatibility with this single stratum.

The whole development schedule for the HYPER system is divided into three phases. The basic concept of the system and the key technical issues are derived in Phase I (1997-2000). Some experiments will be performed to confirm the key technical issues in Phase II (2001-2003). A thermal hydraulic test for the Pb-Bi, an irradiation test for the fuel and a spallation target test are the major experiments that KAERI is considering. In Phase III (2004-2006), a conceptual design for HYPER system will be finished by completing the development of design tools based on the experiments

^{99}Tc and ^{129}I are being considered to be transmuted among long-lived fission products. The fission product targets are loaded in the middle ring of the core in order to make the support ratio of fission product similar to that of TRU. The FP target region is designed to have very localised thermal neutrons for the efficient burning of ^{99}Tc and ^{129}I.

The preliminary results of the basic material studies have shown that a pure metallic form is the most desirable one for the incineration of ^{99}Tc; a fabrication route for casting the technetium metal has been developed and irradiation experiments did not show any evidence of the swelling or disintegration of the metal [1]. On the other hand, an elemental form was found not to be acceptable for iodine because of its volatility and chemical reactivity. Thus, metal iodides are being considered. Sodium iodide (NaI) and calcium iodide(CaI_2) are the desirable forms. Sodium iodide is expected to have melting problems when the sodium is liberated from iodine due to the transmutation.

In this study, a design optimisation of the FP target is performed to maximise the transmutation of ^{99}Tc and ^{129}I without causing any core safety problems in the HYPER system.

Figure 1. **Material flow in the HYPER system**

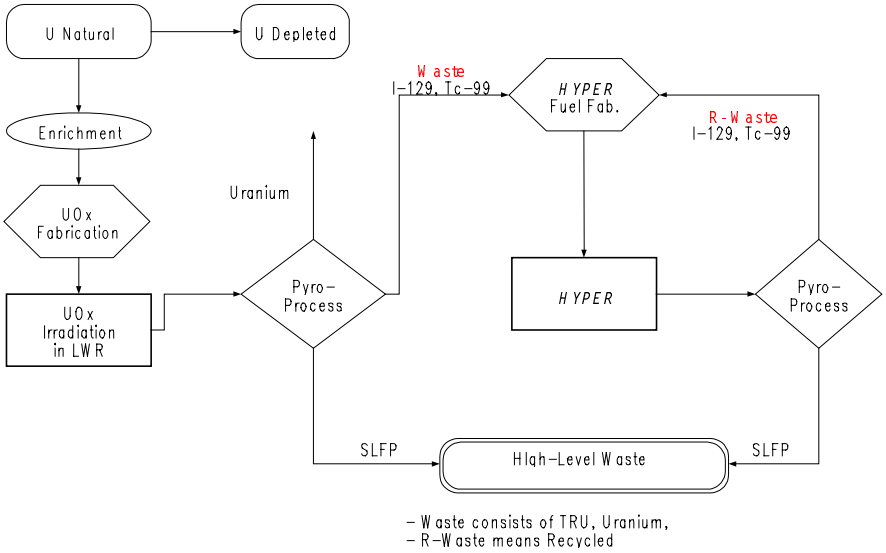

2. General description of the core

The HYPER core adopts a hexagonal type fuel array to render the core compact and to achieve a hard neutron energy spectrum by minimising neutron moderation. Table 1 represents the design parameters of the HYPER core. In order to keep the radial assembly power peaking within the design target value of 1.5, the core is divided into three zones. A low TRU fraction fuel is designed to be loaded in the innermost zone and a high TRU fraction fuel is loaded in the outermost region. The refuelling is to be performed based on scattered loading with 3 batches for each zone. The core configuration is shown in Figure 2. The HYPER core has a relatively small amount of fertile nuclides. This raises two problems in terms of core neutronic behaviours. The first is small Doppler coefficient that contributes to making the fuel temperature coefficient negative. Preliminary calculations show a Doppler coefficient of about -0.36 pcm/K. The coolant void and temperature coefficients were also found to be negative though they are very small. The homogeneous void coefficient for BOC is about ~-140 pcm/%void. However, the local void coefficient in the central region of the core was evaluated as slightly positive. The coolant temperature coefficient is about -2.1 pcm/^{o}C.

The second problem is the relatively large reactivity swing in the core. As the TRU burns up, the reactivity inside the core is reduced and more accelerator power is needed to maintain constant power. However, the reactivity runs down so quickly that the system cannot be operated effectively with a desirable cycle length (~1 year). To avoid such a large amount of reactivity change and minimise the fluctuation of the required accelerator beam power due to the TRU burn-up, the burnable absorber is employed. 90% enriched B_4C is used as a burnable absorber [2]. Two different loading types of burnable absorber are being investigated. The first one coats the inside of the cladding with B_4C to a thickness of 0.002 cm. The second replaces some of the TRU fuel rods with burnable absorber rods. The coating method is evaluated to reduce the reactivity swing by about 38% compared to the non-burnable absorber cases for the depletion period of 180 days. In addition, the introduction of burnable absorber is believed to make the core neutron energy spectrum much harder. The HYPER core is to transmute about 370 kg of TRU a year. This corresponds to a support ratio of ~5.

Either TRU-Zr metal alloy or (TRU-Zr)-Zr dispersion fuel is considered as a blanket fuel for the HYPER system. In the case of the dispersion fuel, the particles of TRU-Zr metal alloy are dispersed in a Zr matrix. A blanket rod is made of sealed tubing containing actinide fuel slugs in columns. The blanket-fuel cladding material is ferritic-martensitic steel. It is expected that the dispersion fuel will generally withstand significantly higher burn-up than alloy fuel. If the fuel particles are separated sufficiently, the areas damaged by fission fragments will not overlap and remains a continuous metal phase which is essentially undamaged by fission fragment. This relatively undamaged metal matrix can withstand higher burn-ups without significant swelling than is possible with alloy fuel. As a result, the dispersion fuel does not need as much gas plenum as the alloy fuel needs. In addition, it is not easy to control the vaporisation of americium nuclides in the fabrication process of an alloy type fuel rod.

Pb-Bi is employed as a coolant for the HYPER system. According to Russian results, the maximum allowable temperature of Pb-Bi coolant is approximately 650^{o}C. The lower limit of the coolant temperature can be started from the Pb-Bi melting point, 125^{o}C. For safe operation, Pb-Bi temperature must be sufficiently above 125^{o}C. Therefore 125 and 650^{o}C can be the basic temperature limits of Pb-Bi coolant. The core inlet and outlet temperature of Pb-Bi coolant were determined to be 340 and 510^{o}C, respectively. This temperature range marginally satisfies the basic temperature limits. Resulting core flow rate in order to cool 1 000 MW thermal power is 46569 kg/s. Coolant velocity of primary cooling system can also cause a design constraint. Coolant velocity affects the integrity of structural materials and the pumping load. The primary cooling system of the HYPER should be designed with low coolant velocity as long as it can satisfy another design requirements. Since Pb-Bi does not significantly absorb or moderate neutrons, it allows the use of a loose lattice that favours lower coolant velocity. The P/D (Pitch-to-Diameter) of the HYPER's core is chosen to be 1.5 and the

corresponding Pb-Bi velocity is 1.1 m/s, which is a relatively low coolant velocity compared to that of typical power reactors. Instead of wire spacer commonly used for tight lattice, grid spacers are suitable to ensure proper separation of the fuel rod. A loop type configuration was selected for the preliminary design of the HYPER system and three-loop system was chosen as the optimal one for the HYPER. The number of loop is determined by considering the coolant velocity and pressure drop across the loop.

Table 1. **Major system design parameters**

Parameter (unit)	Values	Parameter (unit)	Values
System			
- Core thermal power (MW)	1 000	- Ave. neutron energy (keV)	600
- Active core height (m)	1.2	- Ave. neutron flux (n's/sec-cm^2)	6×10^{15}
- Effective core diameter (m)	3.8		
- Total fuel mass (TRU-Kg)	2 961	Assembly	
- System multiplication factor	0.97	- Ass. pitch (cm)	19.96
- Accelerator beam power (MW)	~6	- Flow tube outer surface flat-to-flat distance (cm)	19.52
- Ave. discharge burn-up (%at)	~25		
- Transmutation capability (Kg/yr)	380	- Tube thickness (cm)	0.3556
- Number of fuel assembly	183	- Tube material	HT-9
- Ave. linear power density (KW/m)	13.5	- Rods per assembly	331

Figure 2. **Core configuration**

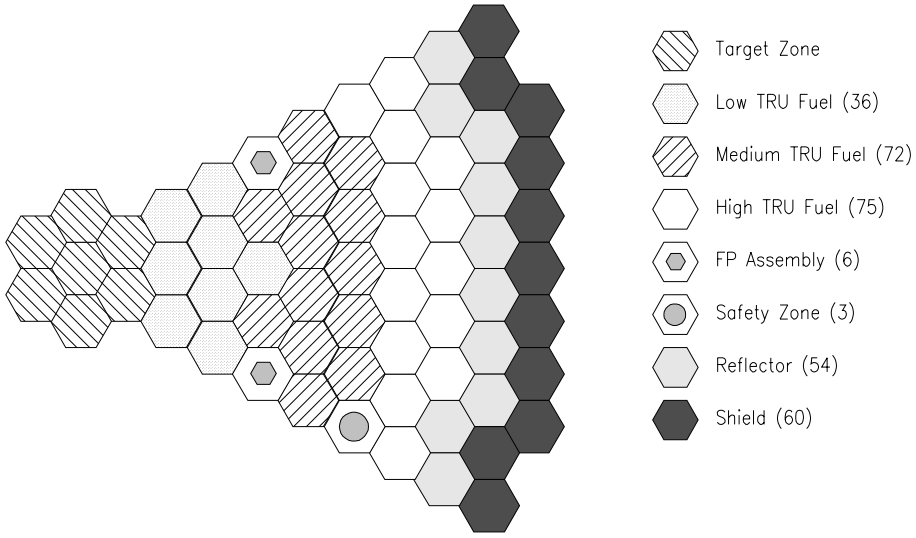

The core coolant is also used as the spallation target. Pb-Bi comes from the bottom of the reactor and encounters the beam window before going out of the top of the reactor. A single beam window is adopted so that there is no independent window cooling system. There are some design goals for the stable and safe operation of the target and reasonable lifetime of the beam window. We set the maximum allowable temperature and stress of the beam window at 700°C and 200 MPa, respectively. The temperature of Pb-Bi is set to be less than 600°C and the lifetime of the beam window is set to be 1 year.

3. Basic characteristics of FP transmutation

The transmutation rate is a function of the neutron flux level and the cross-section($\Phi n\sigma_a$). The introduction of moderator slows down the neutron energy. The moderation reduces the neutron flux level but increase the absorption cross-section of fission product. The preliminary studies were performed to evaluate the effectiveness of local moderator. They were based on the constant volume model (moderator volume + FP volume = FP target volume = constant) because the total volume of a FP target can not be larger than the volume of a TRU assembly. The evaluation showed that the transmutation rate could be improved considerably for ^{129}I while there was not much difference in the transmutation of ^{99}Tc (Figure 3). In addition, a graphite and calcium hydride were evaluated in terms of their effectiveness for moderation. The calculational results showed that a calcium hydride is much better for the production of localised thermal neutrons [3].

In order to decide the way of loading moderator into the FP target, two basic types of FP target configuration were studied in terms of their impact on core power peaking factor. The first one (defined as the outer moderating) is to install the moderating material at the outer region of the FP target. This kind of configuration resulted in unacceptably high core power peaking factors at the TRU assemblies surrounding FP target. The second one (defined as the inner moderating) is to install the moderating material at the central region of the FP target assembly. In this case, the power peaking could be reduced to a certain acceptable level. However, the TRU assemblies around ^{129}I showed relatively high power peaking compared to those of ^{99}Tc (Figure 4). The loaded ^{129}I (NaI) target assembly was found to be less effective to screen out thermal neutrons because of its low density and chemical form.

Figure 3. **Total reaction rate**

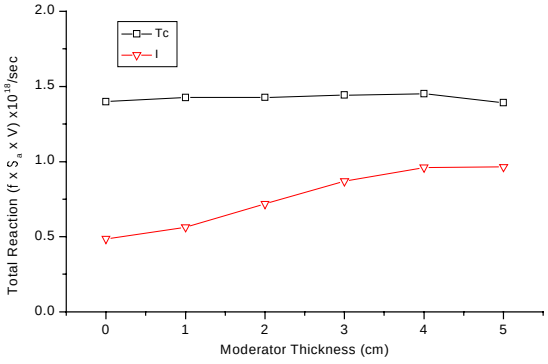

Figure 4. **Pin power peaking factor**

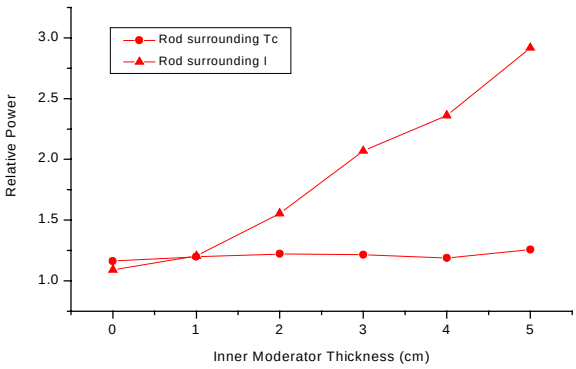

Based on the preliminary investigations, the configuration that ^{99}Tc is loaded in the outer most region and ^{129}I is loaded in the inner region of target is suggested to be the desirable one.

4. Effect of ^{99}Tc thickness

^{99}Tc is to be loaded in the outer most region of target to cut off the streaming of thermal neutron into the surrounding TRU assemblies. The plate type loading was believed to be the best form to minimise the leakage of thermal neutrons into the surrounding TRU assemblies. An investigation to estimate the variation of pin power peaking of TRU assemblies as a function of ^{99}Tc plate thickness was performed using MCNAP based on ENDF-B/VI [4]. All surrounding TRU assemblies were described by pin-by-pin model. Figure 5 shows the cross-sectional view of the calculational model for

the fission product target. The rods (calcium hydride or ^{99}Tc) are installed using triangular array with the P/D ratio of 1.19 in FP target.

Table 2 represents the variation of pin power peaking in the TRU assemblies surrounding FP target. As expected, the increase of ^{99}Tc plate thickness reduces the pin power peaking. The pin power for Model #1 can be used as a reference value. The thickness more than 2.4 cm is believed to be not necessary in terms of pin power control. The transmutation rate of ^{99}Tc is increased from 4.86%/yr to 6.09%/yr by using the localized thermal neutrons.

Figure 5. **Calculational model**

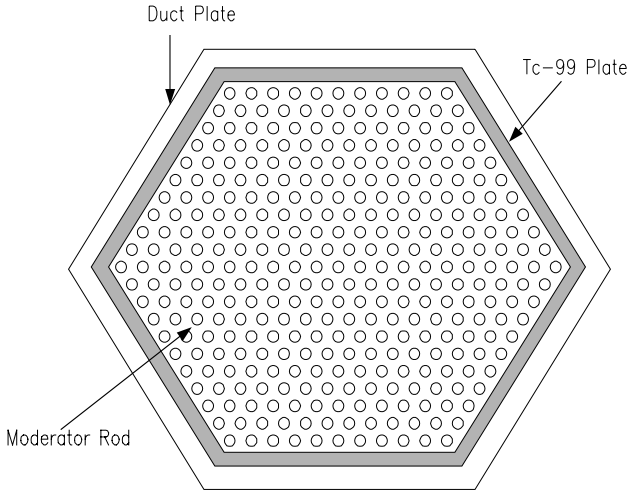

Table 2. **Pin power peaking variation vs ^{99}Tc plate thickness**

Model No.	Thickness (cm)	No. of moderator rings	Transmutation rate (%/yr)	Pin power peaking
1	All Rods are Tc	0	4.86	1.158
2	0.5	13	–	3.763
3	1.5	11	–	1.685
4	2.4	10	6.09	1.193

5. Optimum configuration of FP assembly

Two types of target configurations were investigated on whole core basis as shown in Figure 6. ^{129}I is loaded as a plate type of NaI at the just inner side of ^{99}Tc plate in Type A. On the other hand, ^{129}I is loaded as a rod type of NaI mixed with the moderating rods in Type B. Type A was designed to increase the loading amount of ^{129}I while Type B was to reduce the self-shielding effects. Some pre-calculations decided the thickness of 1.9 cm and 1.3 cm for ^{99}Tc and ^{129}I plate, respectively.

Figure 6. **FP target configuration**

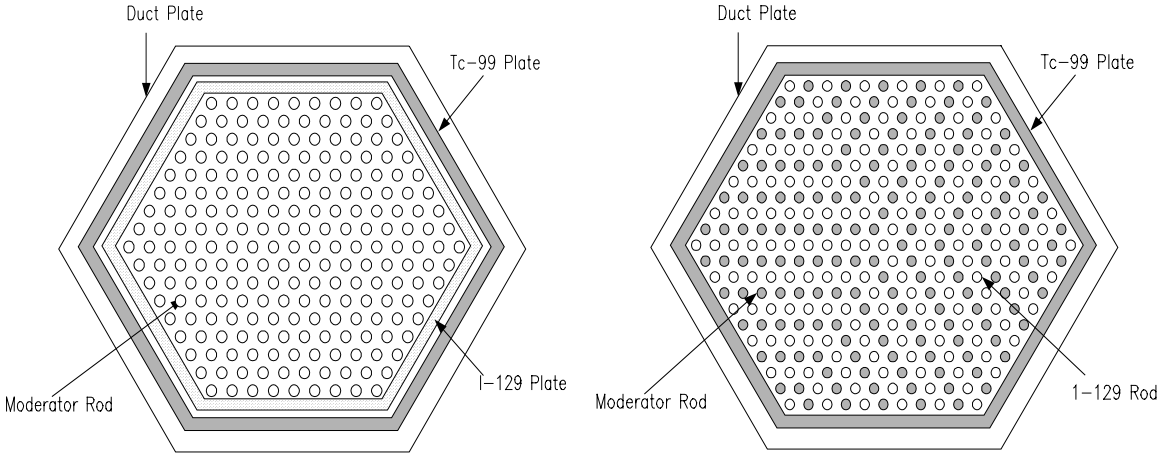

a) Plate Type for I-129 b) Rod Type for I-129

Table 3 shows the results of evaluations. The higher transmutation rate for both ^{99}Tc and ^{129}I are achieved in Type B than Type A. The loading amount of ^{129}I for Type B is reduced by 30% compared to that of Type A. However, there is not much difference between two types in terms of the total amount of the transmuted ^{129}I. In addition, the pin power peaking is kept within an acceptable range in both types.

Table 3. **Performance of FP Targets in the HYPER System**

Target configuration		**Initial loading (kg)**	**Transmuted (kg/yr)**	**Transmutation rate(%/yr)**	**Pin power peaking**
Type A	^{99}Tc	901.8	54.2	6.01	1.211
	^{129}I	129.72	13.12	10.09	
Type B	^{99}Tc	901.8	57.8	6.41	1.232
	^{129}I	93.8	13	13.90	

As mentioned before, the support ratio of the HYPER is expected to be about ~5. In terms of material balance, the HYPER system is desired to have the support ratio for ^{99}Tc and ^{129}I similar to that of TRU. The optimised configuration Type B can transmute 57.8 kg, 13 kg of ^{99}Tc and ^{129}I, respectively. In general, LWR (1.0 GWth) produces about 8.826 kg of ^{99}Tc and 2.721 kg of ^{129}I a year. The HYPER system itself generates about 7.9 kg and 2.3 kg of ^{99}Tc and ^{129}I due to the TRU transmutation. As results, the net support ratios of the HYPER are estimated to be 5.7 and 4.0 for ^{99}Tc and ^{129}I, respectively. The fission product support ratios are very close to that of TRU in the HYPER system.

6. Safety factor evaluation

As mentioned, the localised thermal flux increases the pin power peaking of TRU assemblies. The target configuration is optimised to minimise such an impact. Figures 7 and 8 represent the neutron energy spectrum for the target configuration of Type A and B. The energy spectrum for the

fuel rods are at the TRU assembly the most far away from the core centre among the TRU assemblies surrounding FP target. It can be seen that the neutron energy spectrum of the fuel rods near by FP target become much softer due to the incoming thermal neutron from FP target region. The neutron energy spectrum for ^{99}Tc and fuel rods are very similar in both cases. However, Type B has slightly softer spectrum than Type a for NaI region. In addition, the resonance absorptions of ^{99}Tc in epithermal region are detected in both cases.

The effects of FP target loading on the coolant void and Doppler coefficients were investigated. The loading amount of TRU was adjusted to make the initial k_{eff} of the core about 0.97. Monte Carlo Code, MCNAP with ENDF-B/VI was adopted for the evaluation. Table 4 shows the results of the evaluation. The designed FP target makes the coolant void coefficient more negative but Doppler coefficient less negative though the change is very small. As results, the optimised FP targets with a localised thermal flux are expected to cause no severe core safety problems.

Table 4. **Void and Doppler coefficient change due to FP target**

Core type	**No void k_{eff} (std)**	**10% void k_{eff} (std)**	**Void coeff. (pcm/%void)**	**Fuel temp 300 K k_{eff} (std)**	**Fuel temp 1 100 K k_{eff} (std)**	**Doppler coeff. (pcm/K)**
Reference (No. FP)	0.96897 (0.00050)	0.95619 (0.00048)	-138	0.96897 (0.00050)	0.96628 (0.00049)	-0.36
Type A FP loading	0.96075 (0.00049)	0.94707 (0.00051)	-150	0.96075 (0.00049)	0.95929 (0.00051)	-0.14
Type B FP loading	0.96355 (0.00047)	0.95015 (0.00051)	-146	0.96355 (0.00047)	0.96157 (0.00044)	-0.26

7. Summary

^{99}Tc and ^{129}I are selected to be transmuted in the HYPER system. A study has been performed to develop an optimum configuration for the fission product target. The introduction of moderator to generate a local thermal flux is concluded to considerably increase the transmutation rate of fission product without causing any severe core safety problems. The configuration that ^{99}Tc is loaded as a plate type in the outer most region and ^{129}I is loaded as a NaI rod mixed with calcium hydride rod in the inner region of fission product target is estimated to be one of the best configurations.

The support ratios of the HYPER system for ^{99}Tc and ^{129}I are estimated to be 5.7 and 4.0, respectively. The support ratio for ^{99}Tc is slightly larger while that for ^{129}I is less compared to the support ratio for TRU. Some minor consideration has to be given for the adjustment. In addition, the cooling problems for the FP target will be investigated in near future.

Figure 7. **Neutron energy spectrum for Type A configuration**

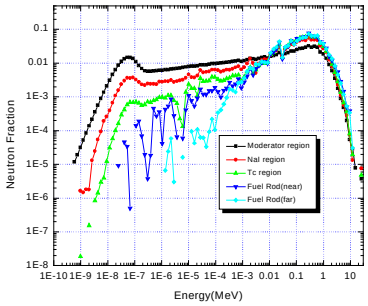

Figure 8. **Neutron energy spectrum for Type B configuration**

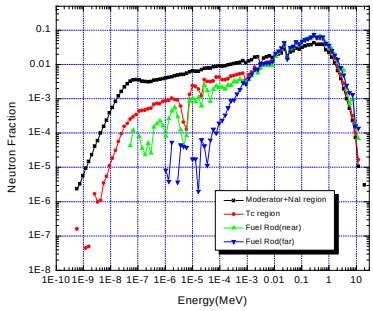

Acknowledgements

The authors greatly appreciate the financial supports of Ministry of Science & Technology (MOST) for this study.

REFERENCES

[1] D.W. Wootan *et al.*, *Irradiation Test of Tc-99 and I-129 Transmutation in the Fast Flux Test Facility,* ANS Trans. 64, 125, 1991.

[2] Y.H. Kim *et al.*, *A Study on Burnable Absorber for a Fast Sub-critical Reactor HYPER*, 6th Information Exchange Meeting on Actinide and Fission Product Partitioning and Transmutation, Madrid, Spain (2000), EUR 19783 EN, OECD Nuclear Energy Agency, Paris (France), 2001.

[3] J.S. Chung, Y. H. Kim and W.S. Park, *Design of the Fission Product Assembly in the Sub-critical System HYPER*, Proceedings of Korean Nuclear Society Spring Meeting, 2000.

[4] H.J. Shim *et al.*, *Monte Carlo Depletion Analysis of a PWR with the MCNAP*, M&C 99 Int. Conf. on Mathematics and Computation, reactor physics and Environmental Analysis in Nuclear Applications, Sept. 1999, Madrid, Spain, Vol. 2, 1026-1035, 1999.